NOTICE

CERTAIN DATA CONTAINED IN THIS DOCUMENT MAY BE DIFFICULT TO READ IN MICROFICHE PRODUCTS.

SAND--88-1203

DE91 000455

SAND88-1203
Unlimited Release
Printed August 1990

EXPLORATORY SHAFT SEISMIC DESIGN BASIS WORKING GROUP REPORT

C. V. Subramanian
Sandia National Laboratories

J. L. King
Science Applications International Corp.

D. M. Perkins
U.S. Geological Survey

R. W. Mudd
Fenix & Scisson

A. M. Richardson
Parsons Brinckerhoff Quade & Douglas, Inc.

J. C. Calovini
Holmes & Narver, Inc.

E. Van Eeckhout
Los Alamos National Laboratory

D. O. Emerson
Lawrence Livermore National Laboratory

ABSTRACT

This report was prepared for the Yucca Mountain Project (YMP), which is managed by the U. S. Department of Energy. The participants in the YMP are investigating the suitability of a site at Yucca Mountain, Nevada, for construction of a repository for high-level radioactive waste. An exploratory shaft facility (ESF) will be constructed to permit site characterization. The major components of the ESF are two shafts that will be used to provide access to the underground test areas for men, utilities, and ventilation. If a repository is constructed at the site, the exploratory shafts will be converted for use as intake ventilation shafts. In the context of both underground nuclear explosions (conducted at the nearby Nevada Test Site) and earthquakes, the report contains discussions of faulting potential at the site, control motions at depth, material properties of the different rock layers relevant to seismic design, the strain tensor for each of the waveforms along the shaft liners, and the method for combining the different strain components along the shaft liners. The report also describes analytic methods, assumptions used to ensure conservatism, and uncertainties in the data. The analyses show that none of the shafts' structures, systems, or components are important to public radiological safety; therefore, the shafts need only be designed to ensure worker safety, and the report recommends seismic design parameters appropriate for this purpose.

This document was prepared under Quality Assurance Level I procedures under WBS 1.2.4.1.2.

WORKING GROUP

REPORT

ES SEISMIC DESIGN BASIS

Prepared By

3/25/88
Fenix & Scisson

3/21/88
Parsons, Brinkerhoff, Quade & Douglas, Inc.

4/6/88
Los Alamos National Laboratory

4/11/88
Lawrence Livermore National Laboratory

3/7/88
3/7/88
Holmes & Narver, Inc.

3/10/88
3/14/88
Science Application International Corp.

3/3/88
Sandia National Laboratories

U.S. Geological Survey

March 1, 1988

ACKNOWLEDGMENTS

In addition to the organizations called out on the front page of this report, others helped put it together. These contributors include J. Kimball of the Department of Energy/Headquarters, J. S. Phillips of Division 7111 of Sandia National Laboratories, G. N. Owen of URS/John A. Blume & Associates, R. Lee (a consultant to URS/Blume), and R. P. Kennedy of Structural Mechanics Consulting (a consultant to Holmes & Narver). Their contributions include participating in the working group meetings, providing technical consultation and input to the working group, providing text for the report, reviewing the report's contents, and helping resolve review comments on the report. Their contributions are gratefully acknowledged.

CONTENTS

		Page
	ACKNOWLEDGMENTS	iv
	EXECUTIVE SUMMARY	x
1.0	INTRODUCTION	1
2.0	GROUND MOTION CAUSED BY EARTHQUAKES	6
	2.1 Relevant Earthquake Sources	6
	2.2 Control Values for Peak Ground Motions	9
	2.3 Checks on Design Basis Motions	12
	2.4 Factors That May Influence Ground Motion	12
	2.5 Further Recommendations	14
3.0	CONTROL MOTIONS FROM UNDERGROUND NUCLEAR EXPLOSIONS	16
4.0	COMBINATION OF INDIVIDUAL COMPONENT WAVE EFFECTS	21
5.0	DEVELOPMENT OF STRAIN TENSORS	23
	5.1 Strain Tensors for Earthquakes	23
	5.2 Strain Tensors for UNEs	26
	5.3 Controlling Strain Combinations Caused by Earthquakes and UNEs	30
6.0	DYNAMIC ROCK PROPERTIES	32
7.0	FAULTING CONSIDERATIONS	37
	7.1 Objectives	37
	7.2 Faulting Potential	38
	7.3 Design Basis Faulting	39
8.0	REFERENCES	40
APPENDIX A-1	Incidence Angle of Seismic Body Waves	A-1-1
APPENDIX A-2	Discussion of the Prediction of UNE Ground Motions	A-2-1
APPENDIX A-3	Determination of Controlling Strain Combination for Design	A-3-1
APPENDIX A-4	Depth Attenuation Behavior of UNE Ground Motions at Yucca Mountain	A-4-1
APPENDIX B	Information Used in This Report From the Reference Information Base, and Candidate Information for the Reference Information Base and Site Engineering Data Base	B-1

TABLES

Table		Page
2-1	Predicted Peak Ground Motion Values at the ESF Site for an Earthquake on the Bare Mountain Fault and Recommended Peak Ground Motion Values for Consideration in ESF Design	10
3-1	Recommended Motions for the Design Basis UNE	19
5-1	Free-Field and Bending Strains for Body Waves with Angle of Incidence θ	27
5-2	Free-Field and Bending Strains in Terms of Ground Motion Control Parameters for Earthquakes	28
5-3	Free-Field and Bending Strains in Terms of Ground Motion Control Parameters for Body Waves with Shallow Angles of Incidence	31
6-1	Reference Information Base Data for Bulk Density, Poisson's Ratio for Rock Mass, and Poisson's Ratio for Intact Rock	34
A-2.1	Prediction Equations for Acceleration, Velocity, and Displacement	A-2-2
A-3.1	Free-Field and Bending Strains Caused by Earthquakes	A-3-2
A-3.2	Free-Field and Bending Strains in Terms of Ground Motion Control Parameters for Earthquakes	A-3-3
A-3.3	Strains Caused by Earthquakes for $45° < 0 \leq 90°$	A-3-4
A-3.4	Wave Particle Velocities and Accelerations	A-3-5
A-3.5	Stresses and Strain for Earthquake Motion	A-3-7
A-3.6	Stresses and Strain for UNE Motions	A-3-8
A-4.1	Ratio of Peak Surface and Downhole Ground Motions	A-4-5
A-4.2	Values Used to Determine Ratios of Surface and Downhole Ground Motions	A-4-10
A-4.3	Summary of Depth Attenuation Curves for Peak UNE Ground Motions	A-4-15
A-4.4	Depth Attenuation of Component Ground Motions	A-4-15
A-4.5	Ratios of Surface and Downhole PSRVs 1, 2, and 5 Hz	A-4-27
A-4.6	Values Used to Determine Ratios of Surface and Downhole PSRVs for 1, 2, and 5 Hz	A-4-29

TABLES
(Concluded)

Table		Page
A-4.7	Summary of PSRV Depth Attenuation Curves for 1, 2, and 5 Hz	A-4-40
A-4.8	Depth Attenuation of PSRVs at 1, 2, and 5 Hz	A-4-40

FIGURES

Figure		Page
2-1	Location of ESF and Faults in the Repository Site Vicinity	7
3-1	Locations of Current and Proposed Testing Areas at the NTS and the Yucca Mountain Site	17
5-1	Orientation of Incident Waves with Respect to the Coordinate System	24
5-2	Relationship Between Peak Ground Motion Control Parameters and Particle Motions Caused by Each Wave Type	29
6-1	Interpretation of Seismic Velocities from USW G-4 Data	33
A-1.1	Approximate Velocity Structure for the Southern Great Basin	A-1-1
A-1.2	Depiction of the Ray Path Along Which the Largest-Amplitude Waves from a Potential Earthquake Source May Emerge at the ESF	A-1-3
A-4.1	Ideal Situation for Determining Depth Attenuation Behavior	A-4-1
A-4.2	Actual Situation for Determining Depth Attenuation Behavior	A-4-2
A-4.3	Surface/Downhole Ratios vs Depth for Vertical Acceleration	A-4-16
A-4.4	Surface/Downhole Ratios vs Depth for Vertical Velocity	A-4-17
A-4.5	Surface/Downhole Ratios vs Depth for Vertical Displacement	A-4-18
A-4.6	Surface/Downhole Ratios vs Depth for Radial Acceleration	A-4-19
A-4.7	Surface/Downhole Ratios vs Depth for Radial Velocity	A-4-20
A-4.8	Surface/Downhole Ratios vs Depth for Radial Displacement	A-4-21
A-4.9	Surface/Downhole Ratios vs Depth for Transverse Acceleration	A-4-22
A-4.10	Surface/Downhole Ratios vs Depth for Transverse Velocity	A-4-23

FIGURES
(Concluded)

Figure		Page
A-4.11	Surface/Downhole Ratios vs Depth for Transverse Displacement	A-4-24
A-4.12	Surface/Downhole Ratios vs Depth for PSRVs of Vertical Motions at 1 Hz	A-4-31
A-4.13	Surface/Downhole Ratios vs Depth for PSRVs of Vertical Motions at 2 Hz	A-4-32
A-4.14	Surface/Downhole Ratios vs Depth for PSRVs of Vertical Motions at 5 Hz	A-4-33
A-4.15	Surface/Downhole Ratios vs Depth for PSRVs of Radial Motions at 1 Hz	A-4-34
A-4.16	Surface/Downhole Ratios vs Depth for PSRVs of Radial Motions at 2 Hz	A-4-35
A-4.17	Surface/Downhole Ratios vs Depth for PSRVs of Radial Motions at 5 Hz	A-4-36
A-4.18	Surface/Downhole Ratios vs Depth for PSRVs of Transverse Motions at 1 Hz	A-4-37
A-4.19	Surface/Downhole Ratios vs Depth for PSRVs of Transverse Motions at 2 Hz	A-4-38
A-4.20	Surface/Downhole Ratios vs Depth for PSRVs of Transverse Motions 5 Hz	A-4-39

EXECUTIVE SUMMARY

This report, which was prepared by a special working group (WG) authorized by the Exploratory Shaft (ES) Interface Control Working Group (ICWG), provides recommendations for the seismic design parameters for the design of the shafts associated with the exploratory shaft facility (ESF) of a proposed repository for high-level radioactive waste at Yucca Mountain, Nevada.* Although directly intended for the design of ESF shaft liners, much of this design basis is also appropriate for the seismic design of other shafts and underground structures that do not affect public safety. The recommendations include parameters both for natural earthquakes, which may possibly occur at or near the repository site, and for underground nuclear explosions (UNE), which are regularly detonated at the Nevada Test Site (NTS). An evaluation was conducted in February 1988 to evaluate the functions of the shafts during the preclosure period of the repository. Based on this evaluation and other studies conducted to support the conceptual design for site characterization, it was concluded that a failure of an ES will not affect the radiological safety of the public and consequently that the shafts need only be designed adequately to provide for worker safety.

Specifically, the recommended control motion values that are to be applied at the surface for an earthquake are

- maximum horizontal component of acceleration, 0.3 g;
- maximum vertical component of acceleration, 0.3 g;
- maximum horizontal component of velocity, 30 cm/sec; and
- maximum vertical component of velocity, 20 cm/sec;

and for a UNE are

---

*This work was performed under the auspices of the U. S. Department of Energy, Office of Civilian Radioactive Waste Management, Yucca Mountain Project, under contract DE-AC04-76DP00789.

- maximum vertical component of acceleration, 0.2 g;
- maximum radial component of acceleration, 0.1 g;
- maximum transverse component of acceleration, 0.1 g;
- maximum vertical component of velocity, 9 cm/sec;
- maximum radial component of velocity, 12 cm/sec; and
- maximum transverse component of velocity, 12 cm/sec.

An evaluation of faulting potential at the ESF site and its vicinity indicates that the annual probability of faulting in excess of a few centimeters (5 cm) is less than 10^{-4}/yr. On the basis of this, the report recommends that faulting effects need not be considered in the design of the ESF. Further, the report provides specific guidance for determining (1) the control motions at depth, (2) the material properties for the different rock layers relevant to seismic design, (3) the strain tensor for each of the waveforms and the maximum strain components along the shaft liner, and (4) the method for combining the different strain components along the shaft liner. Finally, to provide further assurance that the design has adequate conservatism or margin to accommodate uncertainties such as site effects, the WG recommends that the satisfactory performance of the ESF be confirmed using best-estimate conditions when subjected to ground motions that are a factor of 1.67 times the proposed design basis motions. This evaluation for the larger motions should provide assurance that major damage to the ESF is not expected at these levels.

The report also lists the assumptions and other conditions used to develop the recommendations. In developing the basis for the recommendations, the WG used currently available site-specific seismic and geologic data. In recognition of the uncertainties in these data, the seismic design parameters recommended include a reasonable degree of conservatism and are consistent with the seismic design requirements used for similar types of facilities.

1.0 INTRODUCTION

This report was prepared by a special working group (WG) authorized by the Exploratory Shaft (ES) Interface Control Working Grcup (ICWG). It provides recommendations for the seismic design parameters to be used for the design of the shafts associated with the exploratory shaft facility (ESF) of a proposed repository for high-level radioactive waste at Yucca Mountain, Nevada. In developing the basis for these recommendations, the WG used currently available site-specific seismic and geologic data. In recognition of the uncertainties in these data, the seismic design parameters recommended include a reasonable degree of conservatism.

There are two shafts in the ESF configuration. These shafts have a two-stage service life. First, as part of the ESF, they will support site characterization by providing access, ventilation, utility support, and emergency egress from the underground test areas; second, if a repository is constructed at Yucca Mountain, the shafts will be converted to intake ventilation shafts in the actual repository, a function they will perform until repository closure. As discussed in the baselined Generic Requirements for a Mined Geologic Disposal System (OGR/B-2) (DOE, Reference 1), four permanent items have been identified that will be designed, procured, or constructed for future incorporation into the repository. The permanent items include underground openings, operational seals, ground support, and shaft liners. This report provides appropriate seismic design recommendations for these permanent items. Other items and structures in the ESF will be designed using other requirements such as those of the Uniform Building Code (UBC) (UBC, Reference 2).

During the operations phase, the ESF shafts will supply approximately 60% of the total air flow needed to support waste emplacement. The remaining air is supplied through the waste ramp. Exhausting fans on the emplacement area exhaust shaft maintain pressures in the emplacement area lower than the pressures in the development (mining) area.

Concrete liners will be installed in the exploratory shafts concurrently with their sinking. Their functions are

- to provide effective structural support to the ground,
- to eliminate minor rockfall hazards,
- to provide a dimensionally consistent cross section and stable anchorage for installation and alignment of shaft equipment, and
- to provide a low-friction surface for efficient ventilation throughout the life of the repository.

Neither of the exploratory shafts will at any time be used to handle radioactive waste, nor are the liners intended to serve as barriers to radionuclide migration or to entry of water into the emplacement area during operations or after closure. (NOTE: Small quantities of contained radioactive materials used as sources for shielding tests or as part of measuring systems such as neutron or gamma-logging tools will be transported through the shafts.)

The shafts are located in unsaturated geologic formations and do not penetrate any aquifers at the site. Further, any perched water zones encountered during shaft sinking are expected to drain fairly quickly; thus, the shaft liners will not be required to prevent or control ground water inflows into the shaft. The construction joints between each concrete pour are not planned to be watertight.

If one or both of the exploratory shafts were to be completely blocked as the result of a failure of a shaft liner (which is highly unlikely), the emplacement area would still be under negative pressure with respect to the development area, and the ventilation leakage path would be maintained in the direction of the emplacement area. If a waste container were to be ruptured simultaneously with the failure of one of the ESF shafts, any potentially contaminated air would still be exhausted via the emplacement area exhaust shaft through high-efficiency particulate air (HEPA) filters. At this time, no credible accident scenarios have been identified whereby failure of one of the shaft liners could result in a release of radiation. Therefore, public safety does not appear to be an issue in shaft liner design.

In addition, a preliminary analysis has been completed to determine which structures, systems, and components are important to public radiological safety. This analysis is described in reports by SNL (Reference 3 and Jardine, draft*). The results of this analysis indicate that there are no shaft structures, systems, or components important to public safety.

Based on the above, the ESF (especially the shaft liners) is not an "essential" or even a "low-hazard" facility (i.e., a facility that does not handle or process plutonium) as defined by the DOE in Reference 4. Based on these reasons, it is justifiable to design the exploratory shaft liners as structures that are required only to provide for worker safety; i.e., permanent items (such as the liners) associated with the exploratory shafts need not be designed as items important to provide public radiological safety but need be designed only for a level of seismic input that is sufficient to ensure worker safety and reasonably uninterrupted functions. For conservatism, the seismic design basis recommendations for the ESF in this report are consistent with those required for a low-hazard or essential facility. Other nonpermanent items and structures in the ESF will be designed using other requirements such as those of the UBC (Reference 2).

The recommendations for the seismic design basis parameters given in Sections 2 and 3 of this report are based on the discussions in the preceding paragraphs. The recommendations include ground motion parameters both for natural earthquakes, which may possibly occur at or near the site, and for underground nuclear explosions (UNE), which may occur at the Nevada Test Site (NTS).

Section 2 of this report provides recommendations for characterizing the wave motions along with conditions and assumptions used for the

---

*L.J. Jardine, "Preclosure Radiological Safety Analysis for the Exploratory Shaft Facilities," SAND88-7072, prepared for Sandia National Laboratories Bechtel National, Inc., San Francisco, CA, draft.

development of control motions for natural earthquakes. Section 3 provides the same information for UNEs. Section 4 describes the rule to be used for combining the maximum strains (responses) caused by the different wave components. Section 5 describes the strain tensors, including bending strains for each of the propagating waves caused by earthquakes and UNEs, which should be considered in the design of the ESF. This section describes the determination of the worst strain combination case for use in the design. Section 6 identifies the recommendations for the rock properties for each rock intersected by the exploratory shaft. Section 7 presents the WG recommendations regarding consideration of potential fault offsets at the site for the ESF design. Finally, the report contains appendices that support the WG recommendations.

The seismic design basis control motions proposed for the ESF are:

- maximum horizontal component of acceleration, 0.3 g;
- maximum vertical component of acceleration, 0.3 g;
- maximum horizontal component of velocity, 30 cm/sec; and
- maximum vertical component of velocity, 20 cm/sec.

These values are consistent with the values of effective peak acceleration in a map found in a report prepared by the Applied Technology Council (ATC) (Reference 5) from which UBC (Reference 2) Zones 2 and 3 are derived for the design of an essential facility. In addition, the proposed recommendations in this report are also consistent with the requirements for important low-hazard facilities as called out by the DOE in Reference 4 and by Kennedy et al., draft.* In Jardine (draft), the use of UBC requirements for seismic loads for such facilities is recommended. Further, the seismic design basis motions being proposed for the ESF are similar to those for nuclear power plant structures, systems, and

---

*R.P. Kennedy et al., "Design and Evaluation Guidelines for Department of Energy Facilities Subjected to Natural Phenomena Hazards, "prepared for the U.S. Department of Energy, Office of Nuclear Safety, report UCRL-15910, draft.

components that may be required for operation of the facility but that are not important to public safety. The Standard Review Plan recommends the use of other industrial codes such as those from the American Petroleum Institute and American Water Works Association, both of which use UBC-type requirements for these structures.

2.0 GROUND MOTION CAUSED BY EARTHQUAKES

In Section 1, it is concluded that the ESF need not be designed as a facility important to public radiological safety. Based on this conclusion, the WG believes that the ESF design should take into account earthquake ground motions (vibratory ground motion and faulting) that are reasonably likely to occur during the operating life (less than 100 yr) of the ESF. Specifically, the WG recommends consideration of ground motion conditions that recur at average intervals of about 1,000 yr, i.e., with about one chance in ten of occurring during the maximum operating life. This rate of occurrence would result in more conservative values of vibratory ground motions than those given by the ATC (Reference 5) on which the UBC (Reference 2) is based.

In June of 1987, design and evaluation guidelines for Department of Energy (DOE) facilities subjected to natural phenomena hazards were prepared (Kennedy et al., draft). These guidelines recommend that, for mission-dependent facilities (where confinement of contents is not essential), a hazard exceedence probability of 1E-3 be used (recurrence of 1,000 yr). These guidelines have been incorporated in a draft revision of Reference 4, which was published in January of 1988. The ESF seismic design recommendation is also consistent with this draft revision.

Deterministic methods are appropriate for establishing conservative levels of ground motion for consideration in the ESF design. Probabilistic methods are appropriate for confirming that the resulting motions are unlikely to be exceeded during the operating lifetime of the ESF.

2.1 Relevant Earthquake Sources

Figure 2-1 shows the location of the ESF with respect to the various faults in the repository site vicinity. There are a large number of faults in the site vicinity. However, as discussed in Section 7.2, faults in the immediate area of the ESF, including the Ghost Dance Fault, appear to slip at intervals measured in tens of thousands of years or longer and,

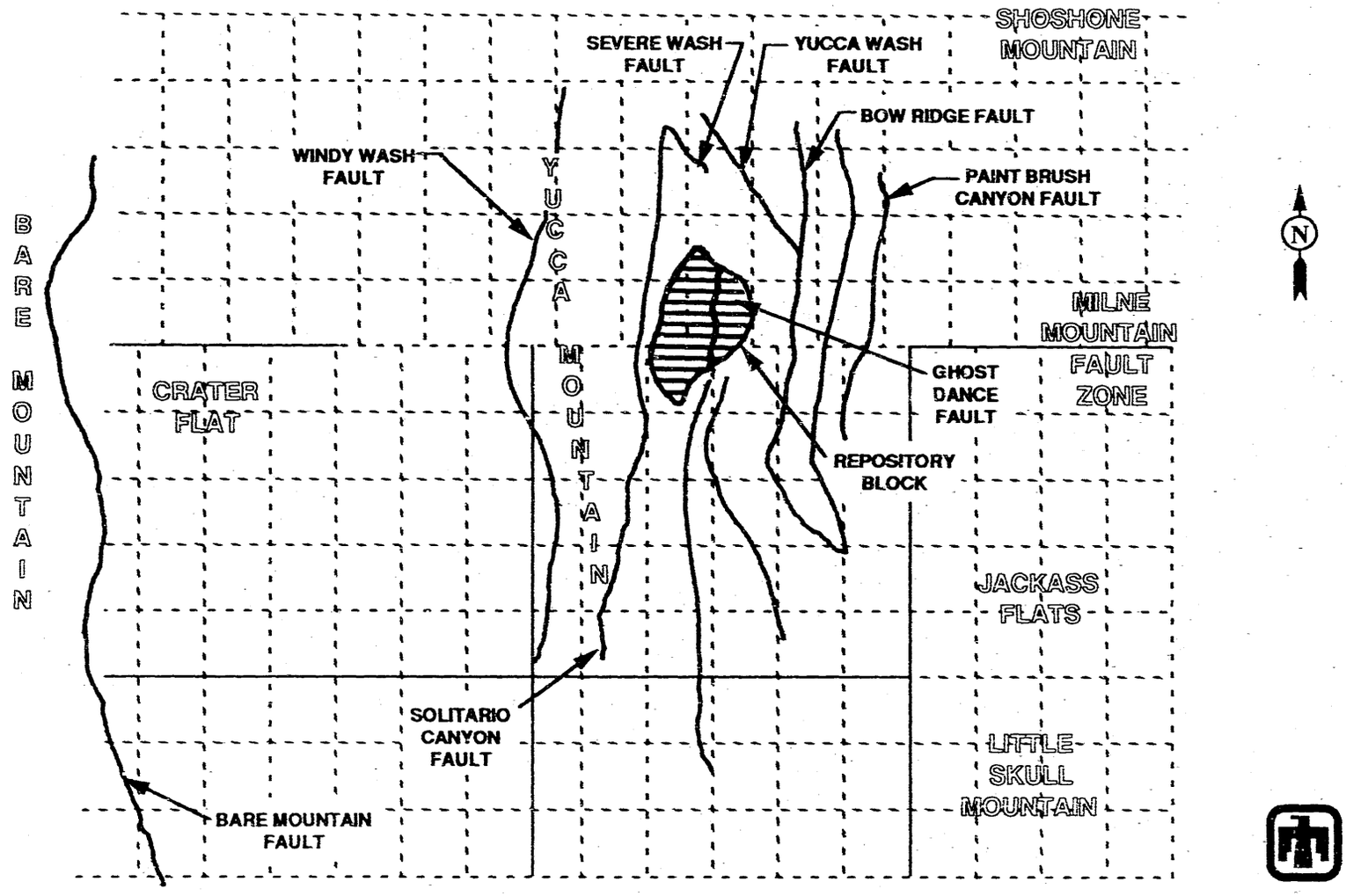

Figure 2-1. Location of ESF and Faults in the Repository Site Vicinity

therefore, are an unlikely source of significant earthquake ground motion during the operating life of the ESF. The average slip rate on local faults during the late Quaternary period appears to be less than about 0.02 mm/yr (Carr, Reference 6). The average recurrence time for magnitude 5-1/2 (potentially damaging) earthquakes on a fault with a slip rate of 0.02 mm/yr exceeds 10,000 yr according to a relationship developed by Slemmons in Reference 7. Larger-magnitude earthquakes (magnitude greater than 5-1/2) would thus have recurrence intervals of longer than 10,000 yr, possibly as long as 100,000 yr. Geologic evidence suggests that slip on one of the more significant local faults, the Windy Wash Fault, results from earthquakes that produce 10 cm or more displacement per event at recurrence intervals of several tens of thousands of years (Whitney et al., Reference 8). Although an earthquake of magnitude 5 or smaller might occur on a local fault during the operating life of the ESF, such events are not known to significantly damage well-engineered structures. In addition, experience with underground facilities indicates that earthquakes of magnitude less than about 6.0 are not expected to cause significant damage to underground facilities (Pratt et al., Reference 9).

The north-trending Bare Mountain Fault, located about 16 km west of the ESF, appears to be the most likely source of potentially severe ground shaking during the lifetime of the ESF. This fault may have an average Quaternary slip rate of up to 0.15 mm/yr (DOE, Reference 10), which indicates that this fault is much more active than faults local to Yucca Mountain. Applying the relationship given by Slemmons (Reference 7) to a fault with a slip rate of 0.15 mm/yr indicates a minimum recurrence interval of about 6,000 yr for a magnitude 6-1/2 earthquake. Based on this and other considerations, including the fact that site ground motions derived from this earthquake are roughly comparable to those from suitably conservative probabilistic hazard analyses (URS/John A. Blume & Assoc., Reference 11, and Perkins et al., Reference 12), a magnitude 6-1/2 earthquake on the Bare Mountain Fault is used in this report as the deterministic basis for establishing ground motion conditions to be considered in the design of the ESF.

2.2 Control Values for Peak Ground Motions

Among the many parameters that influence earthquake ground motion, earthquake magnitude and source distance appear to be the most important. Many recordings of strong motions have been obtained within 20 km of several earthquakes in the magnitude range of 6 to 7. Even though none of these earthquakes is a perfect analog for conditions at Yucca Mountain, the range of observational data is adequate for direct extrapolation.

Regression relationships between peak ground motion parameters and earthquake magnitude, source distance, local site conditions (e.g., rock or soil), and other parameters have been developed by a number of workers (see the references found in Campbell, Reference 13). Two recent and representative sets of regression relations for peak horizontal acceleration and peak horizontal velocity are those in Joyner and Fumal and Campbell (References 14 and 15). Results obtained using these relationships are presented in Table 2-1. The results are obtained based on the assumptions of reverse and thrust mechanisms for conservatism. It is also assumed that the surface trace of the Bare Mountain Fault is 16 km from the ESF location, that the fault is planar, and that it dips eastward at an angle of 70° from the horizontal, the midrange of current estimates (Reference 10). More discussions of this conservative assumption may be found in Section 2.5. For the Campbell relationships given in Reference 15, the closest distance to the zone of seismic energy release, R, was conservatively taken to be the closest distance to the fault plane, 15.0 km. For the Joyner and Fumal relationships given in Reference 14, the distance, d, to the surface projection of the rupture zone was estimated at 10.9 km by assuming a maximum rupture depth of 15.0 km; a shallower rupture depth would increase the distance and would reduce the estimated motions.

Based on the results in Table 2-1 and on other considerations, such as probabilistic hazards, the WG recommends that 0.3 g and 30 cm/s be used as control values for peak horizontal acceleration (larger of two randomly oriented horizontal components) and velocity, respectively. The use of the larger of two randomly oriented horizontal components is more conservative

TABLE 2-1

PREDICTED PEAK GROUND MOTION VALUES AT THE ESF SITE FOR AN EARTHQUAKE ON THE BARE MOUNTAIN FAULT AND RECOMMENDED PEAK GROUND MOTION VALUES FOR CONSIDERATION IN ESF DESIGN

	Peak Horizontal Acceleration[a]			Peak Horizontal Velocity[a]		
M[b]	Joyner and Fumal[c]	Campbell[d]	ESF Design Basis	Joyner and Fumal[c]	Campbell[d]	ESF Design Basis
6.0	0.21 g	0.19 g		11.9 cm/s	10.8 cm/s	
6.5	0.27	0.26	0.30 g	20.9	16.8	30.0 cm/s
6.75	0.31	0.30		27.8	20.7	

a. Predicted median (most probable) peak ground motion values (larger of two randomly oriented components) at the ESF site from an earthquake on the Bare Mountain Fault.

b. M = magnitude.

c. Joyner and Fumal (1985) (Reference 14); distance to the surface projection of the fault rupture, d = 10.9 km, assuming a 70° eastward dip and 15-km maximum rupture depth. Joyner and Fumal do not attempt to obtain distinct regressions for different source mechanisms.

d. Campbell (1987) (Reference 15) "unconstrained" model; acceleration values have been increased by 13% and velocity values by 17% to convert from the mean of two components to the larger of two components. The closest distance to the zone of seismogenic rupture, R, is taken as the closest distance to the fault plane, 15.0 km, assuming a 70° eastward dip. For conservatism, higher values corresponding to the assumption of a reverse or thrust mechanism are calculated.

than the use of the average of the two components by about 13% (Reference 15). The standard practice for defining the design vibratory ground motion for nuclear power plants is to use both of the horizontal components.

Standard engineering practice is to set vertical ground motion values at two-thirds those of the horizontal values. This approach would probably be adequate for peak accelerations from a magnitude 6-1/2 earthquake at a

distance of about 15 km. However, a number of recently obtained close-in recordings of strong motion from large earthquakes have evidenced vertical peak accelerations equal to or even exceeding the peak horizontal accelerations (Shakal et al., Reference 16, and Huang et al., Reference 17). In light of the marginal probability of large vertical accelerations from an earthquake on the Bare Mountain Fault and the marginal probability of an earthquake on one of the closer faults (which could be expected to generate vertical accelerations on the order of the horizontal accelerations), the WG deems it prudent to assume equal peak values for horizontal and vertical acceleration, namely 0.3 g.

Empirical observations indicate that ground velocities do not exhibit such near-field increases in the relative amplitude of the vertical components partly because of the relatively lower frequency content associated with ground velocity as compared with ground accelerations. Consequently, the standard practice of setting the vertical component at two-thirds the value of the horizontal component is used to establish a control value of 20 cm/s for the vertical component of ground velocity.

Whereas earthquake ground shaking results from a myriad of seismic waves, the peak motions from very close earthquakes are expected to be dominated by waves that follow the most direct and efficient route from the earthquake source. As discussed in Appendix A-1, the largest-amplitude waves are expected to emerge at a steep angle, within 30° of vertical, at the ESF location. These body waves include longitudinal P waves and two types of transverse S waves (Bath, Reference 18): horizontally polarized S_h waves and orthogonally polarized S_v waves with a vertical component of motion. Because the ratio of P-wave to S-wave velocities in the earth's crust is nearly constant (ranging from about 1.6 to 1.8, Reference 19), the three types of body waves (P, S_h, and S_v) are expected to emerge at about the same angle. Furthermore, because of the characteristics of earthquake waves, the vertical component of peak motion can be associated with P waves or S_v waves, and the horizontal components can be associated with S_h and S_v waves. However, the amplitude of steeply emerging S_v waves is constrained

by the peak horizontal motions and is therefore limited in its contribution to the vertical motion.

2.3 Checks on Design Basis Motions

Two reconnaissance probabilistic seismic hazard analyses for Yucca Mountain support the adequacy of 0.3 g as a control value for peak horizontal acceleration. Probabilistic seismic hazard analysis integrates the contribution of all known faults and seismic source zones to the probability of exceeding a particular ground motion level and, thus, is a useful means of confirming the adequacy of deterministically derived estimates. A reconnaissance assessment of probabilistic earthquake accelerations at Yucca Mountain by Perkins et al. in Reference 12 indicates that a peak horizontal acceleration of 0.3 g has a return period of about 1,500 to 3,000 yr. A sensitivity study by URS/Blume in Reference 11 suggests a return period on the order of 1,000 yr for 0.3 g. Both analyses are subject to very large uncertainties but tend to confirm that 0.3 g is a conservative estimate of the peak horizontal ground acceleration that could occur during the operating lifetime of the ESF.

2.4 Factors That May Influence Ground Motion

In addition to an earthquake's magnitude and distance from a site, the factors that most influence ground motion at the site include source type (normal, reverse, or strike/slip), rupture dynamics (directivity and variability of stress release on the fault surface), transmission path effects (wave scattering, attenuation, multipathing, and dispersion), and site geology (topography and vertical and lateral variations in soil and rock densities, seismic velocities, and Q values). Considerations of each class of influences are discussed below.

The Bare Mountain Fault is a Basin and Range, range front fault (Carr, Reference 6), with a normal or oblique normal sense of slip. McGarr (Reference 20) has suggested that normal faulting occurs at lower stresses than strike/slip or thrust faulting and that normal fault events are less

energetic at high frequencies than are earthquakes with strike/slip or thrust mechanisms. Because the large majority of data that constrain the empirical relationships used in Table 2-1 are from strike/slip and thrust earthquakes, the use of these relationships would result in the direction of added conservatism in the predicted design basis motions. The Campbell (Reference 15) peak ground motion regressions used in Table 2-1 take into account fault type (strike/slip or reverse and thrust). In order to provide margin for possible re-evaluation of the tectonic environment by ongoing geologic and geophysical studies, the WG has used Campbell's regressions for reverse and thrust earthquake mechanisms. Joyner and Fumal's regressions do not provide for a distinction in ground motion caused by source mechanism.

Effects of rupture dynamics are most influential at distances closer than those being considered here. Close-in strong motion records sometimes evidence (Singh, Reference 21) anomalous or at least identifiable motions that can be attributed to irregularities in the rupture process or to focusing (or defocusing) that results from the approaching (or receding) rupture front. Singh observes that the near-field behavior produces great variability in individual parameters, no one of which is sufficient to account for the variability in near-field damage, and that it is not possible to estimate near-field spectra by using these parameters to set the levels of spectral shapes based on local site conditions. Individual near-field spectra have to be estimated in a site-specific, rupture-specific way. Major effects in the near field are caused by "enhancement of the long-duration pulse called the 'fling,' which is related to the elastic rebound on the fault, and . . . compression of the duration of the strong shaking in the direction of rupture propagation" (Singh, Reference 21). The long-duration pulse is probably most important for damage to longer-period structures. As for the effect of direction of rupture propagation, Singh does not discuss whether the near-field ground motion parameters have greater means or medians than predicted by current attenuation functions if the rupture propagation direction is not known, even though higher ground motions for an approaching rupture and lower ground motions for a receding rupture should be expected. As for the

expected effects at the ESF site, because large normal faulting earthquakes typically initiate at depth and propagate upward (Smith and Richins, Reference 22), away from the site in this case, any bias resulting from rupture dynamics is expected to reduce ground motions at the site.

Data are not yet available to evaluate the possibility of local biases in regional seismic wave transmission characteristics. There are some indications that waves may transmit more efficiently in the southern Great Basin than in California, where most of the relevant strong motion data have been recorded (Rogers, Reference 23). However, the effects of regional differences in attenuation scale with distance and are probably not significant at source receiver distances around 15 km. Also, the soil conditions that are generally associated with increased earthquake motions are not present at a rock site.

Perhaps the biggest single source of dispersion in the observations of earthquake motions results from the effects of the local geology. Based on Campbell's estimates for dispersion from all sources (Reference 24), a site that amplifies motions more than 84% of all sites of the same classification (i.e., a mean-plus-one-standard-deviation site) could result in peak motions about one and one-half times as large as the hypothetical average site. Conversely, a site that amplifies motions to a lesser degree than 84% of the sites (i.e., a mean-minus-one-standard-deviation site) could attenuate motions by a factor of about two-thirds.

Additional considerations are identified below to accommodate possible uncertainties in the determination of ESF design motions.

2.5 Further Recommendations

Until determinations of local site factors are available, added conservatism is warranted to compensate for this source of uncertainty. Specifically, the WG recommends that no credit be taken for attenuation of ground motion with depth below the ground surface or for the reduction in seismic strains that result from the stress-free boundary condition at the

ground surface. Available surface and downhole recordings of motions in the area of Yucca Mountain from UNEs have been compiled in Appendix A-4 and indicate a reduction in ground motions by factors up to a maximum of 3.3. with depth. This indication applies to accelerations, velocities, and displacements with the exception of vertical displacement which does not attenuate with depth.

Finally, to provide further assurance that the design has adequate conservatism or margin to accommodate uncertainties such as site effects, the WG recommends that the performance of the ESF be evaluated using best-estimate conditions when subjected to ground motions that are a factor of 1.67 larger than the design basis motions, i.e., for a peak horizontal acceleration of 0.5 g and a peak horizontal velocity of 50 cm/sec. This evaluation for the larger motions should provide assurance that major damage to the ESF is not expected at these g levels.

3.0 CONTROL MOTIONS FROM UNDERGROUND NUCLEAR EXPLOSIONS

The control motions from the design basis UNE are specified in this section. In addition, background on the design basis UNE and the various assumptions made in the specification of ground motions are also included. Backup material and additional references are provided in Appendices A-2 and A-4.

The Yucca Mountain repository, which is on and adjacent to the NTS, must not limit the ability of the United States government to test nuclear weapons. Therefore, definition of the design basis UNE that is selected must reflect this position. The event chosen has also to produce the maximum ground motions at Yucca Mountain for the maximum credible yield at any given area on the NTS (regardless of current or future treaties). Figure 3-1 shows the current and proposed testing areas at the NTS and their relationship to the Yucca Mountain area. Vortman (Reference 25) used the results of a 1977 USGS real estate availability study of several areas of the NTS and the upper yield limits established for these areas by the Ground Motion and Seismic Evaluation Subcommittee to define the design basis UNE for the repository site. The yield limits were based on offsite damage criteria with special emphasis on damage in Las Vegas. Given the areas selected and the yield limits established, the design basis UNE was chosen as a 700-kt event at a distance of 22.8 km. This event is the largest yield at the closest practical point (from a UNE fielding point of view) in the Buckboard Mesa area of the NTS. This event results in the worst-case situation for ground motions from a UNE at Yucca Mountain.

The prediction of peak ground motions for this UNE is done with empirical equations developed for the NTS. The major assumptions made in the development of these equations are that (1) source geology is considered to be the same and (2) differences in the travel paths are ignored. These equations are based on measured ground motion from many UNEs conducted in the Pahute Mesa area of the NTS. The recording stations used were from several areas of the NTS, including a few at Yucca Mountain. Equations fitting these data were developed using standard linear

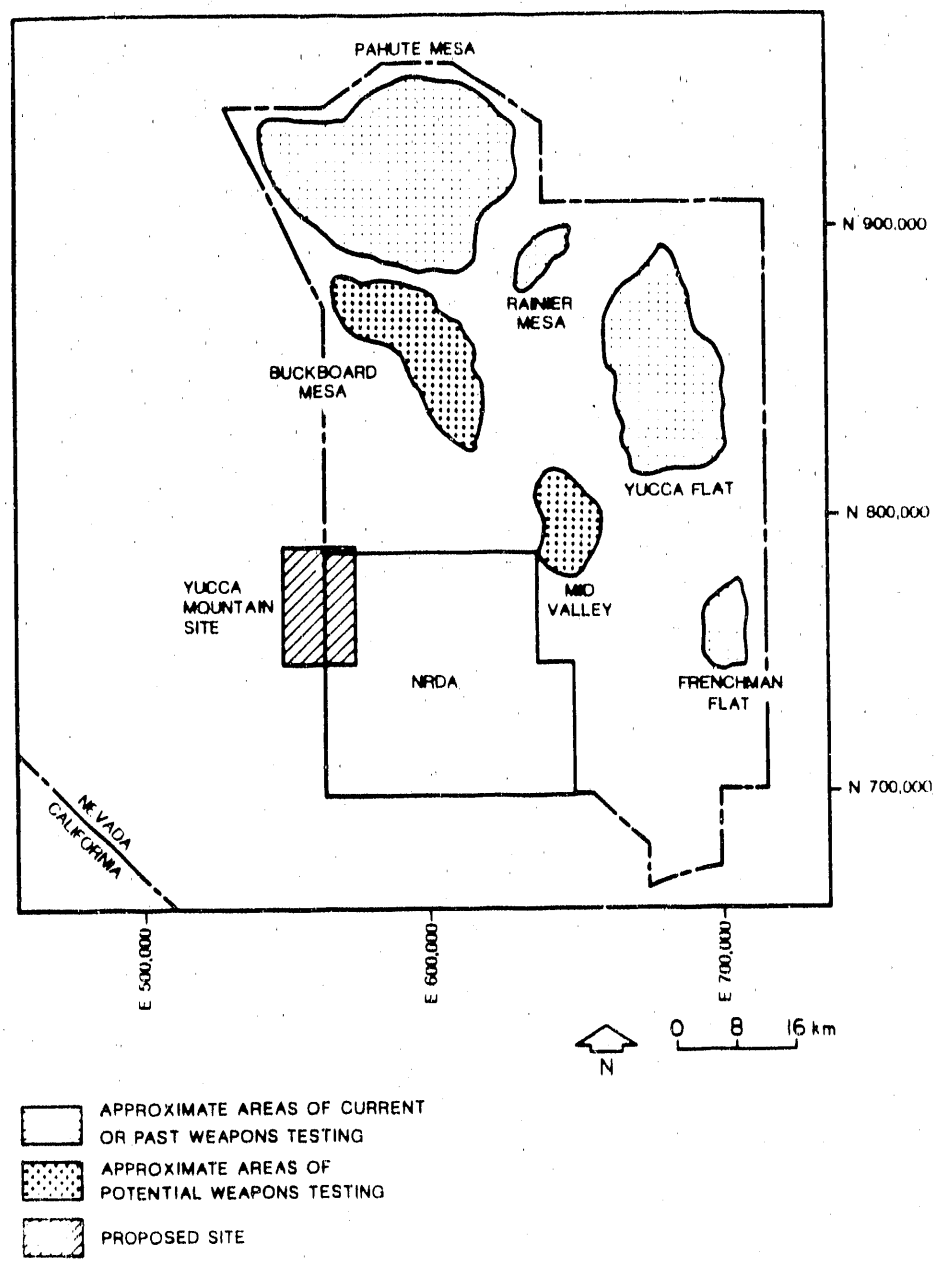

Figure 3-1. Locations of Current and Proposed Testing Areas at the NTS and the Yucca Mountain Site

regression analysis. An evaluation of the ground motion data recorded at Yucca Mountain indicated that observed ground motions were larger than foretold by the prediction equations; however, the underestimation of the ground motions was within the expected accuracy of the prediction equations (i.e., within the expected accuracy of the mean of all observations at the site). Work to be completed as part of site characterization will investigate whether ground motions in the Yucca Mountain region are larger than those in other regions of the NTS. This work will include an accurate confirmation of accelerograph recording site conditions and an assessment of the representativeness of UNE attenuation equations. To provide a conservative estimate of UNE design basis motions, the design basis UNE ground motion parameters specified are given for a nonexceedance probability level of 95% (corresponding to 1.65 times the standard deviation for a normal or lognormal distribution, which increases the most probable values by a factor ranging from 2 to 4). The mean values of the predicted ground motions and the recommended design basis values are summarized in Table 3-1. Further discussions of the prediction equations and the various references are given in Appendix A-2.

Assumptions made and conditions used in the development of the design basis UNE are listed below.

- Potential site effects at Yucca Mountain are not included in the specification of the UNE design basis motions because they are not quantified at this time.

- No attenuation of ground motion with depth will be used in the specification of design motions. This assumption is conservative because UNE ground motions are known to attenuate with depth at Yucca Mountain (Appendix A-4). This assumption, along with the use of design basis motions based on the 95% nonexceedance probability, makes the recommended values conservative and should compensate for potential site effects.

TABLE 3-1

RECOMMENDED MOTIONS FOR THE DESIGN BASIS UNE

Component	Median Predicted Value	Design Basis UNE Values [95% Nonexceedance Level (1.65σ)]
Vertical Acceleration (g)	0.05	0.2
Radial Acceleration (g)	0.03	0.1
Transverse Acceleration (g)	0.03	0.1
Vertical Velocity (cm/s)	4	9
Radial Velocity (cm/s)	4	12
Transverse Velocity (cm/s)	3	12
Vertical Displacement (cm)	1	2
Radial Displacement (cm)	1	3
Transverse Displacement (cm)	1	4

- The angle of incidence for ground motions from the UNE to the ESF is taken as ranging between 0° (vertical propagation) and 90° (horizontal propagation).

- For nearly horizontal propagation (60 to 90°), peak radial response is primarily from P waves, peak vertical response is primarily from the S_V waves, and peak transverse response is primarily from the S_h waves (Rodean, Reference 26).

The incidence angle of the ground motions from UNEs is a function of the speed with which the waves travel through a given material. At first, it may appear that each ground motion component (i.e., P, S_V, and S_h waves) could have its own incidence angle. In practice, however, the incidence

angles (Θ) for all the components are essentially the same. This similarity stems from the way in which the incidence angle is calculated. This calculation uses the change in the arrival times (Δt) of a component of a ground motion from two nearby stations, the distance (Δx) between the two stations, and the material wave speed (v); i.e., $\Theta = \sin^{-1} (\Delta tv/\Delta x)$ (Dobrin, Reference 27). For the same two stations (i.e., Δx is constant), the wave speed and Δt will change for each ground motion component. These changes will be in opposite directions (as wave speed decreases, Δt will increase). These differences will have a tendency to offset one another, causing the incidence angle calculated to be about the same for all components.

This incidence angle can vary from 0 to 90°. A preliminary survey of the UNE ground motion data recorded at Yucca Mountain from Pahute Mesa events indicates that for the P waves, the range of the incidence angle is generally between 10 and 50°. However, because the incidence angle is also a function of distance from the source and because the Yucca Mountain recordings are at distances that are a factor of two more distant from the source than the design basis UNE, there is a reasonably large amount of uncertainty in the definition of this angle for ESF design. To provide adequate conservatism, the incidence angles recommended for use in this report are between 0 and 90°.

The equations used for the prediction of UNE motions were determined from the absolute peak values recorded on the waveform. No effort was made to determine a fit for each component (P, S_V, S_h, and surface waves). In general, peak accelerations observed in UNE recordings are associated with the P wave. Peak vertical and transverse velocity may be the result of P waves or shear waves. All peak displacements are caused by the surface wave components. The design parameter of interest to the designers of the ESF is the peak particle velocity. It is assumed that the velocity corresponding to the P waves is the same as the radial component of velocity and that the velocities corresponding to the S_V and S_h waves are the same as the vertical and transverse components of velocities, respectively.

4.0 COMBINATION OF INDIVIDUAL COMPONENT WAVE EFFECTS

Newmark and Hall (Reference 28) have suggested that peak effects from the three orthogonal components of earthquake input motion be considered to be randomly phased relative to each other and thus be combined probabilistically. They then go on to suggest that a conservative and simpler approach to this probabilistic combination can be obtained by absolute vector addition of 100% of the largest peak effect from any of the three orthogonal components plus 40% of the peak effects from each of the other two components. This approach has come to be known as the 100-40-40 Combination Rule.

This same 100-40-40 Combination Rule can be used for the combination of peak effects from the individual P, S_V, and S_h component waves as long as these peak component effects can be conservatively or realistically treated as randomly phased relative to each other. Such an assumption is reasonable and slightly conservative for both earthquake and UNE control motions. This point is illustrated by the following examples.

The earthquake control motion peak particle velocities for the three orthogonal components are 30, 30, and 20 cm/sec. Using the 100-40-40 Combination Rule, the absolute addition of these three orthogonal components is given by

$$V_c = \sqrt{\left(V_1\right)^2 + (0.4)^2 \left[\left(V_2\right)^2 + \left(V_3\right)^2\right]} \quad , \tag{4-1}$$

where V_c is the combined vector sum, V_1 is the largest orthogonal component effect, and V_2 and V_3 are the other two orthogonal component effects. Using Equation 4-1, together with the three orthogonal component peak particle velocities, leads to a vector sum peak particle velocity of 33.3 cm/sec, which is 11% greater than the largest individual component peak particle velocity. Similarly, peak particle accelerations for the three orthogonal components of the earthquake control motion are each 0.3 g. Using Equation 4-1, the vector sum peak particle acceleration is

0.345 g or 15% greater than the largest individual component peak value. A review of actual earthquake records indicates that the peak vector velocities and accelerations tend to be only 4 to 12% greater than the largest orthogonal component velocities and accelerations; thus, the recommended probabilistic combination of the control motions tends to be on the conservative side for earthquakes.

Actually, this conservatism is increased somewhat by the way peak horizontal and vertical control motions are converted to peak P and S_V wave particle motions for inclined waves. For waves that are inclined 30° from the vertical, the P, S_V, and S_h peak particle velocities for the earthquake control motions become 23.1, 34.6, and 30.0 cm/sec, respectively, which leads to a vector sum peak particle velocity for Equation 4-1 of 37.8 cm/sec or 26% greater than the peak control motion particle velocity of 30.0 cm/sec. Similarly, for the 30° inclined wave case, the vector sum peak particle acceleration becomes 0.392 g, which is 31% greater than the peak control motion particle acceleration of 0.30 g. Thus, the combined effect of converting control motions to P, S_V, and S_h components and then combining these peak component effects by the 100-40-40 Combination Rule introduces significant conservatism for 30° inclined waves.

Conservatism also exists when the effects of the three defined orthogonal components of the UNE control motions are combined by the 100-40-40 Combination Rule. For example, the three orthogonal peak particle velocities defined in Table A-2.1 of Appendix A-2 are 9, 12, and 12 cm/sec; when combined by Equation 4-1, these values lead to a combined vector sum peak particle velocity of 13.4 cm/sec, which significantly exceeds the peak vector velocity of 10 cm/sec listed in Table A-2.1. Similarly, using the three orthogonal peak particle accelerations of 0.2, 0.1, and 0.1 g results in a vector sum peak particle acceleration of 0.21 g using Equation 4-1 versus the vector sum of 0.2 g shown in Table A-2.1.

5.0 DEVELOPMENT OF STRAIN TENSORS

5.1 Strain Tensors for Earthquakes

It is concluded in Appendix A-1 that body waves caused by earthquakes impinge on the shaft with steep angles of incidence, namely, steeper (less) than 30°. Further, as discussed in Section 2.3, it can be assumed that the three wave types--P, S_V, and S_h--emerge along the same ray path, that is, with the same angle of incidence and along the same azimuth.

The coordinate system consists of the z axis oriented downward along the axis of the shaft and the xy plane corresponding to the ground surface. Without loss of generalization, the wave front of each incident wave is normal to the xz plane, as illustrated in Figure 5-1, so that particle motion is either in the xz plane (for P and S_V waves) or normal to the xz plane (for S_h waves). The following notation is used in the subsequent expressions for strain:

θ = angle of incidence for P, S_V, and S_h waves,
C_p = propagation velocity of the P wave,
C_s = propagation velocity of the S_V and S_h waves,
v_p = peak particle velocity of the P wave,
v_{sv} = peak particle velocity of the S_V wave,
v_{sh} = peak particle velocity of the S_h wave,
a_p = peak acceleration of the P wave,
a_{sv} = peak acceleration of the S_V wave,
a_{sh} = peak acceleration of the S_h wave,
v_v = peak particle velocity at the ground in the vertical direction,
v_h = peak particle velocity at the ground in the horizontal direction,
a_v = peak acceleration at the ground in the vertical direction, and
a_h = peak acceleration at the ground in the horizontal direction.

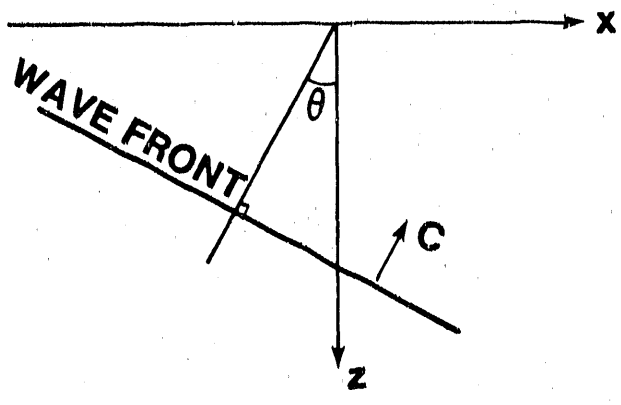

Figure 5-1. Orientation of Incident Waves with Respect to the Coordinate System

The symmetric strain tensor, $\bar{\varepsilon}$, consists of three axial strain components and three shear strain components defined as follows:

$$\bar{\varepsilon} = \begin{bmatrix} \varepsilon_{xx} & \varepsilon_{xy} & \varepsilon_{xz} \\ \varepsilon_{xy} & \varepsilon_{yy} & \varepsilon_{yz} \\ \varepsilon_{xz} & \varepsilon_{yz} & \varepsilon_{zz} \end{bmatrix} = \begin{bmatrix} \varepsilon_{xx} & \frac{1}{2}\gamma_{xy} & \frac{1}{2}\gamma_{xz} \\ \frac{1}{2}\gamma_{xy} & \varepsilon_{yy} & \frac{1}{2}\gamma_{yz} \\ \frac{1}{2}\gamma_{xz} & \frac{1}{2}\gamma_{yz} & \varepsilon_{zz} \end{bmatrix} ,$$

where

$$\varepsilon_{xx} = \frac{\partial u_x}{\partial x}$$

$$\varepsilon_{yy} = \frac{\partial u_y}{\partial y}$$

$$\varepsilon_{zz} = \frac{\partial u_z}{\partial z}$$

$$\varepsilon_{xy} = \frac{1}{2}\left(\frac{\partial u_x}{\partial y} + \frac{\partial u_y}{\partial x}\right)$$

$$\varepsilon_{xz} = \frac{1}{2}\left(\frac{\partial u_x}{\partial z} + \frac{\partial u_z}{\partial x}\right)$$

$$\varepsilon_{yz} = \frac{1}{2}\left(\frac{\partial u_y}{\partial z} + \frac{\partial u_z}{\partial y}\right)$$

u_x, u_y, u_z, = particle displacement in the x, y, and z directions, respectively.

The "engineering shear strain," denoted by γ, is defined as two times the tensor shear strain, i.e., $\gamma_{xy} = 2\varepsilon_{xy}$.

The extreme fiber-bending strain, ε_b, induced in the liner by the passage of waves is defined by

$$\varepsilon_b = R \cdot \kappa \quad ,$$

where

R = radius of the liner

κ = curvature of the shaft axis.

Along the ray paths, a P wave generates axial strain given by

$$\varepsilon = \frac{v_p}{C_p} \quad ,$$

while a shear wave generates pure shear strain given by

$$\gamma = \frac{v_s}{C_s} \quad .$$

Transforming these strains to the xyz-coordinate system yields the expressions for free-field strains shown in Table 5-1.

Curvature along an axis is given by the acceleration normal to the axis divided by the square of the apparent wave speed along that axis. This relationship is used to derive the expressions for bending strain, also shown in Table 5-1.

For the case of earthquakes, the particle motions in the P, S_V, and S_h waves will be controlled by the ground motion control parameters in the z, x, and y directions, respectively. Comparing the components shown in Figure 5-2a with those in Figure 5-2b, the particle velocities are given as

$$v_p = v_v/\cos\theta,$$
$$v_{sv} = v_h/\cos\theta, \text{ and}$$
$$v_{sh} = v_h.$$

The same relations hold for acceleration, where a is substituted for v. The substitution of these relations in the expressions in Table 5-1 yields the expressions in Table 5-2.

5.2 Strain Tensors for UNEs

It is not known at this time how much of the incident wave energy impinging on the shaft from a UNE will be associated with shallow incidence angles versus energy associated with steeper angles. However, it is not

TABLE 5-1

FREE-FIELD AND BENDING STRAINS FOR BODY WAVES WITH ANGLE OF INCIDENCE θ

Wave Type	Free-Field Strains						Bending Strains
	ε_{xx}	ε_{yy}	ε_{zz}	γ_{xy}	γ_{yz}	γ_{xz}	ε_b*
P	$\frac{v_p}{C_p} \sin^2 \theta$	0	$\frac{v_p}{C_p} \cos^2 \theta$	0	0	$\frac{v_p}{C_p} \sin 2\theta$	$\frac{R\, a_p}{C_p^2} \sin \theta \cos^2 \theta$ (in xz-plane)
S_v	$\frac{v_{sv}}{C_s} \sin \theta \cos \theta$	0	$\frac{v_{sv}}{C_s} \sin \theta \cos \theta$	0	0	$\frac{v_{sv}}{C_s} \cos 2\theta$	$\frac{R\, a_{sv}}{C_s^2} \cos^3 \theta$ (in xz plane)
S_h	0	0	0	$\frac{v_{sh}}{C_s} \sin \theta$	$\frac{v_{sh}}{C_s} \cos \theta$	0	$\frac{R\, a_{sh}}{C_s^2} \cos^2 \theta$ (in yz plane)

*ε_b = extreme fiber-bending strain.

TABLE 5-2

FREE-FIELD AND BENDING STRAINS IN TERMS OF GROUND MOTION CONTROL PARAMETERS FOR EARTHQUAKES

Wave Type	Free-Field Strains						Bending Strains
	ε_{xx}	ε_{yy}	ε_{zz}	γ_{xy}	γ_{yz}	γ_{xz}	ε_b
P	$\frac{v_v}{c_p}\frac{\sin^2\theta}{\cos\theta}$	0	$\frac{v_v}{c_p}\cos\theta$	0	0	$\frac{v_v}{c_p}2\sin\theta$	$\frac{R\,a_v}{c_p^2}\sin\theta\cos\theta$ (in xz plane)
S_v	$\frac{v_h}{c_s}\sin\theta$	0	$\frac{v_h}{c_s}\sin\theta$	0	0	$\frac{v_h}{c_s}\frac{\cos 2\theta}{\cos\theta}$	$\frac{R\,a_h}{c_s^2}\cos^2\theta$ (in xz plane)
S_h	0	0	0	$\frac{v_h}{c_s}\sin\theta$	$\frac{v_h}{c_s}\cos\theta$	0	$\frac{R\,a_h}{c_s^2}\cos^2\theta$ (in yz plane)

Note: These expressions are valid only for steeply emerging body waves, i.e., $\theta = 30°$ or less.

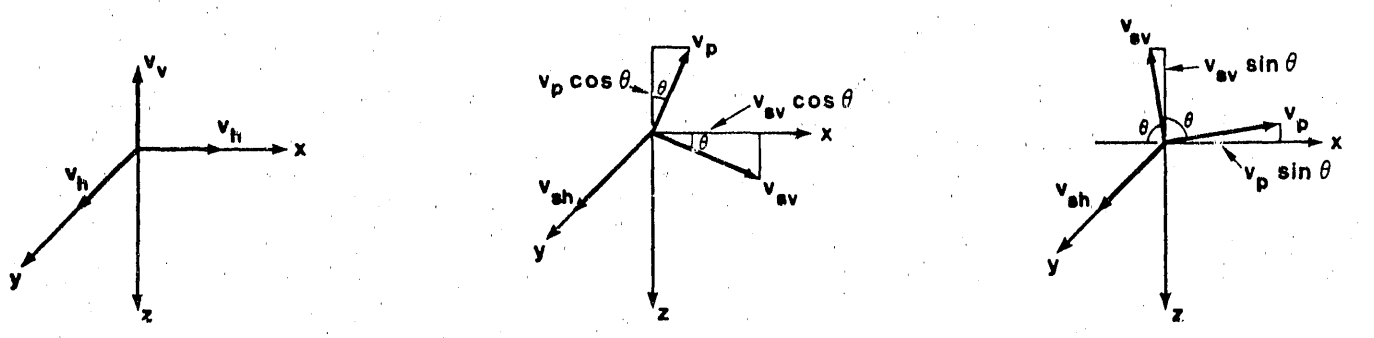

(a) DIRECTION OF CONTROL PARAMETERS (REPRESENTED BY PEAK GROUND MOTION VELOCITIES)

(b) DIRECTION OF PARTICLE MOTIONS IN STEEPLY EMERGING WAVES (REPRESENTED BY PARTICLE VELOCITY)

(c) DIRECTION OF PARTICLE MOTIONS IN SHALLOW EMERGING WAVES (REPRESENTED BY PARTICLE VELOCITY)

Figure 5-2. Relationship Between Peak Ground Motion Control Parameters and Particle Motions Caused by Each Wave Type.

necessary to know the distribution of the incident wave energy with incidence angle because the strains caused by earthquakes will be an upper bound on the strains caused by UNEs, as demonstrated in Section 5.3.

The maximum strains generated by earthquake waves emerging with Θ between 0 and 30° are compared with the maximum strains caused by UNE waves emerging with Θ between 0 and 90°. The strains caused by steeply emerging waves (i.e., between Θ = 0 and 30°), whether generated by earthquakes or UNEs, are computed from the expressions in Table 5-2. New expressions are derived for shallow emerging waves (i.e., between Θ = 60 and 90°).

For UNE waves emerging at shallow angles (Θ = 60 to 90°), P, S_V, and S_h waves will be controlled by the ground motion control parameters in the x, z, and y directions, respectively. Comparing Figures 5-1a and 5-2c, the particle velocities are given as (for shallow emerging waves)

$$v_p = v_h/\sin\Theta,$$
$$v_{sv} = v_v/\sin\Theta, \text{ and}$$
$$v_{sh} = v_h.$$

The same relations hold for acceleration, where a is substituted for v. Substitution of these relations in the expressions in Table 5-1 yields the expressions in Table 5-3.

5.3 Controlling Strain Combinations Caused by Earthquakes and UNEs

For the design basis parameters recommended in Sections 2 and 3 for earthquakes and UNEs, it can be shown (Appendix A-3) that, of all the various incidence angles (0 to 30° for earthquakes and 0 to 90° for UNEs) that need to be evaluated for design, with three possible combinations of P, S_V, and S_h waves, only one case controls all aspects of the shaft design:

- earthquake control motion,
- 30° incidence angle, and
- 100% S_V peak effects plus 40% P and S_h peak effects (using the probabilistic Combination Rule 100-40-40).

Both hoop stress or strain and total axial strain are controlled by earthquake waves emerging at an angle of 30° from the vertical. For the specified design basis motions, UNEs will never control the design; hence, it is recommended that the designer use only the above combination for design evaluation of the ESF.

TABLE 5-3

FREE-FIELD AND BENDING STRAINS IN TERMS OF GROUND MOTION CONTROL PARAMETERS FOR BODY WAVES WITH SHALLOW ANGLES OF INCIDENCE

Wave Type	Free-Field Strains						Bending Strains
	ε_{xx}	ε_{yy}	ε_{zz}	γ_{xy}	γ_{yz}	γ_{xz}	ε_b
P	$\frac{v_h}{C_p} \sin\theta$	0	$\frac{v_h}{C_p} \frac{\cos^2\theta}{\sin\theta}$	0	0	$\frac{v_h}{C_p} 2\cos\theta$	$\frac{R\, a_h}{C_p^2} \cos^2\theta$ (in xz plane)
S_v	$\frac{v_v}{C_s} \cos\theta$	0	$\frac{v_v}{C_s} \cos\theta$	0	0	$\frac{v_v}{C_s} \frac{\cos 2\theta}{\sin\theta}$	$\frac{R\, a_v}{C_s^2} \frac{\cos^3\theta}{\sin\theta}$ (in xz plane)
S_h	0	0	0	$\frac{v_h}{C_s} \sin\theta$	$\frac{v_h}{C_s} \cos\theta$	0	$\frac{R\, a_h}{C_s^2} \cos^2\theta$ (in yz plane)

Note: These expressions are valid for θ between 60 and 90°.

6.0 DYNAMIC ROCK PROPERTIES

This section describes the procedure used to determine dynamic rock properties for use in analyses of underground openings at the ESF when subjected to transient free-field strains caused either by earthquakes or UNEs. The properties important to such analyses are

velocity of compression waves, C_p;
velocity of shear waves, C_s;
dynamic deformation modulus, E_d; and
dynamic Poisson's ratio, ν_d.

These properties should be determined for each rock unit in which underground openings are located. Analyses of the openings for transient free-field strains, based on the ground support relative to rock mass stiffness, must use the corresponding dynamic material properties. Static loadings may be analyzed independently, using static material properties, and the result may be superimposed over the results of the dynamic analyses.

Figure 6-1 illustrates the stratigraphy of the borehole nearest the ESF site (USW G-4), and includes plots of the measured in situ P-wave velocities, as presented by Spengler et al. in Reference 29, and of the measured laboratory P-wave velocities, as presented by Anderson in Reference 30. The plot of in situ values also shows a smooth curve that represents the average of the measured values over each identified rock unit. The remaining plots on this figure represent the recommended P-wave and S-wave velocities as determined by the evaluation described herein.

The most recent Reference Information Base (RIB) for the Nevada Nuclear Waste Storage Investigations (YMP) Project (Reference 31) recommends the rock mass bulk densities, rock mass Poisson's ratios, and intact Poisson's ratios given in Table 6-1.

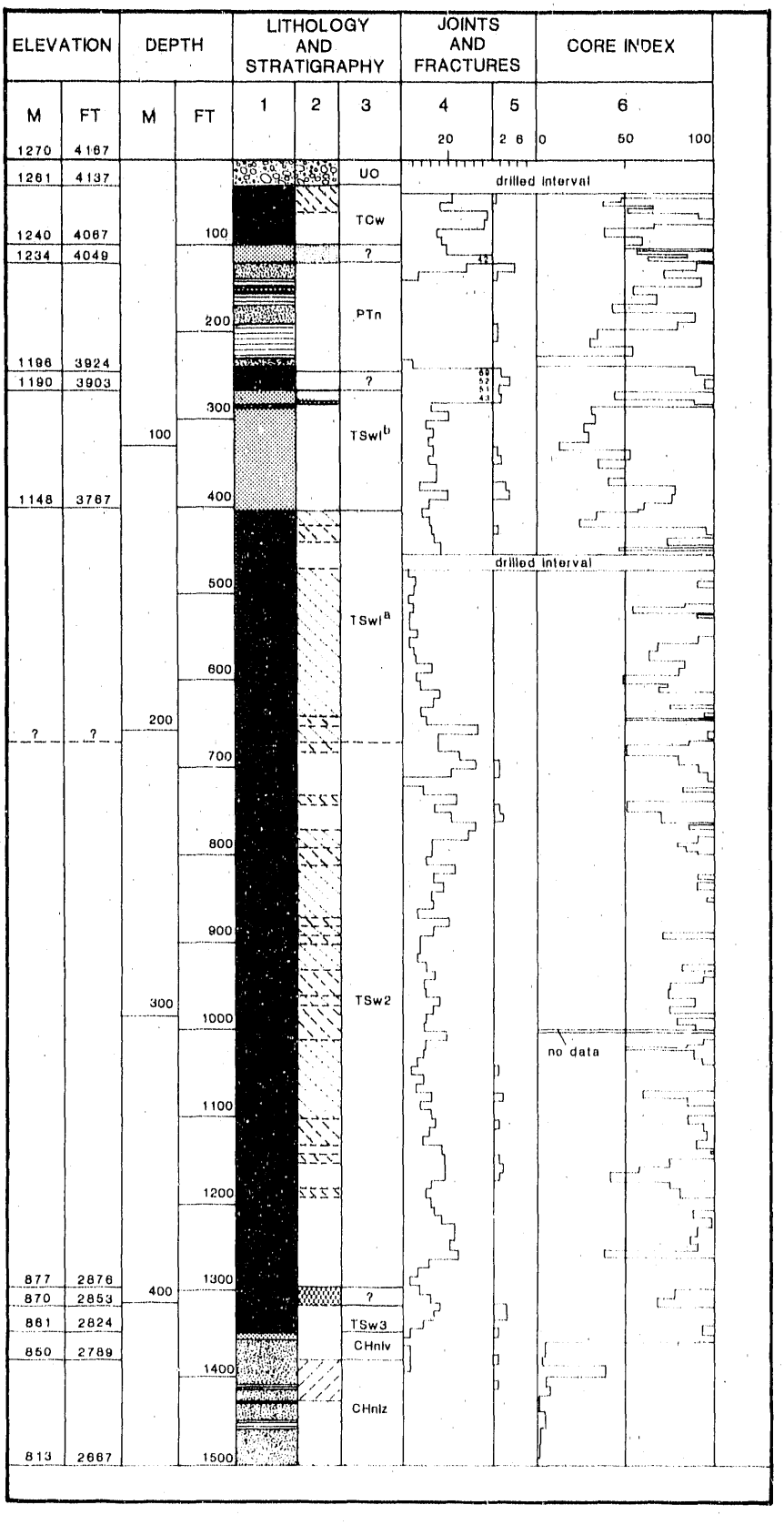

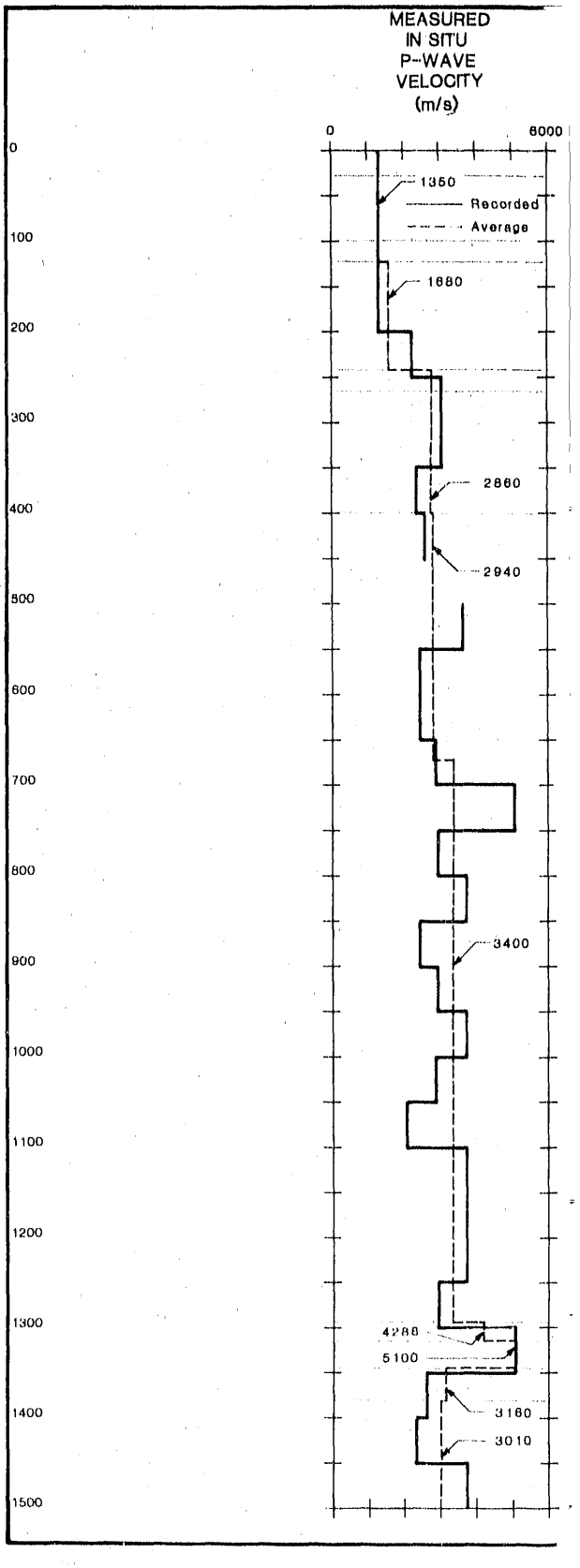

NOTES.

1.) Lithology, joint planes, shear fractures, core index, and measured in situ P-wave velocity are all taken from USGS-OFR-84-789 for USW G-4 boring.

2.) Measured laboratory P-wave velocity is taken from USGS-OFR-84-552.

3.) Reliable recommendations for the seismic velocities of the TCw unit can not be made from the available measurements. However, the seismic velocities of the PT unit represent a lower bound to the TCw unit values.

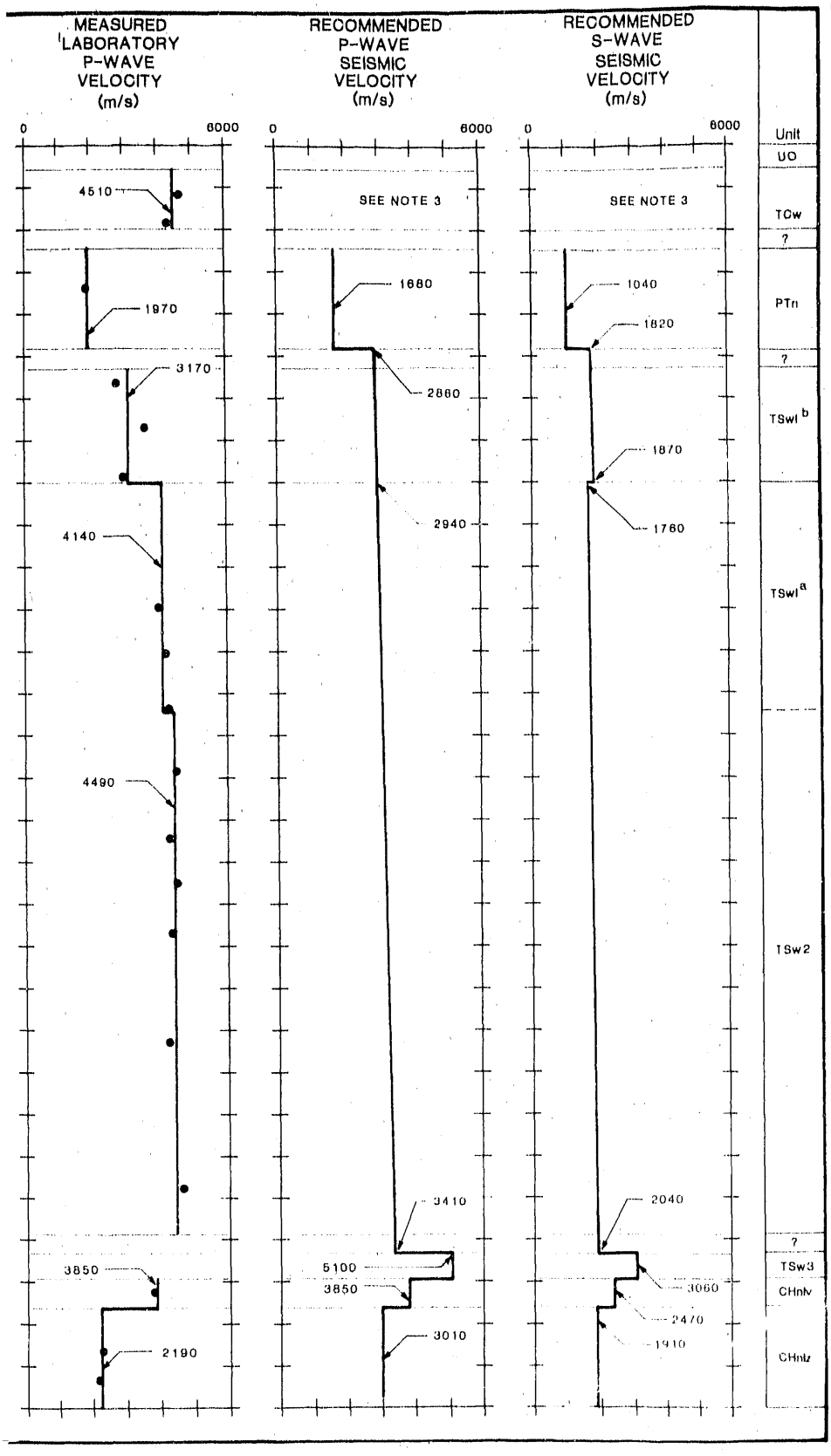

LEGEND

(1) Welded and bedded zones

Densely welded; Moderately welded; Non-to partially welded; Vitrophyre; Bedded; Alluvium

(2) Crystallized and altered zones

Vitric; Vapor phase; Devitrified; Lithophysal (devitrified) — Sparse, Abundant; Devitrified (slightly argillic); Zeolitized and argillic; Zeolitized upper--slightly lower--moderately

(3) Stratigraphic units

UNIT	Lithology
TCw	Densely welded devitrified tuff
PTn	Non welded, vitric tuff
TSwl [b]	Moderately welded, vapor phase tuff
TSwl [a]	Densely welded, devitrified, lithophysal rich tuff
TSw2	Densely welded, devitrified, lithophysal poor tuff
TSw3	Vitrophyre tuff
CHnlv	Non welded, vitric tuff
CHnlz	Partially welded, zeolitized tuff

(4) Joint planes

0 20

Number of measured joint planes per 10-foot interval

(5) Shear fractures

0 6

Number of fracture planes per 10-foot interval along which differential movement was recognized

(6) Core index

$$\text{Core index} = \frac{(\text{ft broken}) + (\text{ft core loss}) + (1/3\ \text{joints})}{(\text{drilled interval, ft})} \times 100$$

FIGURE 6-1

Interpretation of Seismic Velocities From USW-G4 Data

TABLE 6-1

REFERENCE INFORMATION BASE DATA FOR BULK DENSITY, POISSON'S RATIO FOR ROCK MASS, AND POISSON'S RATIO FOR INTACT ROCK

Rock Unit	Bulk Density (g/cm^3)	Poisson's Ratio for Rock Mass	Poisson's Ratio for Intact Rock
TCw	2.31	0.10	0.24
PTn	1.58	0.19	0.16
TSw1[a]	1.84[b]	0.16	0.16
TSw1[c]	2.25	0.22	0.25
TSw2	2.32	0.22	0.24
TSw3	2.32	0.22[b]	0.24[b]
CHn1v	1.82	0.15	0.16
CHn1z	1.92	0.16	0.16

a. Lithophysal rich, vapor phase.
b. Value shown is assumed; RIB indicates that value is not available.
c. Lithophysal rich, devitrified.

The S-wave velocity (C_s) and the dynamic deformation modulus (E_d) can be determined from the bulk density (D), dynamic Poisson's ratio (v_d), and P-wave velocity (C_p) by the following elastic relationships:

$$C_s = C_p[(1 - 2v_d)/(2 - 2v_d)]^{0.5} \quad \text{and}$$

$$E_d = DC_p^2(1 + v_d)(1 - 2v_d)/(1 - v_d) \quad .$$

Based on current, relatively limited data on rock properties, it is recommended that the rock mass Poisson's ratio, as given in the RIB, be used as the dynamic Poisson's ratio and that the bulk density at in situ saturation, as given in the RIB, be used.

The recommended P-wave velocities were determined as described below.

TCw

The in situ measurements differ significantly from the laboratory values. It is not possible to resolve this conflict with the data currently available. Therefore, the only recommendation provided for this unit is that the P-wave velocity of the underlying PTn unit represents a reasonable lower bound to the P-wave velocity of the TCw unit (i.e., PTn values are conservative for the TCw unit).

PTn

The average of the in situ measurements over this unit is approximately 85% of the single laboratory measurement. This is considered to be a very reasonable correlation, and the recommended P-wave velocity is specified as the average of the in situ measurements and equal to 1,680 m/sec.

$TSw1^a$, $TSw1^b$, and TSw2

The average of the in situ measurements over each of these units varies between 75 and 90% of the corresponding laboratory measurements. As with the PTn unit, the relative magnitude of the average in situ measurements, as compared with the laboratory measurements, is reasonable. Both sets of measurements indicate a slight increase in P-wave velocity with depth. Therefore, the recommended P-wave velocity is specified as a linear variation between the average in situ measurement for the $TSw1^a$ unit (2,860 m/sec) at the top of the $TSw1^a$ unit to the average in situ measurement for the TSw2 unit (3,400 m/sec) at the bottom of the TSw2 unit. This linear variation is further extended through the unnamed transition layer between the TSw2 and TSw3 units.

TSw3

There are no laboratory P-wave velocity measurements in the TSw3 material to use as confirmation of the in situ measurements. In addition, the thickness of the unit is less than the interval tested in situ; thus,

the in situ measurement may be biased. Because the measured in situ value of P-wave velocity is the fastest recorded in the rock units of interest, it seems reasonable to assume that the actual unit velocity is greater than the recorded value. Therefore, the average in situ P-wave velocity measurement (5,100 m/sec) for the TSw3 unit is recommended as a conservative value.

CHn1v

The in situ measurement for this unit differs significantly from the single laboratory value. The in situ measurements of P-wave velocity for this thin unit appear to be biased by the underlying CHn1z unit. In lieu of better data, a value equal to the laboratory measurement (3,850 m/sec) is recommended.

CHn1z

The average in situ measurement for this unit is greater than the laboratory measurements. It seems reasonable that this nonwelded material is very sensitive to disturbance and/or confining pressure. Therefore, the average of in situ P-wave velocity (3,010 m/sec) is recommended.

Applying the aforementioned equations for S-wave velocity and dynamic deformation modulus to the recommended P-wave velocities and summarizing the dynamic properties at the base of each unit yields the results given in Table 6-1.

As indicated earlier, these recommended properties are based on currently available but limited site data, which have significant uncertainties. Hence, the WG recommends that additional data be obtained from the site at the earliest opportunity to supplement and confirm the available data and recommended properties.

7.0 FAULTING CONSIDERATIONS

7.1 Objectives

Several faults have been identified in the area of Yucca Mountain that show evidence of movement during the Quaternary period; hence, the possibility of faulting at the ESF location and vicinity must be considered. None of the known faults with evidence of Quaternary movement intersects the ESF. The potential hazard of a fault that may have thus far gone undetected can be assessed and bounded within reasonable limits. This assessment requires consideration of what is currently known about the characteristics of faulting in the surrounding area, including uncertainties. Consideration of the potential impact of faulting on the ESF provides a basis for assessing the relevance of possible undetected faults.

As discussed in Section 1, the ESF shafts will not at any time be used to transport any high-level waste materials. During repository operations, the ESF shafts will be converted to serve as ventilation supply shafts. Exhausting fans on the emplacement area exhaust shaft will at all times maintain negative pressure in the emplacement area relative to the pressure in the development area, which is ventilated with forced ventilation; hence, there is no potential for the ESF shafts to become exhaust shafts rather than intake shafts. Based on these discussions, any fault displacement through the ESF does not appear to affect public safety, nor does it seem to be a serious threat to operations or worker safety unless the fault offsets are significant. Fault displacements in excess of about 5 cm could possibly pose a threat to workers' safety during ESF operations.

The faulting hazard does not merit special design, provided there is reasonable assurance that fault displacement in excess of 5 cm is not likely to occur during the preclosure period. Limiting the possibility to less than one chance in 10 during the preclosure period is judged to be adequate to provide such an assurance. However, because of uncertainties in current understanding of how the ESF would perform if subjected to significant fault displacement and because of uncertainties in current

understanding of the local tectonic conditions, the measure for adequate assurance is made more stringent by an additional factor of 10. Accordingly, faulting hazards need not be considered in the design of the ESF (which has a 100-yr maintainable design life) if the annual probability for exceeding 5 cm of displacement is no greater than 10^{-4}/yr. The characteristics of a fault that might pose a hazard can then be expressed as one that has moved during the Quaternary or late Quaternary at an average rate > 5 cm/10,000 yr (0.005 mm/yr).

7.2 Faulting Potential

Evidence of Quaternary displacement has not been identified on any fault that intersects the ESF or the underground waste disposal area. Except for the Ghost Dance Fault, recognized offsets of faults within the repository block do not exceed 5 m (DOE, Reference 10, pp. 1-127). The Ghost Dance Fault, which intersects the repository block but not the ESF, displaces Tertiary tuff units by 38 m and has a mapped length of 6 km (DOE, Reference 10). Although evidence for movement on this fault during the Quaternary period has not been identified, the possibility cannot be ruled out from available data. However, it appears unlikely that repeated movements during the late Quaternary could have gone undetected.

The Ghost Dance Fault is an obvious geologic feature, yet its potential for movement appears to be insignificant as compared with the faulting characteristics identified in Section 7.1 to be of primary concern in designing the ESF. Although the more significant faults that bound Yucca Mountain to the east and west do not intersect the ESF, their rates of movement are closer to the threshold of concern for the ESF. The Paintbrush Canyon Fault appears to have the highest average rate of displacement during the late Quaternary, about 0.006 mm/yr (DOE, Reference 10, Table 1-8). The average rate of late Quaternary displacement for the Windy Wash Fault is estimated to be about 0.0015 mm/yr. Because these mapped faults displace Tertiary tuff units by 200 m or more (DOE, Reference 10, Table 1-8), similar faults in the proximity of the ESF could have easily been detected.

7.3 Design Basis Faulting

No faults with evidence of Quaternary movement have been found in the immediate area of the ESF or in the larger area of the repository block. More distant faults, which bound Yucca Mountain along the east and west flanks, have moved repeatedly during the Quaternary period. Significant movement on these faults appears unlikely during a typical 100-yr period, and sympathetic displacement in excess of a few centimeters through the shaft is an unlikely response to a local earthquake. The annual probability that faulting in excess of a few centimeters will occur in the ESF shafts is judged to be well below 10^{-4}/yr. Therefore, faulting need not be considered in the design of the ESF.

8.0 REFERENCES

1. DOE (U.S. Department of Energy)(1986), "Generic Requirements for a Mined Geologic Disposal System," Office of Civilian Waste Management, Washington, DC. (NNA.870605.0001)

2. Uniform Building Code (1988 edition), International Conference of Building Officials, Whittier, CA. (NNA.890713.0164)

3. SNL (Sandia National Laboratories) (September 1987), "Site Characterization Plan Conceptual Design Report," SAND84-2641, Sandia National Laboratories, Albuquerque, NM. (NNI.88092.0014-.0019)

4. DOE (U.S. Department of Energy), DOE 6430.1, "United States Department of Energy's General Criteria Manual," Washington, DC. (HQS.880517.2268)

5. ATC (Applied Technology Council) (1978), ATC-3-06, "Tentative Provisions for the Development of Seismic Regulations for Buildings; a cooperative effort with the design professions, building code interests, and the research community," Structural Engineers Association of California, U.S. Bureau of Standards Special Publ. 510, Palo Alto, CA. (NNA.891109.0122)

6. Carr, W. J. (1984), "Regional Structural Setting of Yucca Mountain, Southwestern Nevada, and Late Cenozoic Rates of Tectonic Activity in Part of the Southwestern Great Basin, Nevada and California," USGS OFR-84-0854, U.S. Geological Survey, Denver, CO. (HQS.880517.2634)

7. Slemmons, D. B. (1982), "Determination of Design Earthquake Magnitudes for Microzonation," Proc. of 3rd International Earthquake Microzonation Conference, June 28-July 1, 1982, Seattle, WA, pp. 119-130. (NNA.890713.0188)

8. Whitney, J. W., Shroba, R. R., Simonds, F. W., and Harding, S. T. (1986), "Recurrent Quaternary Movement on the Windy Wash Fault," Nye County, Nevada, [abs.] Geol. Soc. Am., Abstracts with Programs, p. 787. (HQS.880517.1572)

9. Pratt, H. R., Hustrulid, W. A., and Stephenson, D. E. (November 1978), "Earthquake Damage to Underground Facilities," DP-1513, E. I. du Pont de Nemours & Co., Aiken, SC. (HQS.880517.1387)

10. DOE (U.S. Department of Energy) (January 1988), "Site Characterization Plan, Consultation Draft, Yucca Mountain Site, Nevada Research and Development Area, Nevada," Office of Civilian Radioactive Waste Management, Washington, DC. (HQS.881201.0002)

11. URS/John A. Blume & Associates (September 1987), "Technical Basis and Parametric Study of Ground Motion and Surface Rupture Hazard Evaluations at Yucca Mountain, Nevada," SAND86-7013, Sandia National Laboratories, Albuquerque, NM. (HQS.880517.2893)

12. Perkins, D. M., Thenhaus, P. C., Hanson, S. L., and Algermissen, S. T. (1986), "A Reconnaissance Assessment of Probabilistic Earthquake Accelerations at the Nevada Test Site," USGS-OFR-87-199, U.S. Geologic Survey, Denver, CO. (HQS.880517.1381)

13. Campbell, K. W. (1985), "Strong Ground Motion Attenuation Relations: A Ten-Year Perspective," Earthquake Spectra, 1:4, pp. 759-804. (NNA.890714.0072)

14. Joyner, W. B., and Fumal, T. E. (1985), "Predictive Mapping of Earthquake Ground Motion," Ziony, J. I., ed., Evaluating Earthquake Hazards in the Los Angeles Region--An Earth-Science Perspective, USGS PP-1360, U.S. Geological Survey, pp. 203-220. (NNA.891107.0108)

15. Campbell, K. W. (1987), "Predicting Strong Ground Motion in Utah," Hays, W. W., and Gori, P. L., eds., Assessment of Regional Earthquake Hazards and Risk Along the Wasatch Front, Utah, USGS OFR-87-0585, U.S. Geological Survey, Denver, CO, pp. L1-L90. (NNA.890829.0270)

16. Shakal, A. F., Huang, M. J., Parke, D. L., and Sherburne, R. W. (1986), "Processed Data from the Strong-Motion Records of the Morgan Hill Earthquake of 24 April 1984," Report No. OSMS 85-04, Calif. Div. Mines and Geology. (NNA.890808.0109)

17. Huang, M. J., Parke, D. L., Sherburne, R. W., and Shakeal, A. F. (1987), "Processed Strong Motion Data from the Palm Springs Earthquake of 8 July 1986," Report No. OSMS 87-01, Calif. Div. Mines and Geology. (NNA.900403.0378)

18. Bath, M. (1979), Introduction to Seismology, Birkhauser Verlag, Basel, Switzerland. (NNA.900502.0052)

19. Jeffreys, H., and Bullen, K. E. (1958), "Seismological Tables," British Association for the Advancement of Science, London, England. (NNA.890713.0160)

20. McGarr, A. (1984), "Scaling of Ground Motion Parameters, State of Stress, and Focal Depth," Jour. Geophys. Res., 898, pp. 6969-6979. (NNA.890713.0183)

21. Singh, J. P. (1985), "Earthquake Ground Motions: Implications for Designing Structures and Reconciling Structural Damage," Earthquake Spectra, Vol. 1, No. 2, pp. 239-270. (NNA.890713.0220)

22. Smith, R. B., and Richins, W. D. (1984), "Seismicity and Earthquake Hazards of Utah and the Wasatch Front: Paradigm and Paradox," Hays, W. W., and Gori, P. L., eds. USGS-OFR-84-0763, Proc. of Conf. XXVI, A Workshop on Evaluation of the Regional and Urban Earthquake Hazards and Risk in Utah. (NNA.890906.0172)

23. Rogers, A. M., Harmsen, S. C., Herrmann, R. B., and Meremonte, M. E. (1987), "A Study of Ground Motion Attenuation in the Southern Great Basin, Nevada-California, using Several Techniques for Estimates of Q_S, Log A_0, and Coda Q," Journ. Geophys. Res., 92:5, pp. 3527-3540. (NNA.890713.0184)

24. Campbell, K. W. (1981), "Near-Source Attenuation of Peak Horizontal Acceleration," Bull. Seism. Soc. Am., 71:6, pp. 2039-2070. (HQS.880517.1109)

25. Vortman, L. J. (April 1980), "Prediction of Ground Motion From Underground Nuclear Weapons Tests as It Relates to Siting of a Nuclear Waste Storage Facility at NTS and Compatibility with the Weapons Test Program," SAND80-1020/1, Sandia National Laboratories, Albuquerque, NM. (HQS.880517.2895)

26. Rodean, H. C. (1971), "Nuclear Explosion Seismology," AEC Critical Review Series Publications, Lawrence Livermore National Laboratory, University of California, Livermore, CA. (NNA.891107.0120)

27. Dobrin, M. B. (1976), Introduction to Geophysical Prospecting, Third Edition, McGraw-Hill, Inc. (NNA.890713.0200)

28. Newmark, N. M., and Hall, W. J. (May 1978), "Development of Criteria for Seismic Review of Selected Nuclear Power Plants," NUREG/CR-0098, U.S. Nuclear Regulatory Commission, Washington, DC. (NNA.890327.0045)

29. Spengler, R. W., Chornack, M. P., Muller, D. C., and Kibler, J. E. (1984), "Stratigraphic and Structural Characteristics of Volcanic Rocks in Core Hole USW G-4, Yucca Mountain, Nye County, Nevada," USGS-OFR-84-0789, U.S. Geological Survey, Denver, CO. (NNA.870323.0196)

30. Anderson, L. A. (1984), "Rock Property Measurements on Large-Volume Core Samples from Yucca Mountain USW GU-3/G-3 and USW G-4 Boreholes, Nevada Test Site, Nevada," USGS-OFR-84-552, U.S. Geological Survey, Denver, CO. (NNA.870323.0195)

31. DOE (U.S. Department of Energy) (December 1987), "Yucca Mountain Project Reference Information Base," Version 03.001, Office of Civilian Radioactive Waste Management, Las Vegas, NV. (NNA.880105.0023)

APPENDIX A-1

INCIDENCE ANGLE OF SEISMIC BODY WAVES

Strong ground shaking is primarily the result of seismic body waves that propagate through the earth along ray paths. The ray paths curve or refract in response to gradual or abrupt changes in material velocity. As illustrated in Figure A-1.1, the inherent velocity of materials in the earth generally increases with depth, which causes the ray paths for emerging seismic waves to steepen as they approach the earth's surface. The curvature of ray paths is explained by Snell's Law, which requires a constant phase velocity in directions that are parallel to the interface of two different materials as waves pass from one material to the other. Snell's Law is used to examine the range of incidence angles to be expected at the ESF from local earthquakes.

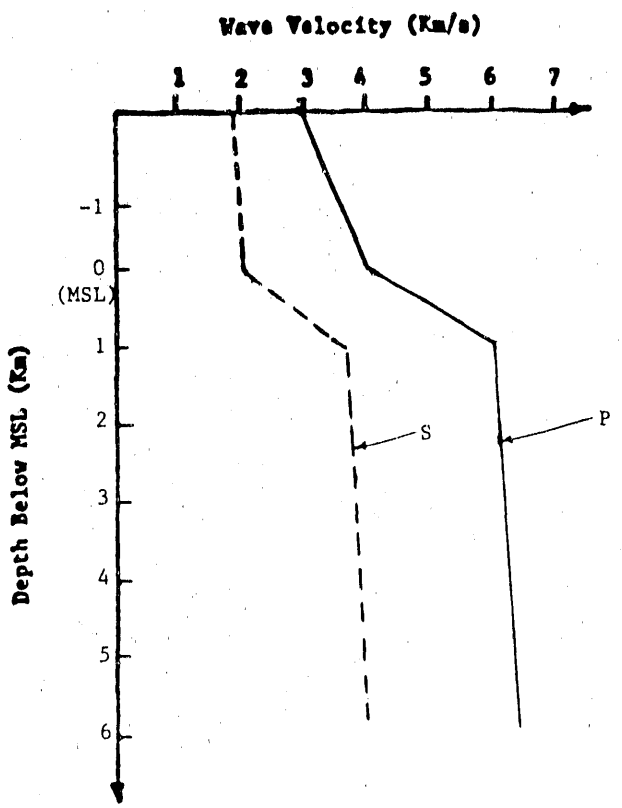

Figure A-1.1. Approximate Velocity Structure for the Southern Great Basin [after Rogers et al., Reference A-1-1].

A-1.1 Earth Properties

The velocity structure in the Great Basin increases rather dramatically with depth (Figure A-1.1). The average P- and S-wave velocities for the Tertiary tuff units at Yucca Mountain are about 3 km/sec and 1.8 km/sec, respectively (Section 6). At a depth of about 3 km below mean sea level, the respective values have increased to about 6.15 km/sec and 3.6 km/sec (Rogers et al., Reference A-1-1).

This increase of a factor of two or more in the velocity of rock with depth is indicative of significant increases in the stiffness and strength properties of rock with depth. The capacity of rock to support large tectonic stresses also increases with depth, at least to a depth of several kilometers. Consequently, the earthquake rupture of most importance to ground motion hazards originates at a depth of a few kilometers or more. Also, the relatively large stiffness and strength properties of rock at these depths are required to efficiently transmit the largest-amplitude waves away from the immediate source area.

A-1.2 Incidence Angle

A local earthquake of unspecified location is postulated for estimating the range of incidence angles that would be expected for the largest-amplitude body waves. As illustrated in Figure A-1.2, the analysis uses the following notation:

v_s = velocity of rock at the source depth responsible for the largest-amplitude waves;

v_{ESF} = velocity of rock at the ESF (approximately $\simeq 1/2\ v_s$);

θ_s = takeoff angle at the source, measured from vertical, for body waves enroute to the ESF; and

θ_{ESF} = incidence angle at the ESF, measured from vertical.

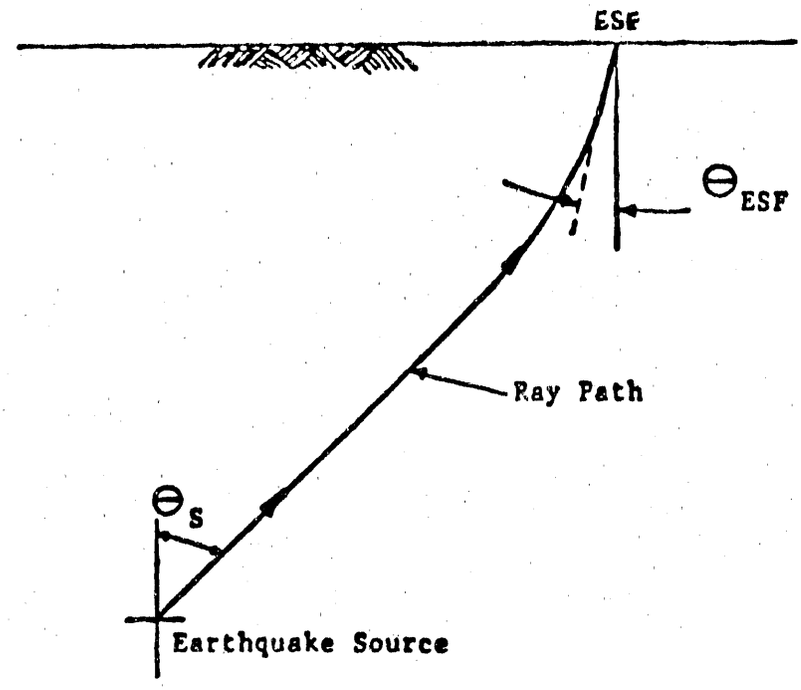

Figure A-1.2. Depiction of the Ray Path Along Which the Largest-Amplitude Waves from a Potential Earthquake Source May Emerge at the ESF

The largest variations in velocity occur with depth. For simplicity, the earth is assumed to comprise horizontal layers of homogeneous material, i.e., vertically stratified. Repetitious application of Snell's Law to ray paths passing from one layer to the next indicates that the horizontal phase velocity would be constant along the entire ray path (Richter, Reference A-1-2). Equating the horizontal phase velocity for waves transmitted at the source with those emerging at the ESF location gives

$$\frac{v_s}{\sin \Theta_S} = \frac{v_{ESF}}{\sin \Theta_{ESF}} \quad .$$

The incidence angle at the ESF is then obtained from

$$\sin \Theta_{ESF} = \frac{v_{ESF}}{v_s} \sin \Theta_S \leq 1/2 \quad ,$$

assuming that $v_s \simeq 2\ v_{ESF}$ for both P and S waves at the source depth responsible for the predominant earthquake waves. Thus, the

largest-amplitude body waves are expected to emerge at the ESF at an angle steeper than about 30° from vertical. Intervening heterogeneities and alternate wave paths are not expected to significantly alter this conclusion.

A-1.3 References

A-1-1. Rogers, A. M., S. C. Harmsen, W. J. Carr, and W. Spence (1983), "Southern Great Basin Seismological Data Report for 1981 and Preliminary Data Analysis," USGS OFR-83-0669, U.S. Geological Survey, Denver, CO.

A-1-2. Richter, C. F. (1958), Elementary Seismology, W. H. Freeman and Company, San Francisco, CA.

APPENDIX A-2

DISCUSSION OF THE PREDICTION OF UNE GROUND MOTIONS

This appendix summarizes background information concerning the prediction equations given in Table A-2.1 and used for the prediction of UNE ground motions. In this table, the mean values shown are calculated for a 700 kt shot at 22.8 km distance. The background information includes discussions of how the design basis UNE was selected, the data used in the development of the equations (including the rationale used in the analysis of the data and the recommended prediction equations), and a brief discussion of wave propagation from a UNE. Additional detail on the development of the prediction equations may be found in Reference A-2-1, Long (draft),* and Phillips (draft).**

A-2.1 Selection of the Design Basis UNE

The locations of present and proposed testing areas are shown in Figure 3-1. Testing areas in current use are those at Pahute Mesa, Rainier Mesa, and Yucca Flats. Possible future sites have been defined (Fernald, Reference A-2-2) because they are required in the event that existing sites are consumed. The two possible future sites of concern are the Buckboard Mesa area and Mid Valley.

The upper limits on yield for each of the testing areas have been defined based on offsite damage. Special emphasis has been placed on potential damage in Las Vegas. These limits are

---

* J.W. Long, "Component Ground Motion at the Nevada Test Site from Pahute Mesa Underground Nuclear Explosions," SAND86-0439, Sandia National Laboratories, Albuquerque, NM, draft.

**J.S. Phillips, "Evaluation of Equations Used for the Prediction of Peak Ground Motions at Yucca Mountain from Underground Nuclear Explosions in Pahute Mesa," SAND87-1811, Sandia National Laboratories, Albuquerque, NM, draft.

TABLE A-2.1

PREDICTION EQUATIONS FOR ACCELERATION, VELOCITY, AND DISPLACEMENT[a,b]

Component	Equation[c]	Mean Value	1.65 σ Value
Vertical Acceleration (g)	$0.487\ W^{0.491}\ R^{-1.792}$	0.05	0.2
Radial Acceleration (g)	$0.239\ W^{0.382}\ R^{-1.425}$	0.03	0.1
Trans. Acceleration (g)	$0.246\ W^{0.326}\ R^{-1.371}$	0.03	0.1
Vector Acceleration (g)	$0.511\ W^{0.482}\ R^{-1.717}$	0.06	0.2
Vertical Velocity (cm/s)	$8.390\ W^{0.679}\ R^{-1.584}$	4	9
Radial Velocity (cm/s)	$6.861\ W^{0.544}\ R^{-1.352}$	4	12
Trans. Velocity (cm/s)	$5.873\ W^{0.458}\ R^{-1.208}$	3	12
Vector Velocity (cm/s)	$12.040\ W^{0.628}\ R^{-1.593}$	5	10
Vertical Displacement (cm)	$1.319\ W^{0.737}\ R^{-1.699}$	1	2
Radial Displacement (cm)	$1.024\ W^{0.719}\ R^{-1.486}$	1	3
Trans. Displacement (cm)	$0.598\ W^{0.603}\ R^{-1.165}$	1	4
Vector Displacement (cm)	$2.683\ W^{0.675}\ R^{-1.640}$	1	2

a. The vector values at the 1.65 σ level for acceleration, velocity, and displacement are less than or equal to the maximum individual component because the standard deviation for the vector quantities is much smaller than that of the individual components and that of the round-off effects.

b. For stations on rock.

c. W denotes field in kt; R denotes range from event location to point of interest in km.

- Pahute Mesa--1,300 kt,
- Yucca Flats--300 kt,
- Frenchman's Flat--300 kt, and
- Buckboard Mesa area--750 kt.

The yield limit for Mid Valley has not been addressed specifically because the geology will restrict yields to well below those at the other sites.

Using the information given above, predictions were made for UNEs in the testing area closest to Yucca Mountain with the highest yield limits (Pahute Mesa and Buckboard Mesa area, Vortman, Reference A-2-3. The smallest possible distance between these particular testing areas and Yucca Mountain was scaled from a map, and this distance was used in the prediction equations. The design basis UNE was selected as the UNE that produced the largest ground motions at Yucca Mountain, which was a 700-kt event in the Buckboard Mesa area at 22.8 km away (700 kt was used instead of 750 kt because of the small differences in the predicted values and the already conservative approach of assuming the closest point for the largest yield). Although the yield limit for Pahute Mesa is greater, Pahute Mesa is sufficiently far away that the ground motion at the repository site would be less than that from the nearest location in the Buckboard Mesa area.

A-2.2 Development of the UNE Prediction Equations

The major objectives for the analyses included in Reference A-2-1, Long (draft), and Phillips (draft) were (1) to develop a regional prediction model for the NTS and (2) to identify and quantify the differences in ground motion behavior at Yucca Mountain when compared to those at the NTS. To this end, data from a number of UNEs were analyzed.

The data set used to develop the prediction equations includes ground motions recorded from a total of 34 UNEs. These events were conducted between 1966 and 1984. The yield variation in the data set is from 80 kt to 1,400 kt (9 UNEs had yields >500 kt; 7 UNEs had yields between 150 and 500 kt; 18 UNEs had yields between 80 and 150 kt). Ground motion has been

recorded at about 50 different locations. Of these 50 locations, 10 have been located in the Yucca Mountain area. Ground motion from a total of eight of these events was recorded at Yucca Mountain stations. This data set was chosen based on the need for a reasonable variation in yield and distance (from the source) to obtain general prediction equations. All events were conducted in the Pahute Mesa testing area of the NTS (Figure 3-1). Geologies in which stations were located may be placed in two broad categories: rock and alluvium.

The prediction equations that were developed in References A-2-1 and A-2-2 are empirical. The major assumptions made in the development of these equations are (1) the source geology is considered to be the same; (2) the differences in travel path geology are ignored; and (3) the station geology differences are accounted for by providing separate equations for rock and alluvium. In addition, the data are assumed to be lognormally distributed and linearly correlated in a log-log space (i.e., fit with a power curve). These assumptions and approach are not original. An earlier study (Environmental Research Corp., Reference A-2-4) has shown this approach to be reasonable when describing the behavior of UNE ground motions. The equations are developed from multiple linear regressions in which yield and distance are considered to be the independent variables and the ground motion parameter (acceleration, velocity, or displacement) is the dependent variable. The data were subdivided into three major groups (Vortman, Reference A-2-1). Group I included all data in the data set. Data from known anomalous stations [e.g., Nuclear Reactor Development Stations (NRDS) area, Rainier Mesa, Climax Stock, etc.] (Vortman and Long, Reference A-2-5) were excluded to form Group II. The Group III data set consisted of Group II minus the data available from the Yucca Mountain stations at the time of the analyses. In addition to these three major groups, three subdivisions of these groups were made based on the station geology. These subdivisions were (1) all stations regardless of geology; (2) only stations on rock; and (3) only stations on alluvium.

The recommendations from Vortman (Reference A-2-1) and Long (draft) were to use the Group III equations for the appropriate station geology as

the prediction equations at the NTS. These recommendations were based on the fact that inclusion of the anomalous stations would bias the predictions in an unfavorable fashion for a procedure that is meant to predict general NTS ground motions. Inclusion of the Yucca Mountain stations would bias the predictions to lower yields and greater distances, i.e., most UNEs are between 40 and 50 km away from Yucca Mountain.

The recommended prediction equations from Vortman (Reference A-2-1) and Long (draft) were evaluated by Phillips (draft). That study used all data recorded at Yucca Mountain stations between mid-1980 and the end of FY 1986. These events were "predicted" using the recommended equations, and these predicted values were compared with the measured values at Yucca Mountain. Ratios of measured and predicted ground motions were calculated for each event at each Yucca Mountain station, and average ratios for each station were determined. In the analysis of these average station ratios, it was observed that the predicted values were generally less than those measured. The average ratios calculated for each station were always less than the 1σ value of the prediction equation. The individual ratios calculated for each event at a particular station seldom exceeded the 2σ values calculated from the equations (1σ corresponds to the 68% confidence interval for the mean of all the observations at the site or the 84% nonexceedance probability level, and 2σ corresponds to the 95% confidence interval or the 98% nonexceedance probability level). The conclusion of this analysis was that the prediction equations from Vortman (Reference A-2-1) and Long (draft) provided reasonably accurate results, given the statistics of the fits. To attempt to correct for possible site effects with this data set would imply a level of accuracy that does not exist in the data.

As discussed in Section 3 of this report, the predicted ground motions provided for the design of the ESF were specified at the 95% nonexceedance probability level, which corresponds to 1.65σ. These values are also listed with the equations in Table A-2.1.

A-2.3 Wave Propagation from UNEs

The UNE produces a radially expanding compressional shock front at the point of the explosion (Bath, Reference A-2-6). As the distance increases from the source, this compressional front is converted to a complex wave train of various seismic signals. These signals are the result of tectonic release, refractions from layering in the earth, free surface effects at the ground surface, and material anisotropies. At distances of interest to the diagnosis of the ESF, the primary wave types present in the ground motions are body waves and surface waves. Body waves are composed of compressional (P) waves, horizontally polarized shear waves (S_h), and vertically polarized shear waves (S_v) (Rodean, Reference A-2-7). Surface waves are composed of Rayleigh and Love waves (Rodean, Reference A-2-7). The wave types that carry most of the energy are the P, S_h, and S_v waves. Because of the depth of the UNE and the radial nature of the explosion, the following assumptions are made about which wave types cause the component acceleration and velocities observed at distances of interest to the designers of the ESF:

- peak radial motions are the result of the P wave,
- peak transverse motions are the result of the S_h wave, and
- peak vertical motions are the result of the S_v wave.

The peak displacements observed at these distances from a UNE are associated with the surface waves.

A-2.4 References

A-2-1. Vortman, L. J. (February 1986), "Ground Motion Produced at Yucca Mountain from Pahute Mesa Underground Nuclear Explosions," SAND85-1605, Sandia National Laboratories, Albuquerque, NM. (HQS.880517.2896)

A-2-2. Fernald, A. T., Coordinator (January 1977), "Real Estate Availability Study, Potential New Test Areas, Nevada Test Site," U.S. Geological Survey, Denver, CO. (Not publicly available)

A-2-3. Vortman, L. J. (April 1980), "Prediction of Ground Motion from Underground Nuclear Weapons Tests as It Relates to Siting of a Nuclear Waste Storage Facility at NTS and Compatibility with the Weapons Test Program," SAND80-1020/1, Sandia National Laboratories, Albuquerque, NM. (HQS.880517.2895)

A-2-4. Environmental Research Corporation (March 1974), "Prediction of Ground Motion Characteristics of Underground Nuclear Detonations," NVO-1163-239, U.S. Atomic Energy Commission, Nevada Operations Office, Las Vegas, NV. (On order)

A-2-5. Vortman, L. J., and Long, J. W. (May 1982), "Effects of Repository Depth on Ground Motion--the Pahute Mesa Data," SAND82-0174, Sandia National Laboratories, Albuquerque, NM. (HQS.880517.1549)

A-2-6. Bath, M. (1979), Introduction to Seismology, Birkhauser Verlag, Basel, Switzerland. (On order)

A-2-7. Rodean, H. C. (1971), "Nuclear Explosion Seismology," AEC Critical Review Series Publications, Lawrence Livermore National Laboratory, University of California, Livermore, CA. (NNA.891107.0120)

APPENDIX A-3

DETERMINATION OF CONTROLLING STRAIN COMBINATION FOR DESIGN

This appendix gives the data, assumptions, and methods used for determining the controlling strain combination for design of the ESF.

A-3.1 Conditions and Assumptions

A-3.1.1 Earthquake Control Motion

Horizontal: $v_h = 30$ cm/sec $\qquad a_h = 0.3$ g

Vertical : $v_v = 2/3\ v_h$ $\qquad a_v = a_h$

A-3.1.2 UNE Control Motion

Horizontal: $v'_h = 12$ cm/sec $= 0.40\ v_h$ $\qquad a'_h = 0.1$ g $= 0.33\ a_h$

Vertical : $v'_v = 9$ cm/sec $= 0.30\ v_h$ $\qquad a'_v = 0.2$ g $= 0.67\ a_h$

All results will be normalized in terms of v_h and a_h.

A-3.1.3 Earthquake incident angles between 0° (vertical) and 30° (maximum) and free-field strains are given by Table A-3.2, which was derived from Table A-3.1 using

$$v_p = v_v/\cos\theta \qquad v_{sv} = v_h/\cos\theta \qquad v_{sh} = v_h$$
$$a_p = a_v/\cos\theta \qquad a_{sv} = a_v/\cos\theta \qquad a_{sh} = a_h \ .$$

A-3.1.4 UNE incident angles can range from 0° (vertical) to 90° (horizontal).

For $0° \leq \theta \leq 45°$, the assumptions are those used for Condition A-3.1.3 and Table A-3.2.

TABLE A-3.1

FREE-FIELD AND BENDING STRAINS CAUSED BY EARTHQUAKES

Wave Type	Free-Field Strains						Bending Strains
	ε_{xx}	ε_{yy}	ε_{zz}	γ_{xy}	γ_{yz}	γ_{xz}	ε_b
P	$\frac{v_p}{c_p} \sin^2 \theta$	0	$\frac{v_p}{c_p} \cos^2 \theta$	0	0	$\frac{v_p}{c_p} \sin 2\theta$	$\frac{R\, a_p}{c_p^2} \sin \theta \cos^2 \theta$ (in xz plane)
S_v	$\frac{v_{sv}}{c_s} \sin \theta \cos \theta$	0	$\frac{v_{sv}}{c_s} \sin \theta \cos \theta$	0	0	$\frac{v_{sv}}{c_s} \cos 2\theta$	$\frac{R\, a_{sv}}{c_s^2} \cos^3 \theta$ (in xz plane)
S_h	0	0	0	$\frac{v_{sh}}{c_s} \sin \theta$	$\frac{v_{sh}}{c_s} \cos \theta$	0	$\frac{R\, a_{sh}}{c_s^2} \cos^2 \theta$ (in yz plane)

TABLE A-3.2

FREE-FIELD AND BENDING STRAINS IN TERMS OF GROUND MOTION CONTROL PARAMETERS FOR EARTHQUAKES

Wave Type	Free-Field Strains						Bending Strains
	ε_{xx}	ε_{yy}	ε_{zz}	γ_{xy}	γ_{yz}	γ_{xz}	ε_b
P	$\frac{v_v}{C_p} \frac{\sin^2 \theta}{\cos \theta}$	0	$\frac{v_v}{C_p} \cos \theta$	0	0	$\frac{v_v}{C_p} 2 \sin \theta$	$\frac{R\, a_v}{C_p^2} \sin \theta \cos \theta$ (in xz plane)
S_v	$\frac{v_h}{C_s} \sin \theta$	0	$\frac{v_h}{C_s} \sin \theta$	0	0	$\frac{v_h}{C_s} \frac{\cos 2\theta}{\cos \theta}$	$\frac{R\, a_h}{C_s^2} \cos^2 \theta$ (in xz plane)
S_h	0	0	0	$\frac{v_h}{C_s} \sin \theta$	$\frac{v_h}{C_s} \cos \theta$	0	$\frac{R\, a_h}{C_s^2} \cos^2 \theta$ (in yz plane)

Note: These expressions are valid only for steeply emerging body waves, i.e., $\theta = 30°$ or less.

TABLE A-3.3

STRAINS CAUSED BY UNE'S FOR $45° < \Theta \leq 90°$

Wave Type	ε_{xx}	ε_{zz}	γ_{xy}	ε_b
P	$\frac{v'_h}{C_p} \sin\Theta$	$\frac{v'_h}{C_p} \frac{\cos^2\Theta}{\sin\Theta}$	0	$\frac{Ra'_h}{C_p^2} \cos^2\Theta$ (xz plane)
S_v	$\frac{v'_v}{C_s} \cos\Theta$	$\frac{v'_v}{C_s} \cos\Theta$	0	$\frac{Ra'_v}{C_s^2} \frac{\cos^3\Theta}{\sin\Theta}$ (xz plane)
S_h	0	0	$\frac{v'_h}{C_s} \sin\Theta$	$\frac{Ra'_h}{C_s^2} \cos^2\Theta$ (yz plane)

For $45° < \Theta \leq 90°$, use Table A-3.3 derived from Table A-3.1 using

$$v_p = v'_h/\sin\Theta \qquad v_{sv} = v'_v/\sin\Theta \qquad v_{sh} = v'_h \ .$$

These assumptions are very conservative for $30° \leq \Theta \leq 60°$ because they lead to the wave particle velocities and accelerations shown in Table A-3.4.

Table A-3.4 shows that the computed values of v and a are very conservative compared with the design basis UNE values. Despite this conservatism, UNE will not govern.

A-3.1.5 Effects of P, S_v, and S_h will be vector summed using the 100-40-40 Combination Rule based on random phasing. For instance, bending strain, ε_b caused by the S_h wave is 90° to ε_b from P and S_v waves.

$$\text{Thus, } \varepsilon_b = \sqrt{\left(\varepsilon_{b_P} + 0.4\ \varepsilon_{b_{S_v}}\right)^2 + \left(0.4\ \varepsilon_{b_{S_h}}\right)^2}, \text{ etc.}$$

TABLE A-3.4

COMPUTED WAVE PARTICLE VELOCITIES AND ACCELERATIONS

	Wave Particle Velocities (cm/sec)				Accelerations (g)			
Θ	v_p	v_{sv}	$v_h'^*$	$v_v'^*$	a_p	a_{sv}	$a_h'^*$	$a_v'^*$
0°	9.0	12.0	12.0	9.0	0.2	0.1	0.1	0.2
37°	11.3	15.0	14.7	12.6	0.25	0.125	0.19	0.23
45°	12.7	17.0	15.6	15.6	0.282	0.141	0.24	0.24
53°	15.0	11.3	14.7	12.6	0.125	0.25	0.19	0.23
90°	12.0	9.0	12.0	9.0	0.1	0.2	0.1	0.2

*Probabilistic 100-40-40 Combination Rule used to generate these values.

A-3.1.6 The designer is concerned with total axial strain and either maximum hoop strain or maximum hoop stress. Elastic computed maximum hoop stress, σ_h, at unlined opening will serve as a measure of hoop effects. Total axial strain, ε_a, is given by $\varepsilon_a = \varepsilon_{zz} + \varepsilon_b$. The earthquake and UNE incident angles and component combinations that maximize σ_h and ε_a must be determined.

A-3.1.7 Properties Used

Poisson's Ratio: $\nu = 0.19$ (Results insensitive for $0.13 \leq \nu \leq 0.24$)

Wave Speed Ratios: $C_p/C_s = 1.62$ (Results insensitive for $1.53 \leq C_p/C_s \leq 1.71$)

Shear Wave Speed: $C_s \geq 800$ m/sec

Shaft Radius: $R \leq 5$ m

A-3.2 Elastic Hoop Stress for Unlined Opening

Free Field

$$\left.\begin{aligned} (\sigma_x/G) &= 2\varepsilon_{xx} + (\lambda/G)(\varepsilon_{xx} + \varepsilon_{zz}) \\ (\sigma_y/G) &= (\lambda/G)(\varepsilon_{xx} + \varepsilon_{zz}) \\ (\tau_{xy}/G) &= \gamma_{xy} \end{aligned}\right\} \text{--Lame's Equation (Timoshenko and Goodier, Reference A-3-1)}$$

Principal Stresses

$$\sigma_{1,3} = \frac{\sigma_x + \sigma_y}{2} \pm \sqrt{\left[\frac{\sigma_x - \sigma_y}{2}\right]^2 + \tau_{xy}^2} \quad ;$$

$$\therefore (\sigma_{1,3}/G) = \varepsilon_{xx} + (\lambda/G)(\varepsilon_{xx} + \varepsilon_{zz}) \pm \sqrt{\varepsilon_{xx}^2 + \gamma_{xy}^2}$$

Maximum Hoop Stress

$(\sigma_h/G) = 3\ (\sigma_1/G) - (\sigma_3/G)$ --Kirsch's Equation (Timoshenko and Goodier, Reference A-3-1);

$$\therefore (\sigma_h/2G) = \varepsilon_{xx} + (\lambda/G)(\varepsilon_{xx} + \varepsilon_{zz}) + 2\sqrt{\varepsilon_{xx}^2 + \gamma_{xy}^2} \quad , \qquad \text{(A-3-1)}$$

where $(\lambda/G) = \frac{2\nu}{1-2\nu} = \frac{2(0.19)}{1-2(0.19)} = 0.61$ for $\nu = 0.19$.

For both an earthquake and UNE, the incident angle and component combination that maximize $(\sigma_h/2\ G)$ will also maximize hoop effects on the ESF. All results are normalized in terms of $\varepsilon_N = \frac{v_h}{C_s}$.

Axial Strain

$\varepsilon_a = \varepsilon_{zz} + \varepsilon_b$

ε_b is normalized by $\varepsilon_{BN} = \left[\frac{Ra_h}{C_s^2}\right]$

$$\therefore (\varepsilon_a/\varepsilon_N) = \left[\frac{\varepsilon_{zz}}{\varepsilon_N}\right] + \left[\frac{\varepsilon_b}{\varepsilon_{BN}}\right]\left[\frac{\varepsilon_{BN}}{\varepsilon_N}\right]$$

For $R \leq 5$ m and $C_s \geq 800$ m/s

$$(\varepsilon_{BN}/\varepsilon_N) = \frac{Ra_h}{v_h C_s} \leq \frac{(5_m)(0.3\ g)(980\ cm/sec^2 g)}{30\ cm/sec\ (800\ cm/sec)} = 0.061 \quad ;$$

$$\therefore (\varepsilon_a/\varepsilon_N) \leq (\varepsilon_{zz}/\varepsilon_N) + 0.061\ (\varepsilon_b/\varepsilon_{BN}) \quad . \qquad \text{(A-3-2)}$$

Axial effects on the shafts will be maximized when $(\varepsilon_a/\varepsilon_N)$ is maximized.

A-3.3 Earthquake Control Motion

The parameters for UNE earthquake control motion are given in Table A-3.3.

TABLE A-3.5

STRESSES AND STRAIN FOR EARTHQUAKE MOTION

$\theta = 0°$	$\varepsilon_{xx}/\varepsilon_N$	$\varepsilon_{zz}/\varepsilon_N$	$\gamma_{xy}/\varepsilon_N$	$\varepsilon_b/\varepsilon_{BN}$	$\sigma_h/2G\varepsilon_N$	$\varepsilon_a/\varepsilon_N$
P	0	0.41	0	0		
S_v	0	0	0	1.0		
S_h	0	0	0	1.0		
100% $\underset{\sim}{P}$ + 40% ($\underset{\sim}{S}_v$ + $\underset{\sim}{S}_h$)	0	0.41	0	0.57[a]	0.25	0.44
100% $\underset{\sim}{S}_v$ + 40% ($\underset{\sim}{P}$ + $\underset{\sim}{S}_h$)	0	0.16	0	1.08[a]	0.10	0.23
100% $\underset{\sim}{S}_h$ + 40% ($\underset{\sim}{P}$ + $\underset{\sim}{S}_v$)	0	0.16	0	1.08[a]	0.10	0.23
$\theta = 30°$						
P	0.12	0.36	0	0.16		
S_v	0.50	0.50	0	0.75		
S_h	0	0	0.50	0.75		
100% $\underset{\sim}{P}$ + 40% ($\underset{\sim}{S}_v$ + $\underset{\sim}{S}_h$)	0.32	0.56	0.20	0.55[a]	0.61	0.59
100% $\underset{\sim}{S}_v$ + 40% ($\underset{\sim}{P}$ + $\underset{\sim}{S}_h$)	0.55	0.64	0.20	0.87[a]	2.45[b]	0.69[b]
100% S_h + 40% ($\underset{\sim}{P}$ + $\underset{\sim}{S}_v$)	0.25	0.34	0.50	0.83[a]	1.73	0.39

a. Vectorially combined per Condition A-3.1.5 $\underset{\sim}{P}$, $\underset{\sim}{S}_v$, and $\underset{\sim}{S}_h$ indicate vector quantities.
b. Controls.

A-3.4 UNE Control Motion

The parameters for UNE control motion are given in Table A-3.6.

TABLE A-3.6

STRESSES AND STRAIN FOR UNE MOTIONS

$\Theta = 0°$	$\varepsilon_{xx}/\varepsilon_N$	$\varepsilon_{zz}/\varepsilon_N$	$\gamma_{xy}/\varepsilon_N$	$\varepsilon_b/\varepsilon_N$	$\sigma_h/2G\varepsilon_N$	$\varepsilon_a/\varepsilon_N$
P	0	0.19	0	0		
S_V	0	0	0	0.33		
S_h	0	0	0	0.33		
1[a]	0	0.19	0	e	0.12	0.19
2[b]	e	0.08	e	0.36	e	0.10
3[c]	e	0.08	e	0.36	e	0.10
$\Theta = 37°$	$\varepsilon_{xx}/\varepsilon_N$	$\varepsilon_{zz}/\varepsilon_N$	$\gamma_{xy}/\varepsilon_N$	$\varepsilon_b/\varepsilon_{BN}$	$\sigma_h/2G\varepsilon_N$	$\varepsilon_a/\varepsilon_N$
P	0.09	0.15	0	0.12		
S_V	0.24	0.24	0	0.21		
S_h	0	0	0.24	0.21		
1[a]	0.19	0.25	0.10	e	e	e
2[b]	0.28	0.30	0.10	0.27	1.23	0.32
3[c]	0.13	0.16	0.24	e	e	e
$\Theta = 45°$	$\varepsilon_{xx}/\varepsilon_N$	$\varepsilon_{zz}/\varepsilon_N$	$\gamma_{xy}/\varepsilon_N$	$\varepsilon_b/\varepsilon_{BN}$	$\sigma_h/2G\varepsilon_N$	$\varepsilon_a/\varepsilon_N$
P	0.08	0.08	0	0.13		
S_V	0.28	0.28	0	0.17		
S_h	0	0	0.28	0.17		
1[a]	0.19	0.19	0.11	e	0.86	e
2[b]	0.31	0.31	0.11	0.23	1.35[d]	0.32[d]
3[c]	0.14	0.14	0.28	e	0.94	e

TABLE A-3.6

STRESSES AND STRAIN FOR UNE MOTIONS (Concluded)

$\Theta = 53°$	$\varepsilon_{xx}/\varepsilon_N$	$\varepsilon_{zz}/\varepsilon_N$	$\gamma_{xy}/\varepsilon_N$	$\varepsilon_b/\varepsilon_{BN}$	$\sigma_h/2G\varepsilon_N$	$\varepsilon_a/\varepsilon_N$
P	0.20	0.11	0	0.05		
S_v	0.18	0.18	0	0.18		
S_h	0	0	0.32	0.12		
1[a]	0.27	0.18	0.13	e	1.14	e
2[b]	0.26	0.22	0.13	e	e	e
3[c]	0.15	0.12	0.32	e	1.02	e
$\Theta = 90°$	$\varepsilon_{xx}/\varepsilon_N$	$\varepsilon_{zz}/\varepsilon_N$	$\gamma_{xy}/\varepsilon_N$	$\varepsilon_b/\varepsilon_{BN}$	$\sigma_h/2G\varepsilon_N$	$\varepsilon_a/\varepsilon_N$
P	0.25	0	0	0		
S_v	0	0	0	0		
S_h	0	0	0.40	0		
1[a]	0.25	0	0.16	0	1.00	0
2[b]	e	0	e	0	e	0
3[c]	0.10	0	0.40	0	0.99	0

a. 1 = 100% $\underset{\sim}{P}$ + 40% ($\underset{\sim}{S}_v$ + $\underset{\sim}{S}_h$).

b. 2 = 100% $\underset{\sim}{S}_v$ + 40% ($\underset{\sim}{P}$ + $\underset{\sim}{S}_h$).

c. 3 = 100% $\underset{\sim}{S}_h$ + 40% ($\underset{\sim}{P}$ + $\underset{\sim}{S}_v$).

d. Controls.

e. By observation, this cannot control; therefore, it was not computed.

A-3.5 Conclusions

Earthquake control motion, with $\theta = 30°$ and a combination of $100\%\ \underset{\sim}{S}_V + 40\%\ (\underset{\sim}{P} + \underset{\sim}{S}_h)$ } controls

For this case, $\sigma_h/2G\varepsilon_N = 2.45$ and

$$\varepsilon_a/\varepsilon_N \leq 0.69 \quad .$$

The largest UNE effect is at $\theta = 45°$ for $100\%\ \underset{\sim}{S}_V + 40\%\ (\underset{\sim}{P} + S_h)$.

For this case, $\sigma_h/2G\varepsilon_N = 1.35$ = (0.55 * value for earthquake control motion) and

$\varepsilon_a/\varepsilon_N = 0.32$ = (0.46 * value for earthquake control motion).

It is necessary to double the UNE control motion before UNE can govern.

A-3.6 Reference

A-3-1. Timoshenko, S., and Goodier, J. N., Theory of Elasticity, Second Edition, McGraw-Hill Book Company, Inc., New York, NY, 1951. (NNA.890522.0221)

APPENDIX A-4

DEPTH ATTENUATION BEHAVIOR OF UNE GROUND MOTIONS
AT YUCCA MOUNTAIN

The objective of this appendix is to describe the observed attenuation behavior of ground motions at Yucca Mountain with depth. The ideal approach to achieve this objective would be to record ground motions at several depths from the design basis UNE in the hole of interest and to develop attenuation curves for the pertinent parameters (Figure A-4.1). However, data in this form do not exist at the repository site. The data set that is available for this task consists of ground motions from a total of 17 UNEs (conducted from mid-1980 through mid-1987) recorded at a total of six different surface and downhole stations located in the vicinity of Yucca Mountain, of which none is located at the ESF. Each one of these stations has instruments at the surface and at one downhole location. The stations are located in similar but not identical geologies and are separated by distances of as much as 8 km (Figure A-4.2). The distances from the UNEs included in the data base to the ground motion stations range from 40 to 50 km, and the UNE yields range from 80 to 150 kt (as compared with the design basis UNE of 700 kt at a distance of 22.8 km).

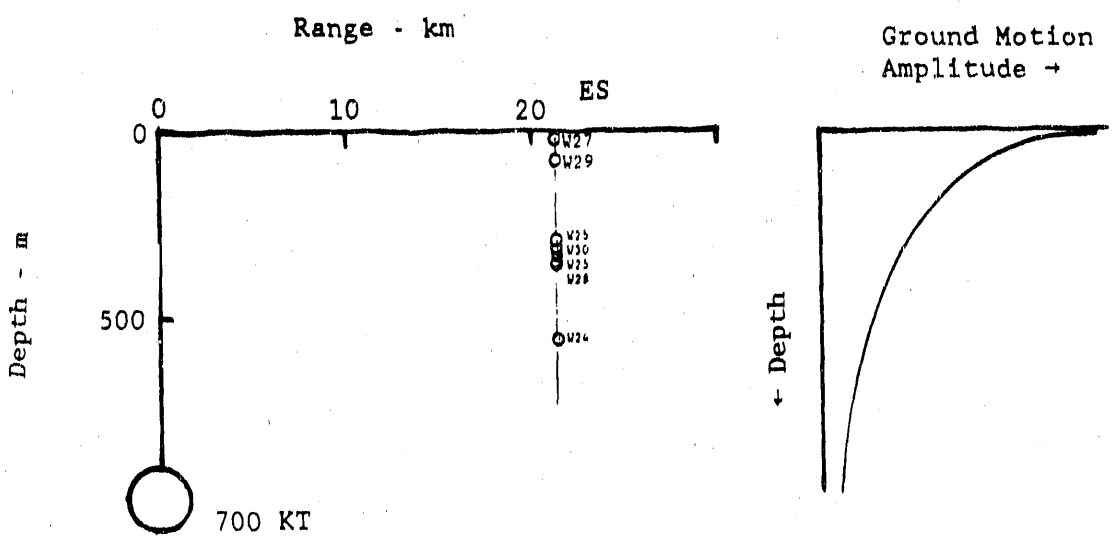

Figure A-4.1. Ideal Situation for Determining Depth Attenuation Behavior

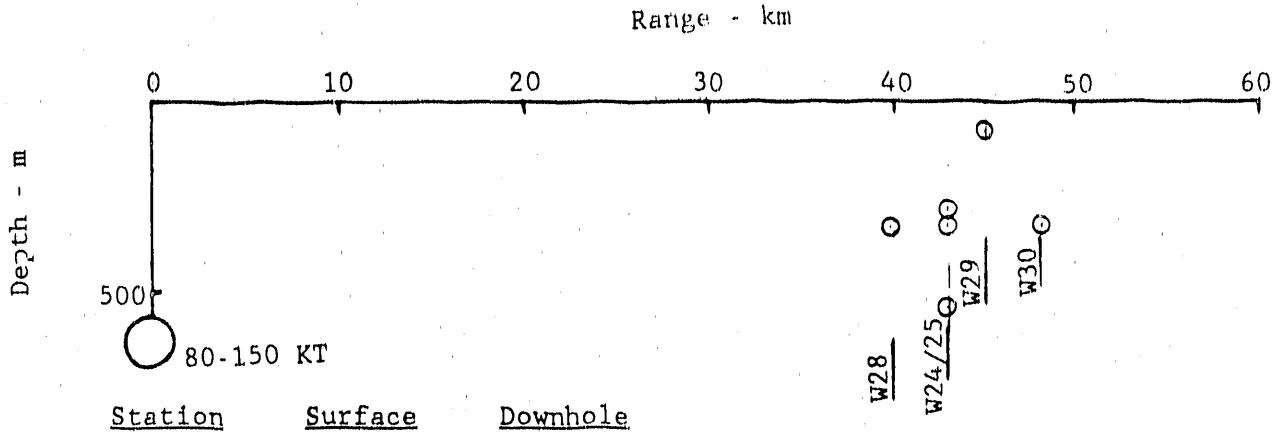

Station	Surface	Downhole
W28	TCW	TSW1
W24	UO	CHn2
W25	UO	TSW2
W29	UO	UO
W30	TCW	TSW2

Figure A-4.2. Actual Situation for Determining Depth Attenuation Behavior

Two different studies were conducted. The first was directed at the attenuation of absolute peak ground motions with depth; the second addressed the depth attenuation behavior of the pseudorelative velocity response spectra (PSRV) at characteristic earthquake frequencies of 1, 2, and 5 Hz. These two studies are discussed below.

A-4.1 Assumptions and Approach

The approach used to develop depth attenuation behavior is to calculate ratios of surface and downhole ground motion and to plot the log of these ratios versus depth. This approach assumes that the geologic differences, as well as the separation distances between the individual stations, are insignificant. In addition, differences in yield, shot point geology, station-to-source distance, and travel path geology are also assumed to be insignificant. Finally, by considering only the absolute peak ground motions, the individual wave types that make up the total ground motion are ignored. All of these assumptions will have the effect of increasing the data scatter and hence the uncertainty in this analysis. In the analysis

of the PSRV ratios, the degree of uncertainty will be reduced because the same wave type will be compared at both the surface and downhole locations.

The considerations that went into the determination of the various fits were as follows:

1. Distance attenuation rates for a specific wave type will differ on the surface from those downhole, and distance attenuation rates of different wave types will differ because geometrical factors and material properties differ in the surface and downhole media. Although these factors are not used explicitly in the development of the depth attenuation curves, they are taken into consideration in the "judgment factor" applied to the derived fits.

2. The surface materials at the ground motion stations are different. These differences will artificially influence the surface-to-downhole ratios because there will only be one surface material at the ESF site.

3. Station W30 was the station farthest from the UNEs. Surface-to-downhole ratios for this station are generally less than those for the other stations at Yucca Mountain. Based on observations of UNE data, the amount of attenuation observed at depth decreases with increasing distance from the source (Phillips, draft*). A possible explanation is that the peak amplitudes at greater distances are driven by surface waves, which do not attenuate significantly (for the wave lengths of the UNE motions) with depth. Because the primary objective here is to predict attenuation behavior for a larger yield at a closer range, the data from W30 were not given much weight in the derived fit.

---

*J.S. Phillips (draft), "Analysis of Component Safety/Downhole Ground Motions at Yucca Mountain for Underground Nuclear Explosions in Pahute Mesa," SAND87-2381, Sandia National Laboratories, Albuquerque, NM.

4. Transverse and radial acceleration data recorded at Station W28 were not heavily weighted in the fit because the anomalous behavior observed there is too sporadic to quantify at this time (Phillips, draft).

5. Singular events that appear to be outside of the norm were essentially ignored in the fitting process.

6. The derived fit is an "eyeball" fit. Blind regression of these data produces results with poor correlation coefficients and suggests a degree of accuracy or understanding (from these data) that is not present.

7. The fits, determined from the average ratios at each station, were compared with the complete data set and were modified as necessary.

A-4.2 Absolute Peak Attenuation

The surface-to-downhole ratios for peak values of acceleration, velocity, and displacement for all UNEs recorded at the Yucca Mountain site were calculated and plotted versus depth of the station. Some of the events have been included in Phillips (draft), but others were conducted after the data for that study had been gathered. Table A-4.1 shows the events, stations, station depths, and calculated surface-to-downhole ratios for each ground motion component. Table A-4.2 repeats the information of Table A-4.1 and includes the actual data values from the events not included by Phillips (draft). The plots of these ratios are included in Figures A-4.3 through A-4.11. The equations determined for the lines shown on these figures are given in Table A-4.3. The amount of depth attenuation predicted for various depths by these equations is summarized in Table A-4.4. All accelerations, velocities, and displacements decreased with increasing depth with the exception of vertical displacement.

In an attempt to evaluate these attenuation curves by comparison with an event more similar to the design basis event, another UNE recorded at a closer range was studied. The event was Nebbiolo, and the station was W-9,

Table A-4.1

Ratio of Peak Surface and Downhole Ground Motions

Ratios of Peak Surface and Downhole Vertical Accelerations

Station	W1	W3	W12-30	W25	W29	W28	W26	W24
Depth - m	35	92	352	358	305	375	354	564
Event								
Chantelle			1.50	3.55				
Cabra			1.41					3.98
Lenpeel	1.71		1.27	5.15				
Salvo		1.65	1.91	4.21		3.16		
Serena		2.13	1.84	4.09		2.37		
Komoka				3.41				
Wide								3.73
Cypress				3.84		2.41		
Lowanda		1.36	1.49	3.85				
Goldstone		2.18	1.53	3.66		2.33		
Jefferson		1.62	1.58	4.50		2.09		
Darwin		2.12	1.29	4.03		1.92		
Ledgeway		1.46	1.51	3.35		2.25		
Belmont		1.39	1.33	3.93		1.68		
Jodie		1.7	1.35			1.54		
Delacar		1.74	1.84					
Parrott		2.1	1.77		1.48		2.45	
Average	1.71	2.03	1.63	3.92		2.08		3.86

Ratios of Peak Surface and Downhole Vertical Velocities

Station	W1	W3	W12-30	W25	W29	W28	W26	W24
Depth - m	35	92	352	358	305	375	354	564
Event								
Chantelle			1.45	1.87				2.10
Cabra			1.94					
Lenpeel	1.41		1.50	2.74				
Salvo		1.78	1.84	1.71		1.84		
Serena		1.79	1.61	1.84		1.67		
Komoka				1.82				
Wide								1.70
Cypress				1.99		1.31		
Lowanda		1.37	1.34	1.90				
Goldstone		1.76	1.73	1.78		1.53		
Jefferson		1.67	1.74	1.91		1.65		
Darwin		1.86	1.67	1.84		1.48		
Ledgeway		1.75	1.70	1.81		1.75		
Belmont		1.70	1.63	1.82		1.46		
Jodie		1.74	1.72			1.63		
Delacar		1.71	1.77					
Parrott		1.81	1.73		1.65		1.68	
Average	1.71	1.78	1.73	1.92		1.74		1.90

Table A-4.1

Ratio of Peak Surface and Downhole Ground Motions (Continued)

Ratios of Peak Surface and Downhole Vertical Displacements

Station	W27	W29	W12/30	W34	W25	W20	W28	W24
Depth - m	35	83	352	350	205.00	335	358	564
Event								
Chancellor			1.02	1.10				
Cabra			0.97					1.17
Kappel	0.99		1.00	1.11				
Galut		1.05	0.98	1.09		1.09		
Serena		1.04	1.02	1.13		1.09		
Sonoma				1.13				
Olema								1.14
Tierra				0.85		1.04		
Lawanda		1.02	0.98	1.08				
Goldstone		1.02	0.98	1.09		1.05		
Lakeside		1.02	0.99	1.10		1.07		
Darwin		1.05	1.00	1.08		1.02		
Lanquard		1.05	0.99	1.13		1.13		
Belmont		1.06	0.95	1.08		1.05		
Bodie		1.03	0.95			0.96		
Delamar		1.02	1.03					
Hardin		0.95	0.99		0.44		1.15	
Average	0.99	1.03	0.99	1.05		0.99		1.16

Ratios of Peak Surface and Downhole Radial Accelerations

Station	W27	W29	W12/30	W34	W25	W20	W28	W24
Depth - m	35	83	352	350	205	335	358	564
Event								
Chancellor			1.03	1.20				1.04
Cabra			1.04					
Kappel	1.08		1.06	0.87				
Galut		2.09	1.10	1.17		1.04		
Serena		2.23	1.08	1.14		0.95		
Sonoma								
Olema								1.20
Tierra				0.87		0.85		
Lawanda		1.23	1.09	1.08				
Goldstone		2.52	1.11	1.19		0.95		
Lakeside		2.19	0.87	1.07		1.00		
Darwin		1.72	1.04	1.12		1.04		
Lanquard		1.52	1.02	1.07		1.07		
Belmont		1.04	1.04	1.13		1.04		
Bodie		1.05	1.05			1.04		
Delamar		2.14	1.11					
Hardin		1.32	1.11		1.11		1.11	
Average	1.15	2.14	1.07	1.09		1.01		1.11

Table A-4.1

Ratio of Peak Surface and Downhole Ground Motions (Continued)

Ratios of Peak Surface and Downhole Radial Velocities

Station	W29	W30	W25	W5	W38	W28	W24
Depth - ft	84	352	356	705	375	358	564
Event							
Cancelled		1.4					
Cabrillo		1.27					2.07
Coyote	1.04	1.28					
Gilroy		1.59			2.49		
Morgan	1.16	1.39			3.22		
Oyster							
Point							1.77
Santa					2.07		
Sawmill		1.83					
Stevens		1.58			2.45		
Stevens		1.61			3.25		
Sycamore		1.56			2.44		
Tennant		1.08			2.41		
Watson							
Wildlife		1.36			2.77		
Williams		1.50					
Yerba		1.44				2.50	
Average		1.55					1.92

Ratios of Peak Surface and Downhole Radial Accelerations

Station	W29	W30	W25	W5	W38	W28	W24
Depth - ft	84	352	356	705	375	358	564
Event							
Cancelled							
Cabrillo							
Coyote							
Gilroy							
Morgan							
Oyster							
Point							
Santa							
Sawmill							
Stevens							
Stevens							
Sycamore							
Tennant							
Watson							
Wildlife							
Williams							
Yerba							
Average							

Table A-4.1

Ratio of Peak Surface and Downhole Ground Motions (Continued)

Ratios of Peak Surface and Downhole Transverse Accelerations

Station	W27	W29	W12/30	W25	W25	W28	W23	W24
Depth - m	35	83	352	358	305	375	358	564
Event								
Chancellor			3.37	9.22				
Cabra			1.99					7.85
Kennett	1.58		2.11	5.34				
Saint		1.44	1.97	4.79		1.11		
Serena		1.47	2.34	9.01		0.63		
Egmont				7.58				
Gibne								3.72
Tierra				3.82		0.30		
Towanda		1.37	2.20	4.16				
Goldstone		1.84	2.33	6.02		1.03		
Jefferson		1.69	2.54	6.94		0.84		
Darwin		1.28	2.95	7.33		2.05		
Labquark		1.36	2.28	6.80		1.17		
Belmont		1.75	2.02	8.91		0.82		
Bodie		1.63	2.66			0.27		
Delamar		1.59	2.17					
Hardin		1.67	4.64		2.69		1.57	
Average	1.69	1.53	2.54	6.99		0.92		5.29

Ratios of Peak Surface and Downhole Transverse Velocities

Station	W27	W29	W12/30	W25	W25	W28	W23	W24
Depth - m	35	83	352	358	305	375	358	564
Event								
Chancellor			1.79	3.28				
Cabra			1.08					2.11
Kennett	1.07		1.21	1.44				
Saint		1.15	2.10	2.18		2.47		
Serena		1.13	1.27	1.66		2.12		
Egmont				1.88				
Gibne								2.5
Tierra				1.56		1.30		
Towanda		1.15	1.70	1.48				
Goldstone		1.13	1.85	2.37		1.92		
Jefferson		1.06	1.14	1.85		2.		
Darwin		1.11	1.13	1.72		1.95		
Labquark		1.16	2.01	1.81		2.37		
Belmont		1.07	1.79	1.97		1.75		
Bodie		1.10	1.52			0.45		
Delamar		1.09	1.48					
Hardin		1.13	1.95		0.79		1.26	
Average	1.07	1.11	1.61	1.91		1.82		1.53

Table A-4.1

Ratio of Peak Surface and Downhole Ground Motions (Concluded)

Ratios of Peak Surface and Downhole Transverse Displacements

Station	W27	W29	W12/30	W25	W25	W28	W9	W24
Depth - m	35	83	352	358	305	375	358	564
Event								
Chancellor			1.33	1.43				
Cedra			1.09					1.39
Kappeli	1.06		1.21	1.05				
Saloi		1.05	1.86	1.64		1.94		
Serena		1.04	1.17	1.17		1.31		
Fremont				1.51				
Gilroy								2.36
Sierra				1.05		1.42		
Towanda		1.09	1.45	1.36				
Goldstone		1.11	1.69	1.37		1.73		
Jefferson		1.01	1.30	1.44		1.54		
Bermio		1.06	1.43	1.30		1.33		
Aqueri		1.05	1.38	1.40		1.57		
Belmont		1.04	1.65	1.40		1.55		
Bodie		1.06	1.44			1.56		
Delamar		1.19	1.25					
Hardin		1.06	1.57		1.48		1.22	
Average	1.06	1.05	1.45	1.35		1.46		1.74

Table A-4.2

Values Used to Determine Ratios of Surface and Downhole Ground Motions

Values Used to Determine Ratios of Peak Surface and Downhole Vertical Acceleration

Station	W27	W29	W12/30	W25	W25	W28	W28
Depth - m	35	83	352	358	305	375	358
Event							
Chancellor			1.58	3.55			
Cabra			1.41				
Kappeli	1.21		1.97	5.15			
Salut		1.62	1.81	4.21		3.16	
Serena		2.13	1.64	4.09		2.37	
Egmont				3.41			
Gilroy							
Tierra				3.84		2.41	
Towanda		1.36	1.49	2.85			
Goldstone	0.08884/0.03243	0.04418/0.02879	0.1947/0.05319		0.09425/0.04082		
Jefferson	0.04426/0.02822	0.04029/0.0261	0.1336/0.02972		0.08289/0.03965		
Darwin	0.05782/0.02729	0.04157/0.03237	0.09713/0.02389		0.05032/0.02617		
Labquark	0.04103/0.02473	0.0309/0.02062	0.08752/0.02332		0.07905/0.03521		
Belmont	0.08817/0.04527	0.04694/0.03547	0.2071/0.05213		0.09635/0.05729		
Bodie	0.05543/0.03212	0.0392/0.02236			0.04941/0.09127		
Delamar	0.05322/0.0305	0.05156/0.028					
Hardin	0.2484/0.06598	0.1673/0.09473		0.16/0.1084		0.1926/0.07852	
Average	1.21	2.03	1.60	3.92		2.08	

Values Used to Determine Ratios of Peak Surface and Downhole Vertical Velocities

Station	W27	W29	W12/30	W25	W25	W28	W28
Depth - m	35	83	352	358	305	375	358
Event							
Chancellor			1.05	1.47			
Cabra			0.97				
Kappeli	1.12		1.5	2.74			
Salut		1.15	1.06	1.31		2.06	
Serena		1.09	1.01	1.74		1.33	
Egmont				1.4			
Gilroy							
Tierra				0.98		1.21	
Towanda		1.13	0.99	1.1			
Goldstone	0.004279/0.003476	0.00461/0.004468	0.006936/0.00305		0.005606/0.003001		
Jefferson	0.003762/0.003711	0.003956/0.003796	0.006011/0.003152		0.005011/0.003465		
Darwin	0.003875/0.003648	0.005705/0.00586	0.005284/0.004626		0.004895/0.003497		
Labquark	0.003103/0.002707	0.00566/0.005481	0.006609/0.005672		0.006729/0.005607		
Belmont	0.00525/0.004793	0.006099/0.006036	0.006792/0.004032		0.006434/0.005635		
Bodie	0.003909/0.003705	0.004531/0.004621			0.002545/0.00561		
Delamar	0.004111/0.004069	0.006322/0.006233					
Hardin	0.006579/0.005081	0.00694/0.006753		0.004142/0.004818		0.00696/0.004955	
Average	1.12	1.12	1.05	1.58		1.34	

Table A-4.2

Values Used to Determine Ratios of Surface and Downhole Ground Motions (Continued)

Vaules Used to Determine Ratios of Peak Surface and Downhole Vertical Displacements

Station	W27	W29	W12/30	W25	W25	W28	W28
Depth - m	35	83	352	358	305	375	358
Event							
Chancellor			1.02	1.1			
Cabra			0.97				
Kappeli	0.99		1	1.11			
Salut		1.05	0.98	1.08		1.08	
Serena		1.04	1.02	1.13		1.09	
Egmont				1.13			
Gibne							
Tierra				0.85		1.04	
Towanda		1.02	0.98	1.08			
Goldstone	0.112/0.11	0.1483/0.1514	0.1074/0.09893		0.1081/0.1028		
Jefferson	0.1108/0.109	0.1249/0.1264	0.105/0.09525		0.1071/0.09963		
Darwin	0.118/0.1123	0.2006/0.2012	0.1561/0.145		0.1237/0.1213		
Labquark	0.09823/0.09327	0.1862/0.1882	0.2056/0.182		0.186/0.1643		
Belmont	0.152/0.1439	0.2001/0.2112	0.1711/0.1583		0.1857/0.1762		
Bodie	0.1089/0.1061	0.1406/0.1474			0.0449/0.1577		
Delamar	0.1147/0.1124	0.2122/0.2124					
Hardin	0.1563/0.1571	0.2043/0.2071		0.07026/0.1614			0.173/0.1928
Average	0.99	1.03	0.99	1.08		0.98	

Vaules Used to Determine Ratios of Peak Surface and Downhole Radial Accelerations

Station	W27	W29	W12/30	W25	W25	W28	W28
Depth - m	35	83	352	358	305	375	358
Event							
Chancellor			1.03	2.7			
Cabra			1.24				
Kappeli	1.36		1.06	4.45			
Salut		2.09	1.7	3.67		1.04	
Serena		2.23	1.34	3.31		0.66	
Egmont							
Gibne							
Tierra				4.83		0.6	
Towanda		1.23	1.49	3.94			
Goldstone	0.08349/0.03315	0.0317/0.02817	0.09765/0.03754		0.06244/0.0653		
Jefferson	0.0577/0.02762	0.0248/0.02843	0.08018/0.03025		0.05006/0.0405		
Darwin	0.05811/0.03381	0.0308/0.01866	0.07624/0.02462		0.05991/0.02657		
Labquark	0.0326/0.02147	0.03319/0.02497	0.07833/0.02216		0.0638/0.0278		
Belmont	0.07586/0.03725	0.0404/0.02693	0.1532/0.04382		0.07954/0.05701		
Bodie	0.06069/0.02291	0.03496/0.02197			0.02636/0.0784		
Delamar	0.05849/0.02777	0.0315/0.02234					
Hardin	0.1775/0.06085	0.08188/0.06788		0.1078/0.09089			0.1602/0.07568
Average	1.36	2.10	1.32	3.48		1.19	

Table A-4.2

Values Used to Determine Ratios of Surface and Downhole Ground Motions (Continued)

Vaules Used to Determine Ratios of Peak Surface and Downhole Radial Velocities

Station	W27	W29	W12/30	W25	W25	W28	W28
Depth - m	35	83	352	358	305	375	358
Event							
Chancellor			1.42	2.22			
Cabra			1.77				
Kappeli	1.04		1.66	2.25			
Salut		1.22	1.59	3.3		2.89	
Serena		1.16	1.39	2.65		2.23	
Egmont				3.05			
Gibne							
Tierra				2.56		2.07	
Towanda		1.12	1.83	2.32			
Goldstone	0.003816/0.002826	0.005512/0.003589	0.005294/0.001816		0.004694/0.001912		
Jefferson	0.008551/0.003708	0.004865/0.003013	0.004281/0.001679		0.005116/0.001575		
Darwin	0.005118/0.004186	0.008371/0.005378	0.005421/0.001958		0.005381/0.007208		
Labquark	0.004227/0.00367	0.005286/0.004898	0.005774/0.00249		0.006026/0.002992		
Belmont	0.005094/0.004366	0.008333/0.007047	0.005275/0.002477		0.008672/0.003091		
Bodie	0.004286/0.003308	0.006688/0.003587			0.003134/0.004375		
Delamar	0.00445/0.004194	0.0082/0.004555					
Hardin	0.00604/0.005615	0.009206/0.006384		0.002759/0.004267		0.00971170.003882	
Average	1.04	1.18	1.55	2.59		2.32	

Vaules Used to Determine Ratios of Peak Surface and Downhole Radial Displacements

Station	W27	W29	W12/30	W25	W25	W28	W28
Depth - m	35	83	352	358	305	375	358
Event							
Chancellor			1.42	1.55			
Cabra			1.61				
Kappeli	0.85		1.64	2.63			
Salut		1.22	1.66	1.72		2.14	
Serena		1.09	1.15	2.98		1.93	
Egmont				2.32			
Gibne							
Tierra				2.78			
Towanda		1.1	1.81	2.45		1.5	
Goldstone	0.095/0.08315	0.1913/0.144	0.08143/0.05783		0.1258/0.05688		
Jefferson	0.2581/0.104	0.1668/0.0993	0.1002/0.05638		0.104/0.04686		
Darwin	0.1484/0.1411	0.2854/0.1716	0.1054/0.04902		0.147/0.06507		
Labquark	0.1021/0.09115	0.1925/0.18	0.2058/0.0959		0.2014/0.1233		
Belmont	0.1446/0.1319	0.2855/0.2432	0.1347/0.08661		0.2256/0.08887		
Bodie	0.1174/0.1105	0.2275/0.1304			0.08256/0.1895		
Delamar	0.1266/0.1319	0.3138/0.1708					
Hardin	0.1804/0.1745	0.3204/0.2074		0.06805/0.1197		0.2573/0.1314	
Average	0.85	1.21	1.52	2.12		1.87	

Table A-4.2

Values Used to Determine Ratios of Surface and Downhole Ground Motions (Continued)

Vaules Used to Determine Ratios of Peak Surface and Downhole Transverse Accelerations

Station	W27	W29	W12/30	W25	W25	W28	W28
Depth - m	35	83	352	358	305	375	358
Event							
Chancellor			3.37	8.22			
Cabra			1.99				
Kappeli	1.68		2.11	5.34			
Salut		1.44	1.97	4.79		1.11	
Serena		1.47	2.34	9.01		0.61	
Egmont				7.58			
Gibne							
Tierra				7.82		0.3	
Towanda		1.37	2.2	4.16			
Goldstone	0.04923/0.0268	0.03457/0.01483	0.1539/0.02558		0.0601/0.05852		
Jefferson	0.0405/0.02393	0.03422/0.01347	0.1384/0.01993		0.04342/0.04854		
Darwin	0.05048/0.03946	0.03763/0.01274	0.09191/0.01254		0.05915/0.02884		
Labquark	0.03816/0.02806	0.02883/0.01262	0.07754/0.0114		0.04343/0.03709		
Belmont	0.05646/0.03233	0.03667/0.01818	0.2365/0.02685		0.05045/0.06186		
Bodie	0.05017/0.0308	0.03895/0.01467			0.02519/0.09315		
Delamar	0.04426/0.03469	0.0291/0.01344					
Hardin	0.1184/0.07014	0.1685/0.03628		0.1476/0.05483			0.0842/0.05352
Average	1.68	1.53	2.54	6.90		0.92	

Vaules Used to Determine Ratios of Peak Surface and Downhole Transverse Velocities

Station	W27	W29	W12/30	W25	W25	W28	W28
Depth - m	35	83	352	358	305	375	358
Event							
Chancellor			1.79	3.28			
Cabra			1.08				
Kappeli	1.07		1.21	1.44			
Salut		1.15	2.1	2.18		2.47	
Serena		1.13	1.27	1.66		2.12	
Egmont				1.88			
Gibne							
Tierra				1.56		1.3	
Towanda		1.19	1.7	1.48			
Goldstone	0.005696/0.005047	0.004878/0.002638	0.006163/0.002599		0.005192/0.002856		
Jefferson	0.005039/0.004666	0.00435/0.003818	0.004868/0.002637		0.004834/0.002292		
Darwin	0.006773/0.006116	0.005195/0.002917	0.004688/0.002726		0.006892/0.003437		
Labquark	0.005052/0.004347	0.008124/0.004034	0.004539/0.002476		0.00605/0.002553		
Belmont	0.007286/0.007047	0.008112/0.004525	0.007039/0.004213		0.009423/0.005264		
Bodie	0.007052/0.005418	0.007011/0.004567			0.003119/0.006894		
Delamar	0.008947/0.008214	0.007461/0.005046					
Hardin	0.008122/0.007184	0.009393/0.005361		0.003614/0.004547			0.007866/0.004684
Average	1.07	1.11	1.61	1.91		1.82	

Table A-4.2

Values Used to Determine Ratios of Surface and Downhole Ground Motions (Concluded)

Vaules Used to Determine Ratios of Peak Surface and Downhole Transverse Displacements

Station	W27	W29	W12/30	W25	W25	W28	W28
Depth - m	35	83	352	358	305	375	358
Event							
Chancellor			1.33	1.43			
Cabra			1.09				
Kappeli	1.06		1.21	1.05			
Salut		1.05	1.86	1.64		1.94	
Serena		1.04	1.17	1.17		1.51	
Egmont				1.51			
Gibne							
Tierra				1.05		1.42	
Towanda		1.09	1.46	1.38			
Goldstone	0.1521/0.1373	0.1813/0.107	0.1156/0.08425		0.1705/0.0952		
Jefferson	0.151/0.1495	0.1724/0.1264	0.1433/0.09934		0.1324/0.08308		
Darwin	0.2669/0.2516	0.1877/0.1311	0.168/0.1201		0.1753/0.1267		
Labquark	0.1405/0.1321	0.294/0.1655	0.1507/0.1079		0.1606/0.1024		
Belmont	0.2807/0.269	0.3291/0.1995	0.2249/0.1605		0.2891/0.1848		
Bodie	0.1808/0.1705	0.2926/0.203			0.09659/0.2473		
Delamar	0.3319/0.303	0.2598/0.2057					
Hardin	0.2594/0.2406	0.3274/0.2084		0.09403/0.1979		0.2428/0.1917	
Average	1.06	1.06	1.45	1.35		1.46	

Table A-4.3

Summary of Depth Attenuation Curves for Peak UNE Ground Motions

Component	Equation
Peak Vertical Accel.	$a_d = a_s / (e^{1.8E-3\ z})$
Peak Vertical Vel.	$v_d = v_s / (e^{7.4E-4\ z})$
Peak Vertical Disp.	$d_d = d_s$
Peak Radial Accel.	$a_d = a_s / (e^{1.2E-3\ z})$
Peak Radial Vel.	$v_d = v_s / (e^{1.2E-3\ z})$
Peak Radial Disp.	$d_d = d_s / (e^{4.4E-4\ z})$
Peak Transverse Accel.	$a_d = a_s / (e^{2.3E-3\ z})$
Peak Transverse Vel.	$v_d = v_s / (e^{1.2E-3\ z})$
Peak Transverse Disp.	$d_d = d_s / (e^{7.8E-4\ z})$

Note: Subscript d is for downhole and s is for surface; z is depth in m.

Table A-4.4

Depth Attenuation of Component Ground Motions

Depth	Vertical			Radial			Transverse		
(m)	Accel	Vel	Disp	Accel	Vel	Disp	Accel	Vel	Disp
0	1	1	1	1	1	1	1	1	1
100	0.8	0.9	1	0.9	0.9	1	0.8	0.9	0.9
200	0.7	0.9	1	0.8	0.8	0.9	0.6	0.8	0.9
300	0.6	0.8	1	0.7	0.7	0.9	0.5	0.7	0.8
400	0.5	0.7	1	0.6	0.6	0.8	0.4	0.6	0.7
500	0.4	0.7	1	0.6	0.6	0.8	0.3	0.6	0.7

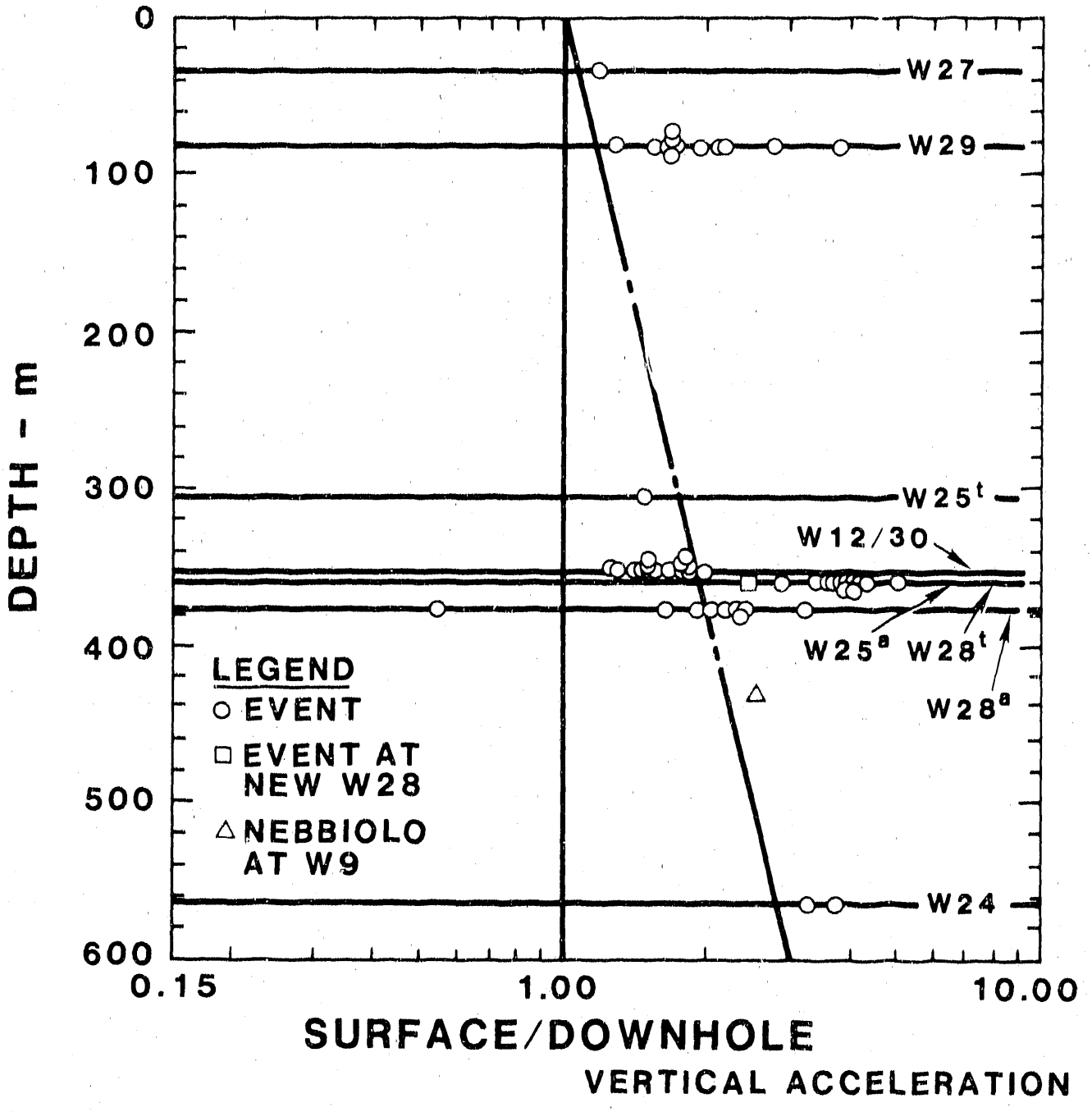

NOTES:
1. DOWNHOLE STATIONS AT W25 and W28 HAVE BEEN INSTALLED AT TWO DIFFERENT DEPTHS. "a" DENOTES THE INITIAL DEPTH. "t" DENOTES THE MOST RECENT DEPTH. THE NEW DEPTH FOR W28 IS THE SAME AS OLD W25.
2. THE LINE SHOWN IS THE FIT DISCUSSED IN THE TEXT.

Figure A-4.3. Surface/Downhole Ratios vs Depth for Vertical Acceleration

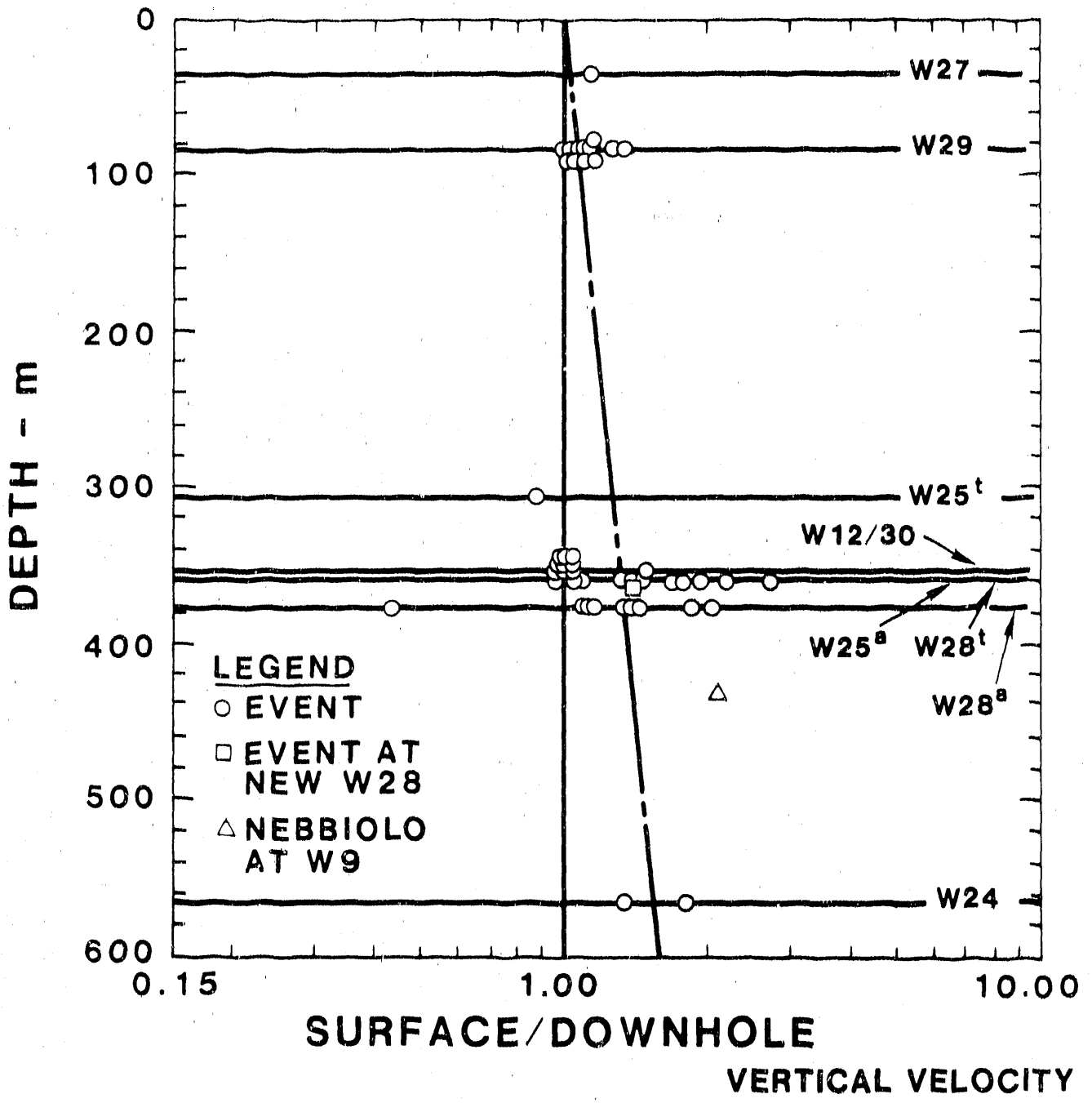

NOTES:
1. DOWNHOLE STATIONS AT W25 and W28 HAVE BEEN INSTALLED AT TWO DIFFERENT DEPTHS. "a" DENOTES THE INITIAL DEPTH. "t" DENOTES THE MOST RECENT. THE NEW DEPTH OF W28 IS THE SAME AS THE OLD FOR W25.
2. THE LINE SHOWN IS THE FIT DISCUSSED IN THE TEXT.

Figure A-4.4. Surface/Downhole Ratios vs Depth for Vertical Velocity

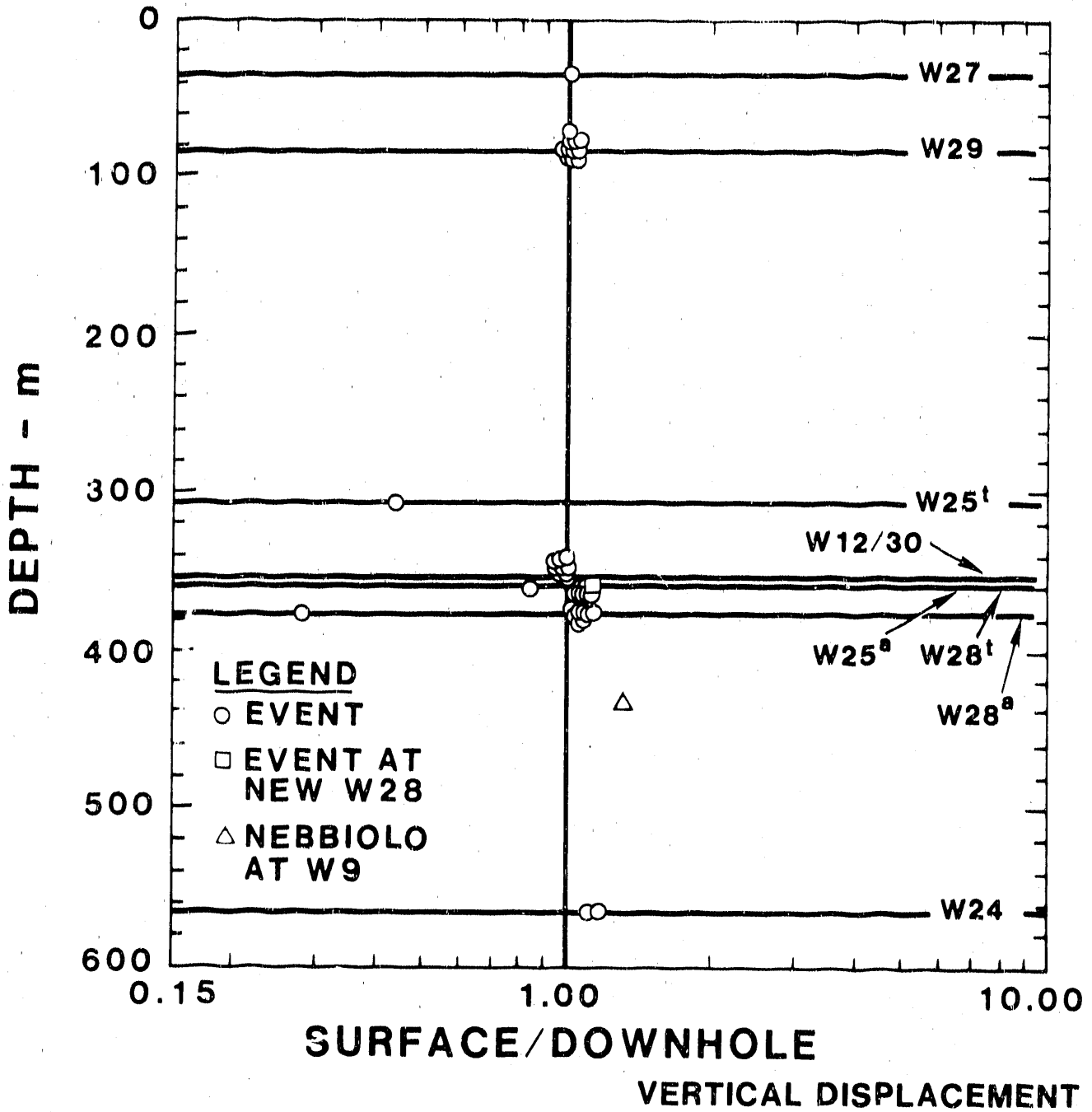

NOTES:
1. DOWNHOLE STATIONS AT W25 and W28 HAVE BEEN INSTALLED AT TWO DIFFERENT DEPTHS. "a" DENOTES ORIGINAL DEPTH. "t" DENOTES NEW DEPTH. NEW DEPTH OF W28 IS THE SAME AS OLD W25.
2. THE FIT FOR THESE DATA IS A VERTICAL LINE AT A RATIO OF 1.

Figure A-4.5. Surface/Downhole Ratios vs Depth for Vertical Displacement

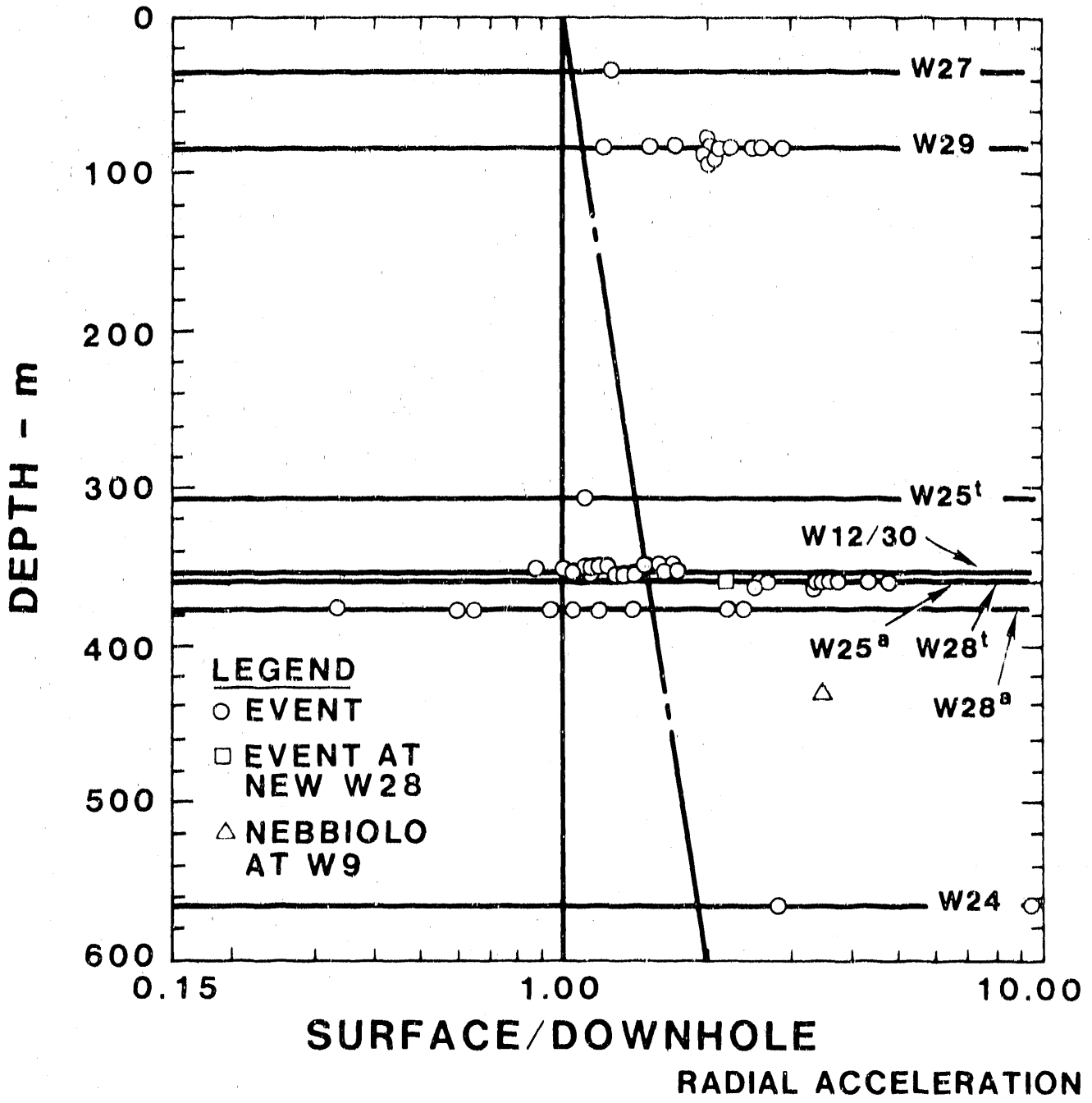

NOTES:
1. DOWNHOLE STATIONS AT W25 and W28 HAVE BEEN INSTALLED AT TWO DIFFERENT DEPTHS. "a" DENOTES ORIGINAL DEPTH. "t" DENOTES NEW DEPTH. NEW DEPTH OF W28 SAME AS OLD W25.
2. LINE SHOWN IS FIT DISCUSSED IN TEXT.

Figure A-4.6. Surface/Downhole Ratios vs Depth for Radial Acceleration

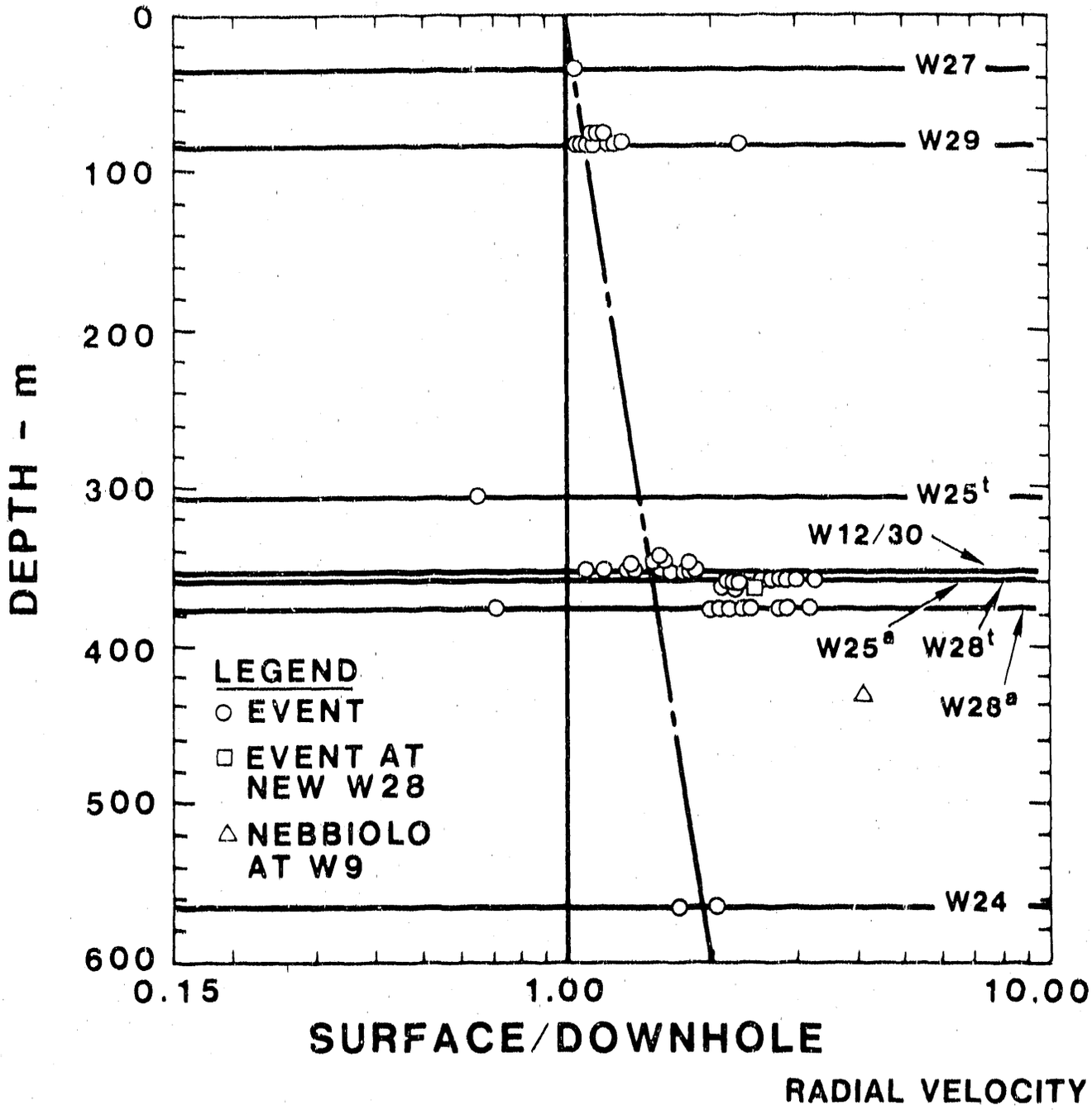

NOTES:
1. DOWNHOLE STATIONS AT W25 and W28 HAVE BEEN INSTALLED AT TWO DIFFERENT DEPTHS. "a" DENOTES ORIGINAL DEPTH. "t" DENOTES NEW DEPTH. NEW DEPTH OF W28 SAME AS OLD W25.
2. LINE SHOWN IS FIT DISCUSSED IN THE TEXT.

Figure A-4.7. Surface/Downhole Ratios vs Depth for Radial Velocity

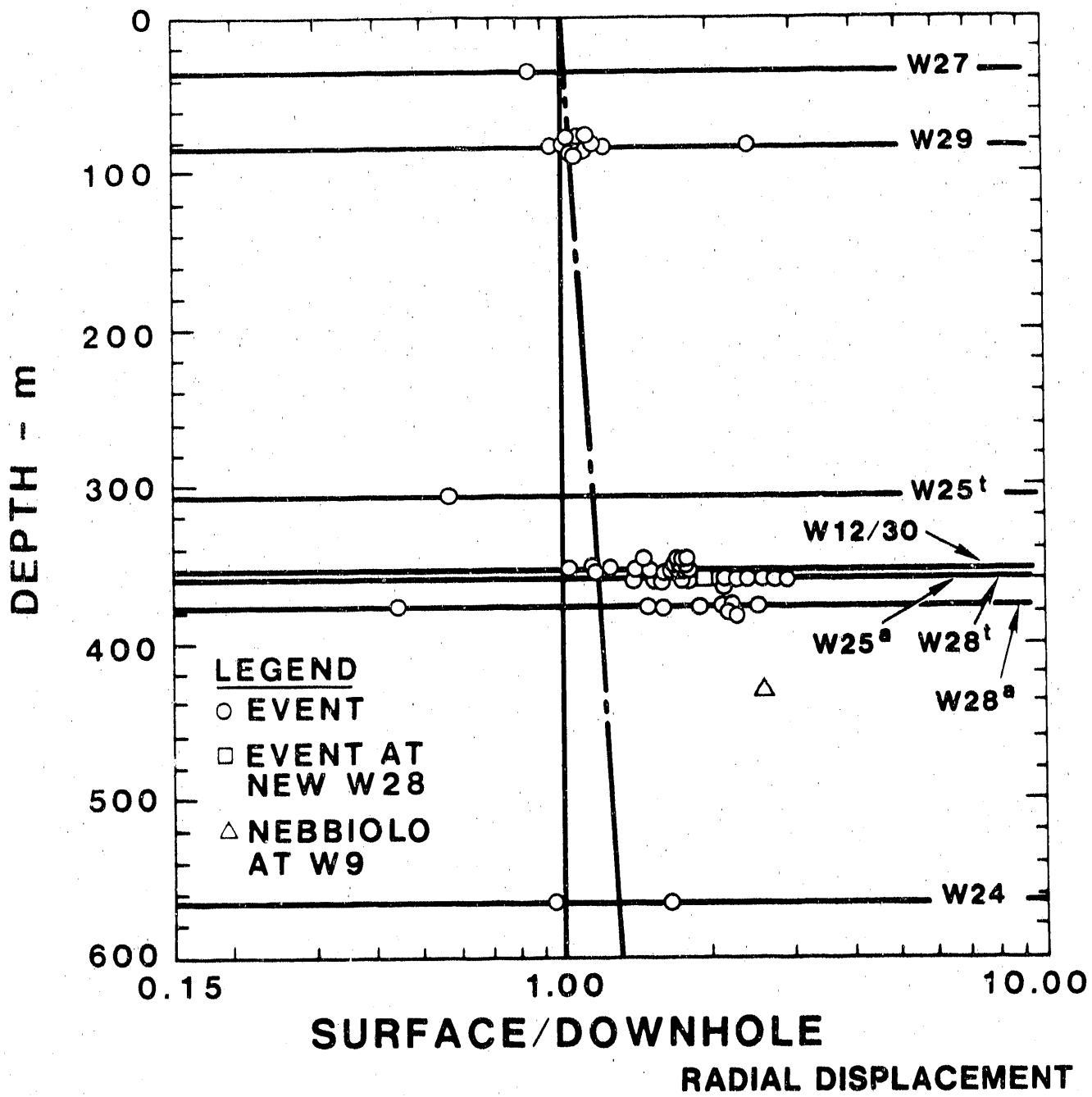

NOTES:
1. DOWNHOLE STATIONS AT W25 and W28 HAVE BEEN INSTALLED AT DIFFERENT DEPTHS. "a" DENOTES ORIGINAL DEPTH. "t" DENOTES NEW DEPTH. NEW DEPTH OF W28 SAME AS OLD W25.
2. LINE SHOWN IS FIT DISCUSSED IN THE TEXT.

Figure A-4.8. Surface/Downhole Ratios vs Depth for Radial Displacement

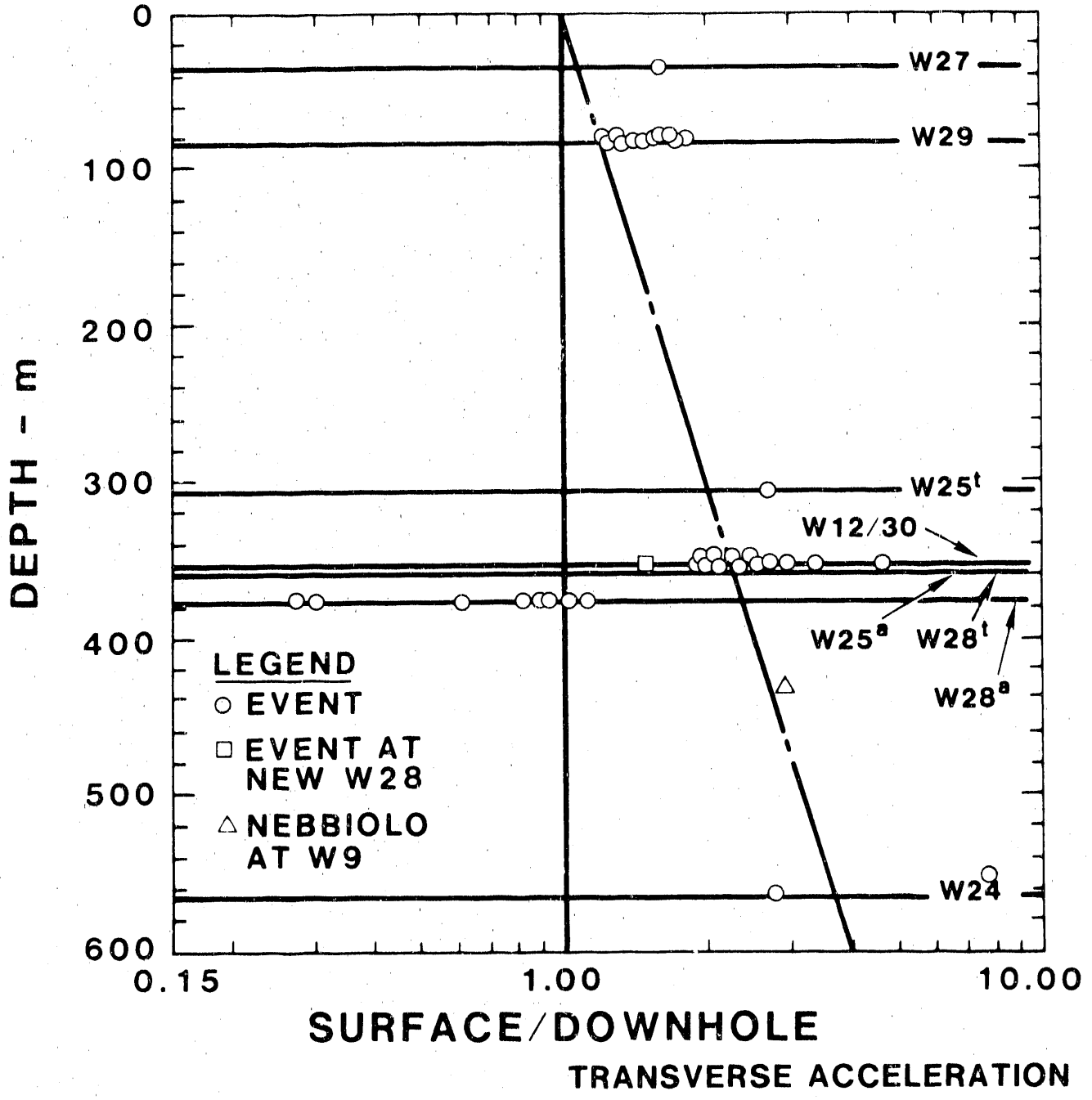

NOTES:
1. DOWNHOLE STATIONS AT W25 and W28 HAVE BEEN INSTALLED AT DIFFERENT DEPTHS. "a" DENOTES ORIGINAL DEPTH. "t" DENOTES NEW DEPTH. NEW DEPTH OF W28 SAME AS OLD W25.
2. LINE SHOWN IS FIT DISCUSSED IN TEXT.

Figure A-4.9. Surface/Downhole Ratios vs Depth for Transverse Acceleration

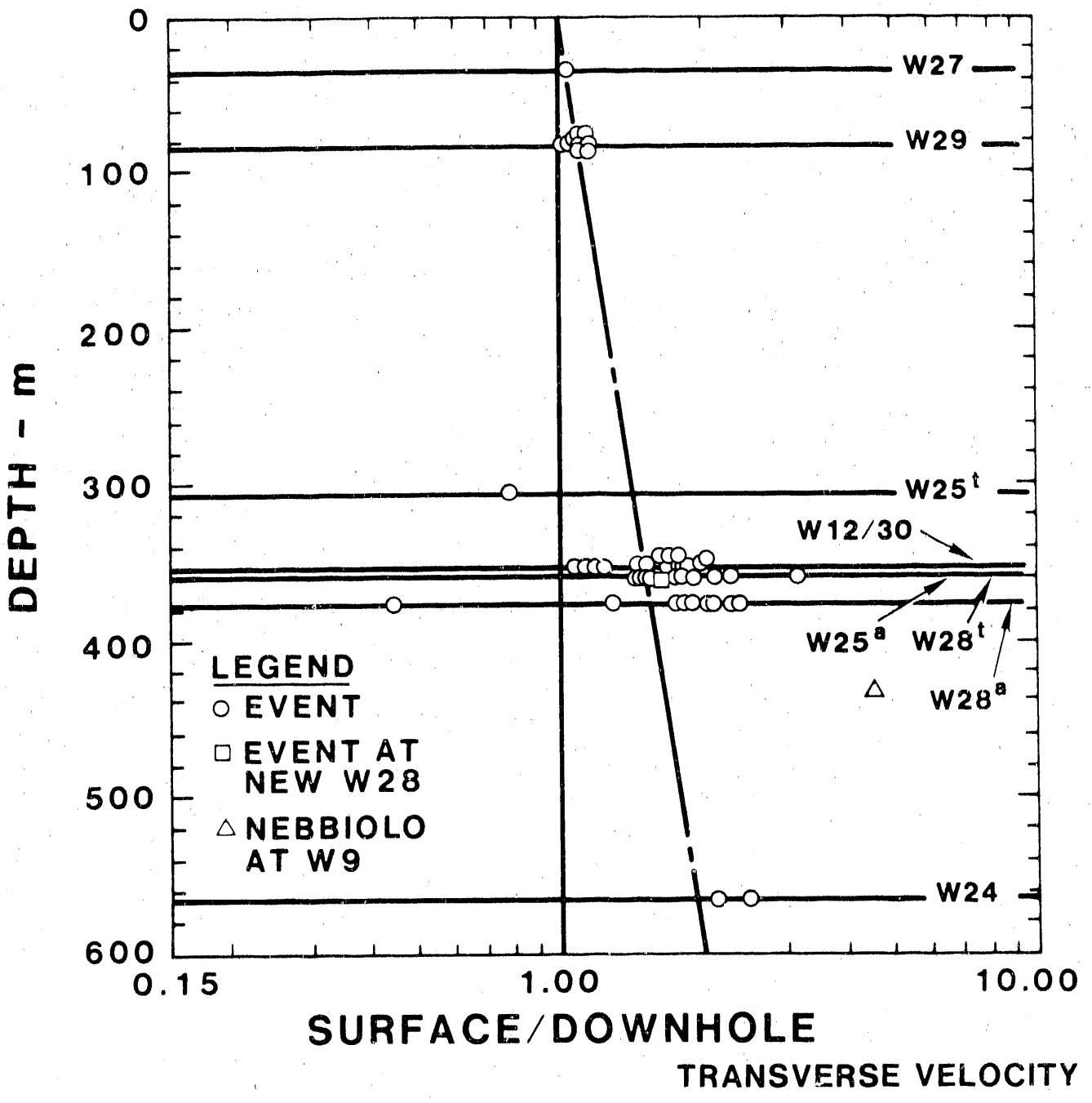

NOTES:
1. DOWNHOLE STATIONS AT W25 and W28 HAVE BEEN INSTALLED AT DIFFERENT DEPTHS. "a" DENOTES ORIGINAL DEPTH. "t" DENOTES NEW DEPTH. NEW DEPTH OF W28 SAME AS OLD W25.
2. LINE SHOWN IS FIT DISCUSSED IN TEXT.

Figure A-4.10. Surface/Downhole Ratios vs Depth for Transverse Velocity

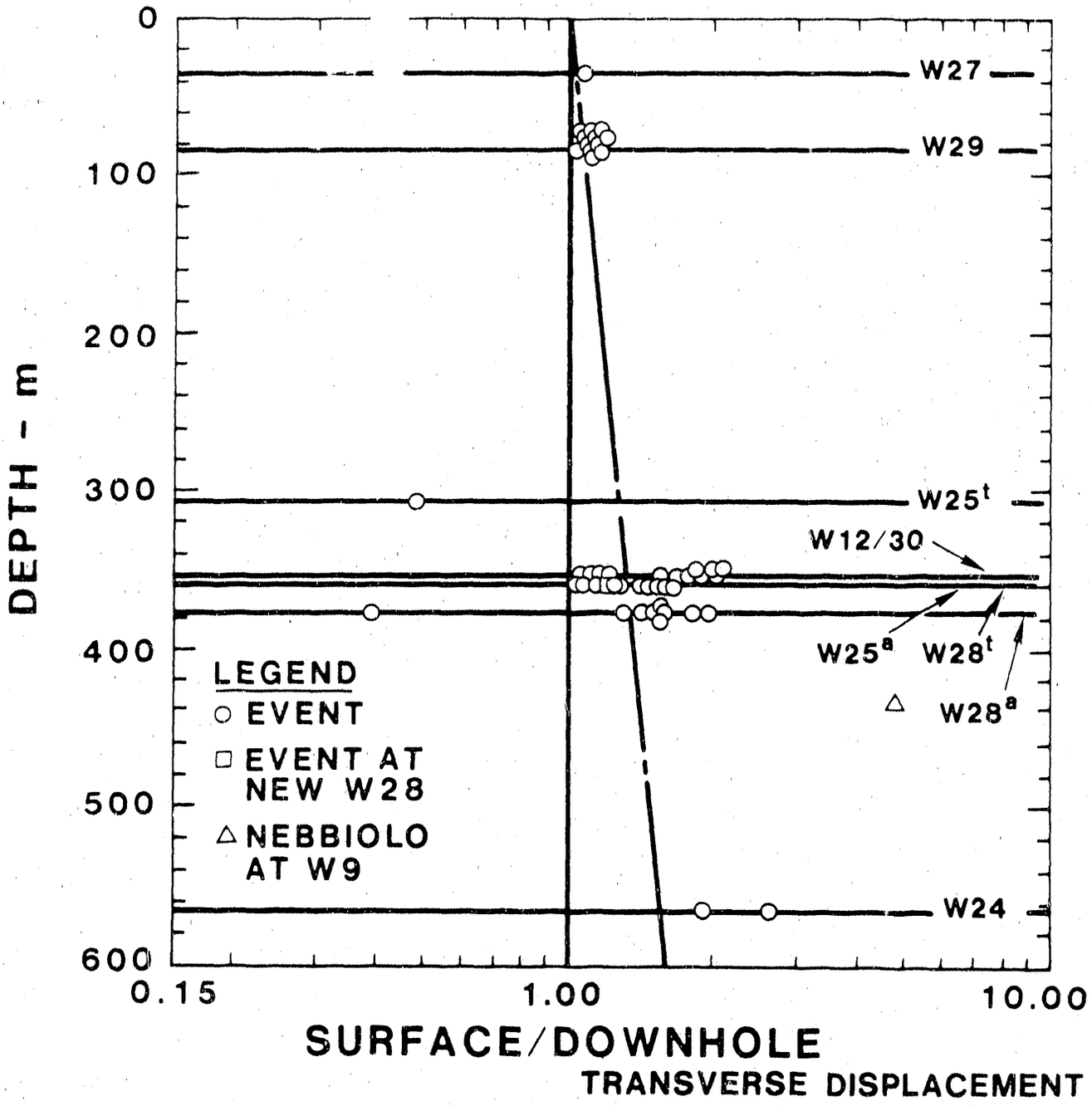

NOTES:
1. DOWNHOLE STATIONS AT W25 and W28 HAVE BEEN INSTALLED AT DIFFERENT DEPTHS. "a" DENOTES ORIGINAL DEPTH. "t" DENOTES NEW DEPTH. NEW DEPTH OF W28 SAME AS OLD W25.
2. LINE SHOWN IS FIT DISCUSSED IN TEXT.

Figure A-4.11. Surface/Downhole Ratios vs Depth for Transverse Displacement

which is located on Rainier Mesa at a distance of 15.9 km from surface ground zero. This combination roughly approximates the design basis UNE and the geology at Yucca Mountain. The depth of the station is 432 m. The surface-to-downhole ratios calculated for this event and station are also shown on Figures A-4.3 through A-4.11, which show that the surface-to-downhole ratios from this event were all greater than what the equations in Table A-4.3 would predict.

A-4.3 PSRV Attenuation

Similar depth attenuation ratios were developed for the PSRV data at 1, 2, and 5 Hz. Table A-4.5 shows the ratios calculated for each station. Table A-4.6 shows the actual PSRV values for the events not included in the study in Phillips (in review). These ratios were plotted with depth and are shown in Figures A-4.12 through A-4.20. The same considerations used for the peak ground motion parameters were used in deriving the depth attenuation curves. The results are similar. The data scatter in the ratios was generally smaller because the same ground motion wave types were compared in the ratios. As would be expected, the 1-Hz signal attenuated at a slower rate than that of the higher frequencies. The equations determined for these fits are given in Table A-4.7. The amount of attenuation predicted from these equations at various depths is summarized in Table A-4.8.

A-4.4 Conclusion

With the exception of the vertical displacement, all absolute peak values of the ground motion components decreased with increasing depth (accelerations at 400-m depth varied between 40 and 60% of the surface value, and velocities at this depth varied between 60 and 70% of the surface value). The PSRV data exhibited a similar decrease in amplitude with increasing depth. All of the frequencies examined had values at the 400-m depth that were between 40 and 60% of the surface values. The conclusion of this study, based on the data recorded at Yucca Mountain, is that UNE ground motions will attenuate with depth at the ESF. The amount of attenuation is subject to a large amount of uncertainty for the reasons

stated earlier. The specification of the design basis for the ESF has not taken depth attenuation into account, and, for this reason, the approach is conservative.

Table A-4.5

Ratios of Surface and Downhole PSRVs 1, 2, and 5 Hz

Station W25

	Vertical			Radial			Transverse		
Event	1 Hz	2 Hz	5 Hz	1 Hz	2 Hz	5 Hz	1 Hz	2 Hz	5 Hz
Labquark	1.7	3.1	2.7	1.2	2.9	3.5	2.5	8.6	7.2
Chancellor	1.5	2.8	2.9	2.4	2.1	3.5	1.8	5.1	8.3
Salut	1.7	3.8	3.8	3.8	2.2	4.9	2.6	5.5	6.6
Kappeli	1.6	5.4	3.8	2.3	1.7	3.5	1.8	6.4	9.3
Jefferson	1.7	5.2	4.7	2.1	2.8	2.9	3.1	4.7	8.6
Serena	1.3	5.1	4.4	2.3	2.2	3.7	1.6	4.8	11.2
Goldstone	1.8	4.0	4.6	3.2	2.8	2.8	1.7	4.5	5.6
Egmont	1.6	2.5	5.7	2.6	4.5	4.5	2.0	5.0	9.5
Towanda	1.5	2.6	2.7	1.6	2.9	4.6	2.5	4.0	5.7
Darwin	1.6	2.1	5.3	3.2	4.4	4.5	2.1	4.3	6.7
Belmont	1.7	4.7	4.5	2.9	2.9	1.7	2.0	3.9	13.0
Hardin #	0.6	1.8	1.7	0.7	1.0	1.2	0.8	1.5	2.3
Average	1.6	3.8	4.1	2.5	2.9	3.6	2.2	5.2	8.7

Station W12/30

	Vertical			Radial			Transverse		
Event	1 Hz	2 Hz	5 Hz	1 Hz	2 Hz	5 Hz	1 Hz	2 Hz	5 Hz
Labquark	1.5	3.6	1.4	1.2	2.5	0.8	2.8	2.3	3.1
Chancellor	1.5	2.7	1.7	1.9	2.7	0.8	3.0	2.1	2.3
Salut	1.5	3.1	1.5	1.5	1.4	1.3	2.1	2.5	1.6
Kappeli	1.5	2.6	1.4	1.4	1.5	1.0	1.6	2.8	1.4
Jefferson	1.5	2.1	1.5	1.3	1.3	0.8	2.4	1.8	1.5
Serena	1.4	2.9	1.6	1.4	1.6	0.7	1.7	2.5	1.6
Goldstone	1.5	3.1	1.8	1.7	1.1	0.8	3.4	2.4	1.9
Cabra	1.5	3.0	1.3	0.9	1.3	1.3	3.3	2.6	1.6
Towanda	1.4	1.8	1.3	1.7	1.9	0.8	2.4	2.0	2.0
Darwin	1.6	2.2	1.5	1.8	1.7	1.1	2.8	2.7	2.3
Delamar	1.4	2.2	1.8	1.8	1.4	1.1	2.2	1.6	1.9
Belmont	1.4	2.8	1.6	1.5	1.4	0.7	2.9	2.7	1.5
Bodie	1.5	1.9	1.4	1.1	1.5	0.8	1.7	2.2	1.7
Hardin	1.5	3.0	1.6	1.6	1.3	0.7	1.6	1.7	1.6
Average	1.5	2.6	1.5	1.5	1.6	0.9	2.4	2.3	1.9

Station W29

	Vertical			Radial			Transverse		
Event	1 Hz	2 Hz	5 Hz	1 Hz	2 Hz	5 Hz	1 Hz	2 Hz	5 Hz
Labquark	1.9	5.0	2.1	3.5	2.9	2.5	2.8	2.2	1.7
Tierra	1.7	3.9	2.5	4.8	3.8	1.1	3.1	1.4	0.8
Salut	2.9	4.0	3.1	3.3	1.9	2.3	4.0	2.6	2.0
Jefferson	2.6	4.2	2.6	5.8	2.3	2.0	2.8	2.9	2.3
Serena	1.4	3.1	2.1	3.3	3.5	1.2	3.7	1.7	1.5
Goldstone	2.9	3.9	2.4	3.3	3.3	1.5	4.1	2.8	2.2
Darwin	2.3	3.3	4.2	4.0	4.0	2.6	4.1	3.6	3.1
Belmont	2.1	3.4	3.3	4.6	3.3	2.1	3.6	1.9	1.9
Bodie	0.7	1.1	0.6	1.9	0.9	0.6	0.8	0.5	0.5
Hardin #	2.1	3.0	3.6	2.9	4.0	2.2	3.6	2.2	1.3
Average	2.1	3.5	2.5	3.7	2.9	1.8	3.2	2.2	1.8

Table A-4.5

Ratios of Surface and Downhole PSRVs 1, 2, and 5 Hz
(Concluded)

Station W29

	Vertical			Radial			Transverse		
Event	1 Hz	2 Hz	5 Hz	1 Hz	2 Hz	5 Hz	1 Hz	2 Hz	5 Hz
Loma Prieta	1.1	1.2	1.4	1.1	1.8	1.4	1.2	1.3	1.8
Salut	1.1	1.3	1.3	1.2	1.6	1.6	1.3	1.9	1.0
Jefferson	1.1	1.3	1.2	2.4	2.4	2.5	1.2	1.1	1.3
Serena	1.1	1.4	2.5	1.2	1.3	1.4	1.2	1.4	1.3
Goldstone	1.1	1.4	1.6	1.1	1.5	2.5	1.2	1.5	1.5
Towanda	1.1	1.4	2.1	1.1	1.7	1.7	1.1	1.8	1.1
Darwin	1.2	1.3	1.3	1.1	1.4	1.7	1.3	1.2	1.2
Delamar	1.2	1.3	1.8	1.2	2.0	2.0	1.3	1.4	1.9
Belmont	1.1	1.3	2.1	1.1	1.8	1.6	1.1	1.6	1.5
Bodie	1.1	1.4	1.6	1.1	2.1	2.4	1.3	1.7	1.2
Hardin	1.1	1.4	3.7	1.2	1.6	1.8	1.2	2.4	1.4
Average	1.1	1.3	1.9	1.3	1.7	1.9	1.2	1.6	1.4

Station W24

	Vertical			Radial			Transverse		
Event	1 Hz	2 Hz	5 Hz	1 Hz	2 Hz	5 Hz	1 Hz	2 Hz	5 Hz
Gibne	3.1	4.2	2.9	4.0	5.8	13.8	1.1	2.5	3.2
Cabra	2.4	3.8	4.6	1.3	2.3	2.3	2.5	6.2	10.9
Average	2.8	4.0	3.8	2.6	4.0	8.1	1.8	4.3	6.6

Station W27

	Vertical			Radial			Transverse		
Event	1 Hz	2 Hz	5 Hz	1 Hz	2 Hz	5 Hz	1 Hz	2 Hz	5 Hz
Kanpelli	1.0	1.1	1.2	0.9	1.1	1.6	1.0	1.3	1.8

Table A-4.6

Values Used to Determine Ratios of Surface and Downhole PSRVs for 1, 2, and 5 Hz

Station W25

	Vertical			Radial			Transverse		
Event	1 Hz	2 Hz	5 Hz	1 Hz	2 Hz	5 Hz	1 Hz	2 Hz	5 Hz
Labquark	1.7	3.1	2.7	1.2	2.9	3.5	2.5	8.6	7.2
Chancellor	1.5	2.8	2.9	2.4	2.1	3.5	1.8	5.1	8.3
Salut	1.7	3.8	3.8	3.8	2.2	4.9	2.6	5.5	6.6
Kappeli	1.6	5.4	3.8	2.3	1.7	3.5	1.8	6.4	9.3
Jefferson	1.7	5.2	4.7	2.1	2.8	2.9	3.1	4.7	8.6
Serena	1.3	5.1	4.4	2.3	2.2	3.7	1.6	4.8	11.2
Goldstone	1.8	4	4.6	3.2	2.8	2.8	1.7	4.5	9.6
Egmont	1.6	2.5	5.7	2.6	4.5	4.5	2	5	9.5
Towanda	1.5	2.6	2.7	1.6	2.9	4.6	2.5	4	5.7
Darwin	1.6/0.97	0.79/0.3	0.95/0.1	2/0.62	1.2/0.27	0.9/0.2	1/0.48	0.95/0.22	1/0.15
Belmont	1.2/0.7	1.5/0.32	1.9/0.42	1.2/0.42	1.7/0.58	1.1/0.64	0.7/0.35	1.5/0.38	3/0.23
Hardin #	0.72/1.3	0.6/0.33	1/0.58	0.72/1.1	0.43/0.4	0.6/0.5	0.47/0.5	0.52/0.35	1/0.43
Average	1.61	3.75	4.10	2.51	2.86	3.65	2.15	5.17	8.70

Station W12/30

	Vertical			Radial			Transverse		
Event	1 Hz	2 Hz	5 Hz	1 Hz	2 Hz	5 Hz	1 Hz	2 Hz	5 Hz
Labquark	1.5	3.6	1.4	1.2	2.5	0.8	2.8	2.3	3.1
Chancellor	1.5	2.7	1.7	1.9	2.7	0.8	3	2.1	2.3
Salut	1.5	3.1	1.5	1.5	1.4	1.3	2.1	2.5	1.6
Kappeli	1.5	2.6	1.4	1.4	1.5	1	1.6	2.8	1.4
Jefferson	1.5	2.1	1.5	1.3	1.3	0.8	2.4	1.8	1.5
Serena	1.4	2.9	1.6	1.4	1.6	0.7	1.7	2.5	1.6
Goldstone	1.5	3.1	1.8	1.7	1.1	0.8	3.4	2.4	1.9
Cabra	1.5	3	1.3	0.9	1.3	1.3	3.3	2.6	1.6
Towanda	1.4	1.8	1.3	1.7	1.9	0.8	2.4	2	2
Darwin	2.8/1.8	0.5/0.23	0.3/0.2	1.8/1	0.38/0.2	0.19/0.1	0.9/0.32	0.38/0.14	0.2/0.08
Delamar	2.1/1.5	0.6/0.27	0.44/0.2	1.5/0.85	0.55/0.4	0.22/0.2	0.8/0.36	0.42/0.26	0.25/0.1
Belmont	2.1/1.5	0.85/0.3	0.3/0.19	1.2/0.8	0.58/0.4	0.2/0.28	1/0.34	0.65/0.24	0.24/0.1
Bodie	2/1.3	0.52/0.2	0.27/0.1	1.1/0.98	0.5/0.33	0.16/0.2	1/0.6	0.67/0.3	0.17/0.1
Hardin	2.1/1.4	0.9/0.3	0.8/0.5	1.8/1.1	0.59/0.4	0.48/0.6	1.6/1	0.63/0.37	0.55/0.3
Average	1.48	2.65	1.53	1.49	1.61	0.91	2.42	2.28	1.86

Station W28

	Vertical			Radial			Transverse		
Event	1 Hz	2 Hz	5 Hz	1 Hz	2 Hz	5 Hz	1 Hz	2 Hz	5 Hz
Labquark	1.9	5	2.1	3.5	2.9	2.5	2.8	2.	1.7
Tierra	1.7	3.9	2.5	4.8	3.8	1.1	3.1	1.4	0.8
Salut	2.9	4	3.1	3.3	1.9	2.3	4	2.6	2
Jefferson	2.6	4.2	2.6	5.8	2.3	2	2.8	2.9	2.3
Serena	1.4	3.1	2.1	3.3	3.5	1.2	3.2	1.7	1.5
Goldstone	2.9	3.9	2.4	3.3	3.3	1.5	4.1	2.8	2.2
Darwin	1.8/0.78	1/0.3	0.67/0.1	2/0.5	1.2/0.3	0.36/0.1	1.9/0.46	0.8/0.21	0.34/0.1
Belmont	1.6/0.75	1.7/0.5	1/0.3	2/0.5	1.5/0.47	0.65/0.3	1.8/0.5	1/0.53	0.34/0.1
Bodie	0.8/1.2	0.98/0.9	0.28/0.4	0.8/0.8	0.7/0.76	0.19/0.3	0.7/0.85	0.43/0.8	0.16/0.3
Hardin #	1.8/0.86	1.9/0.6	1.5/0.58	2/0.7	1.7/0.42	0.92/0.4	2.5/0.7	1.1/0.5	0.41/0.2
Average	2.06	3.55	2.54	3.67	2.87	1.77	3.17	2.20	1.77

Table A-4.6

Values Used to Determine Ratios of Surface and Downhole PSRVs for 1, 2, and 5 Hz (Concluded)

Station W29

	Vertical			Radial			Transverse		
Event	1 Hz	2 Hz	5 Hz	1 Hz	2 Hz	5 Hz	1 Hz	2 Hz	5 Hz
Labquark	1.1	1.2	1.4	1.1	1.8	1.4	1.2	1.2	1.8
Salut	1.1	1.3	1.3	1.2	1.6	1.6	1.3	1.9	1
Jefferson	1.1	1.3	1.2	2.4	2.4	2.5	1.2	1.1	1.3
Serena	1.1	1.4	2.5	1.2	1.3	1.4	1.2	1.4	1.3
Goldstone	1.1	1.4	1.6	1.1	1.5	2.5	1.2	1.5	1.5
Towanda	1.1	1.4	2.1	1.1	1.7	1.7	1.1	1.8	1.1
Darwin	1.7/1.4	0.58/0.4	0.24/0.1	0.98/0.9	0.49/0.3	0.3/0.18	1.3/1	0.56/0.45	0.35/0.3
Delamar	1.4/1.2	0.9/0.7	0.3/0.17	1/0.85	1/0.5	0.38/0.1	1/0.75	0.7/0.5	0.4/0.21
Belmont	1.7/1.6	1.3/1	0.4/0.19	1/0.9	0.75/0.4	0.5/0.31	1/0.91	1/0.62	0.4/0.27
Bodie	1.2/1.1	1/0.72	0.26/0.1	0.75/0.6	0.82/0.4	0.4/0.17	1.9/1.5	0.85/0.5	0.44/0.3
Hardin	1.6/1.4	1.1/0.78	0.73/0.2	1.4/1.2	0.82/0.5	0.8/0.45	2.2/1.9	1.2/0.5	0.8/0.58
Average	1.12	1.33	1.87	1.25	1.74	1.86	1.21	1.57	1.38

Station W24

	Vertical			Radial			Transverse		
Event	1 Hz	2 Hz	5 Hz	1 Hz	2 Hz	5 Hz	1 Hz	2 Hz	5 Hz
Gibne	0.9/0.29	1.3/0.31	1.4/0.48	0.8/0.2	1.1/0.19	1.8/0.13	0.53/0.5	1/0.4	1.6/0.5
Cabra	0.48/0.2	0.75/0.2	0.55/0.1	0.4/0.32	0.5/0.22	0.3/0.13	0.6/0.24	0.8/0.13	0.52/0.0
Average	2.75	3.97	3.75	2.63	4.03	8.08	1.78	4.33	6.60

Station W27

	Vertical			Radial			Transverse		
Event	1 Hz	2 Hz	5 Hz	1 Hz	2 Hz	5 Hz	1 Hz	2 Hz	5 Hz
Kappelli	0.82/0.8	0.9/0.85	0.29/0.2	0.6/0.69	0.8/0.71	0.35/0.2	0.65/0.6	1/0.8	0.39/0.2

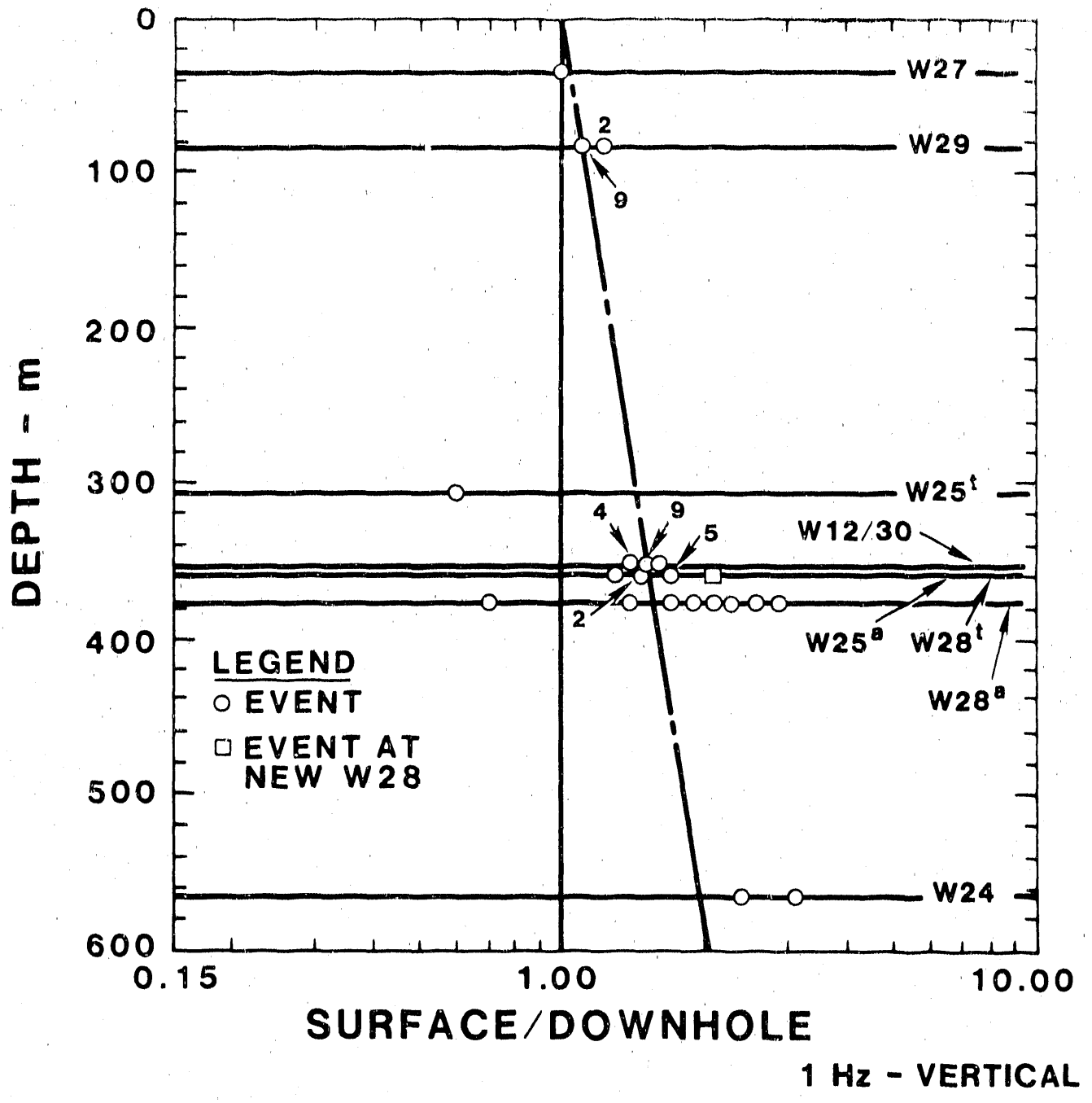

NOTES:

1. **DOWNHOLE STATIONS AT W25 and W28 HAVE BEEN INSTALLED AT TWO DIFFERENT DEPTHS. "a" DENOTES THE INITIAL DEPTH. "t" DENOTES THE MOST RECENT DEPTH. THE NEW DEPTH OF W28 IS THE SAME AS THE OLD DEPTH FOR W25.**
2. **NUMBERS ABOVE THE POINTS INDICATE SEVERAL OF THE EVENTS HAD THE SAME RATIO.**
3. **THE LINE SHOWN IS THE FIT DISCUSSED IN THE TEXT.**

Figure A-4.12. Surface/Downhole Ratios vs Depth for PSRVs of Vertical Motions at 1 Hz

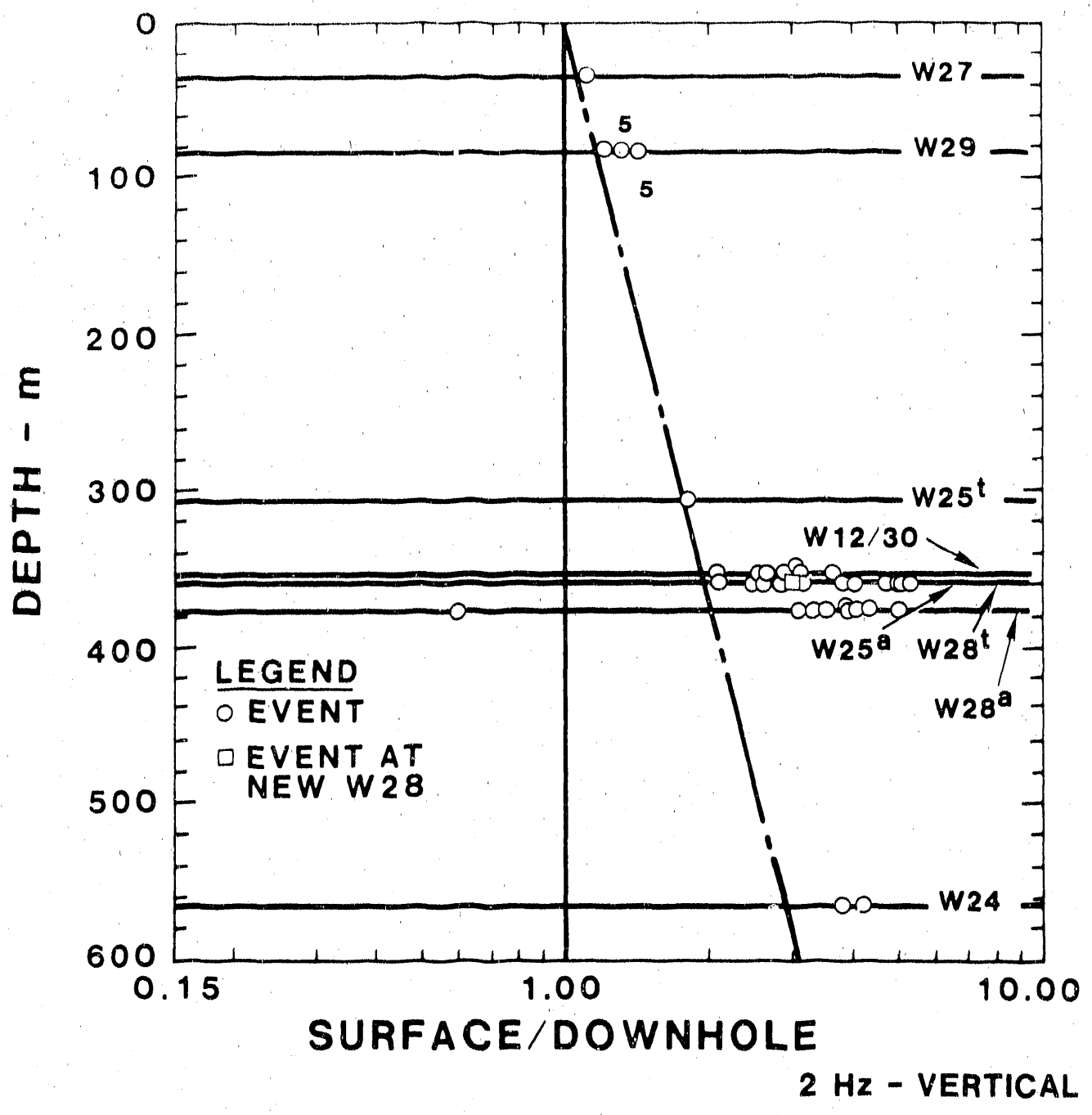

NOTES:
1. DOWNHOLE STATIONS AT W25 and W28 HAVE BEEN INSTALLED AT DIFFERENT DEPTHS. "a" DENOTES OLD DEPTH. "t" DENOTES NEW DEPTH. NEW DEPTH OF W28 SAME AS OLD W25.
2. NUMBER ABOVE POINTS INDICATE SEVERAL EVENTS WITH SAME RATIO.
3. LINE SHOWN IS FIT DISCUSSED IN TEXT.

Figure A-4.13. Surface/Downhole Ratios vs Depth for PSRVs of Vertical Motions at 2 Hz

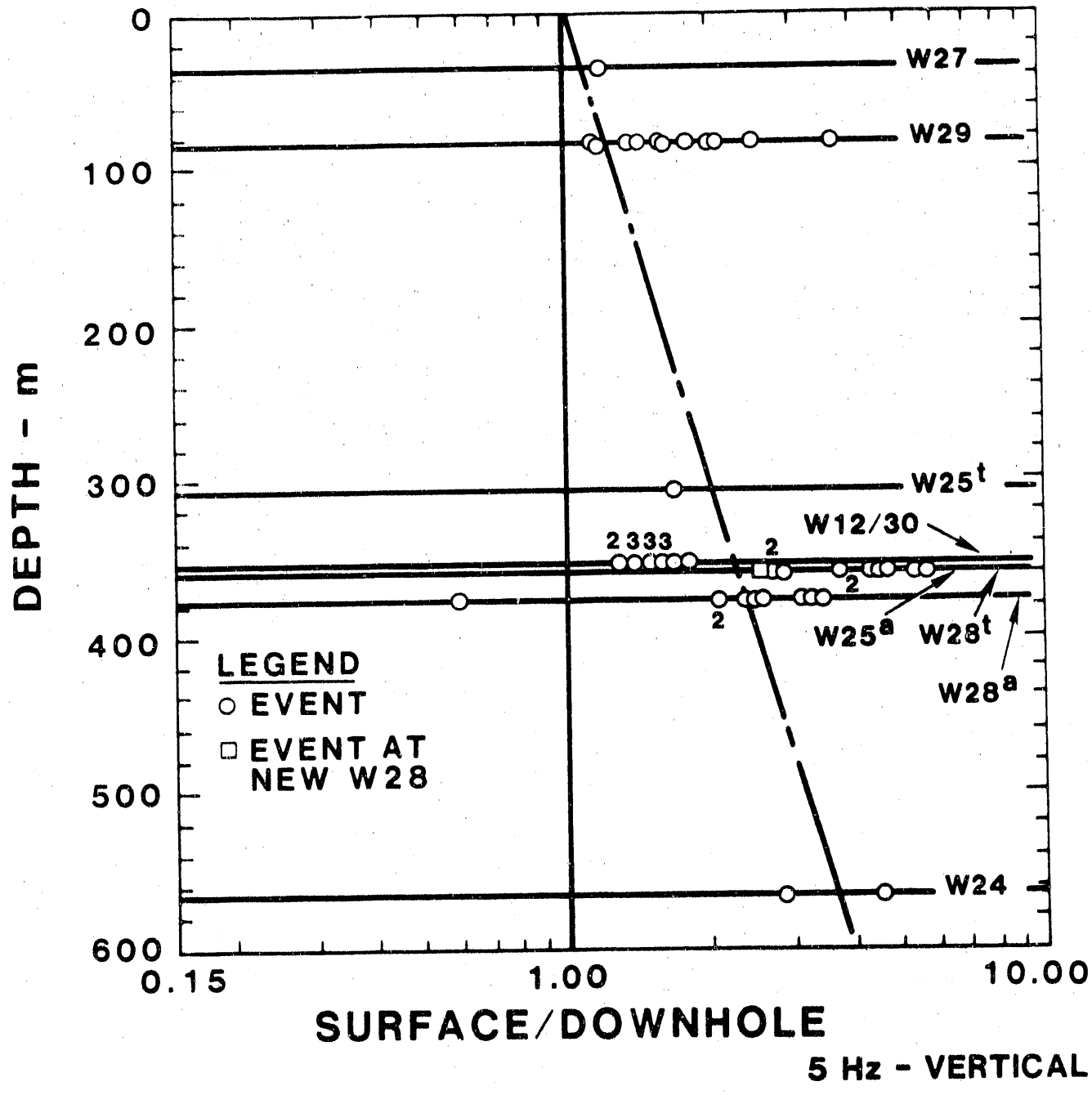

NOTES:
1. DOWNHOLE STATIONS AT W25 and W28 HAVE BEEN INSTALLED AT DIFFERENT DEPTHS. "a" DENOTES OLD DEPTH. "t" DENOTES NEW DEPTH. NEW W28 IS AT SAME DEPTH AS OLD W25.
2. NUMBERS ABOVE POINTS INDICATE SEVERAL EVENTS WITH SAME RATIO.
3. LINE SHOWN IS FIT DISCUSSED IN TEXT.

Figure A-4.14. Surface/Downhole Ratios vs Depth for PSRVs of Vertical Motions at 5 Hz

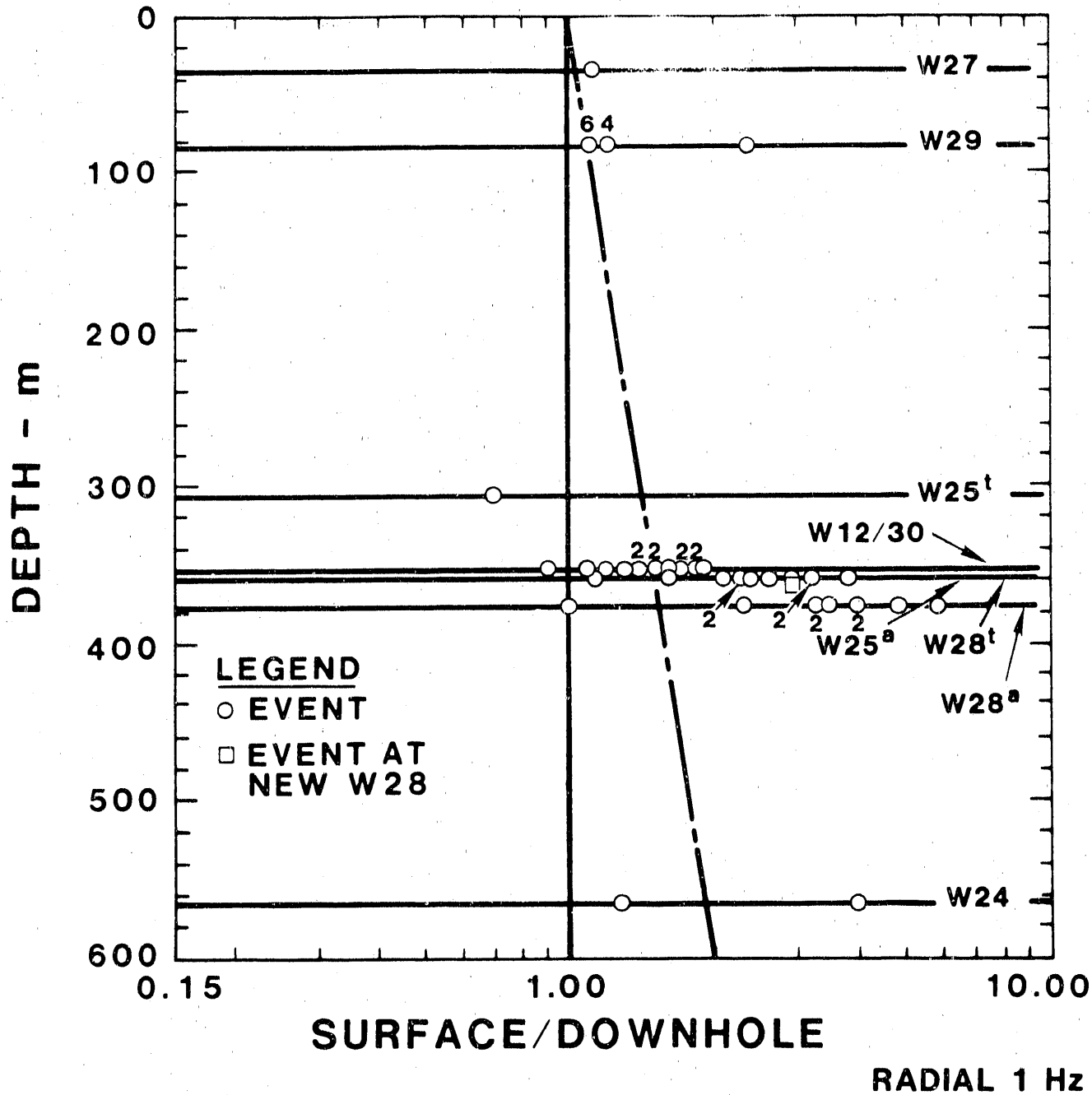

NOTES:
1. **DOWNHOLE STATIONS AT W25 and W28 HAVE BEEN INSTALLED AT DIFFERENT DEPTHS. "a" DENOTES ORIGINAL DEPTH. "t" DENOTES OLD DEPTH. NEW DEPTH OF W28 SAME AS OLD W25.**
2. **NUMBERS ABOVE POINTS INDICATE SEVERAL EVENTS WITH SAME RATIO.**
3. **LINE SHOWN IS FIT DISCUSSED IN TEXT.**

Figure A-4.15. Surface/Downhole Ratios vs Depth for PSRVs of Radial Motions at 1 Hz

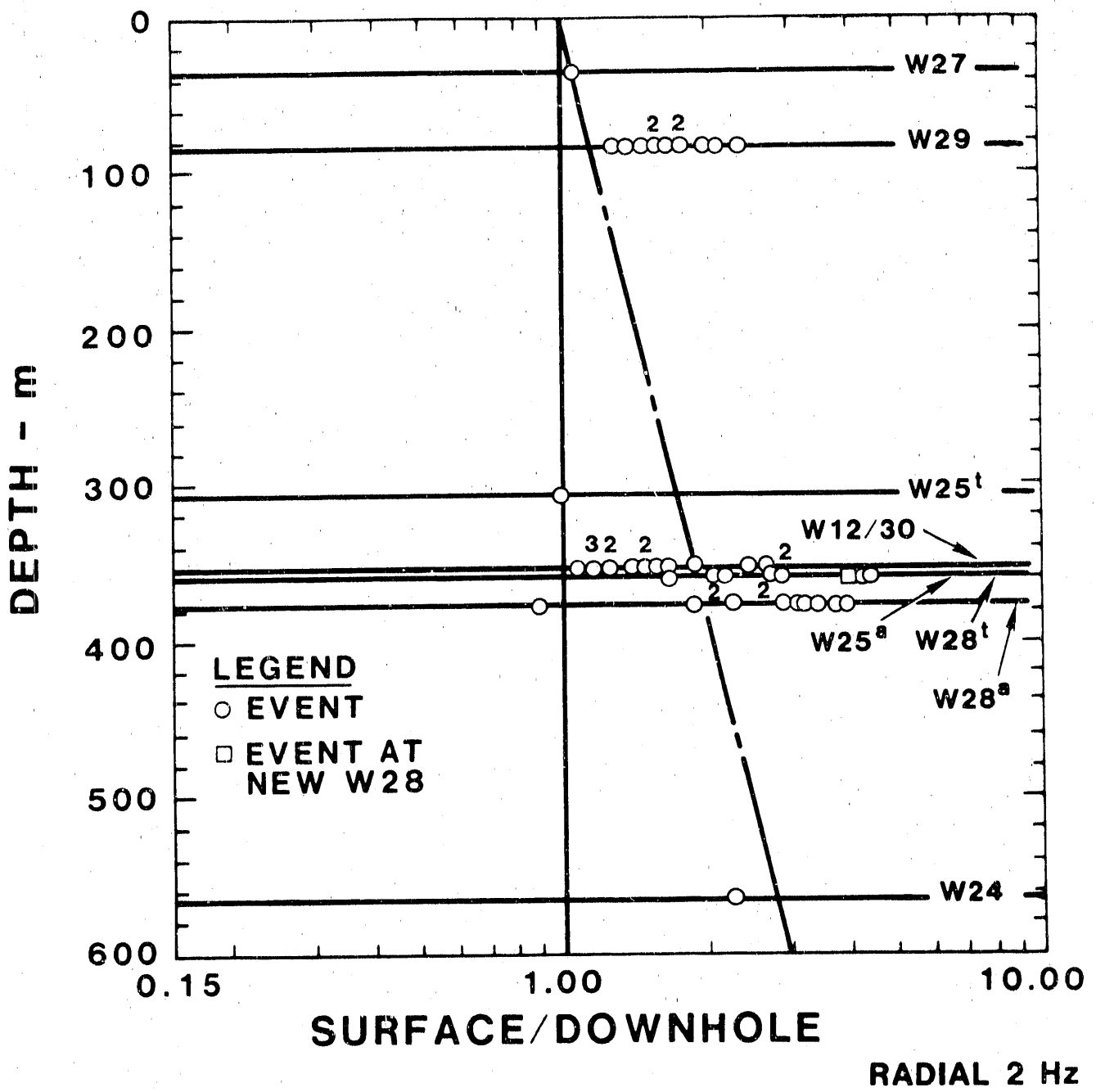

NOTES:

1. **DOWNHOLE STATIONS AT W25 and W28 HAVE BEEN INSTALLED AT DIFFERENT DEPTHS. "a" DENOTES ORIGINAL DEPTH. "t" DENOTES NEW DEPTH. NEW DEPTH OF W28 SAME AS OLD W25.**
2. **NUMBERS ABOVE POINTS INDICATE SEVERAL EVENTS WITH SAME RATIO.**
3. **LINE SHOWN IS FIT DISCUSSED IN TEXT.**

Figure A-4.16. Surface/Downhole Ratios vs Depth for PSRVs of Radial Motions at 2 Hz

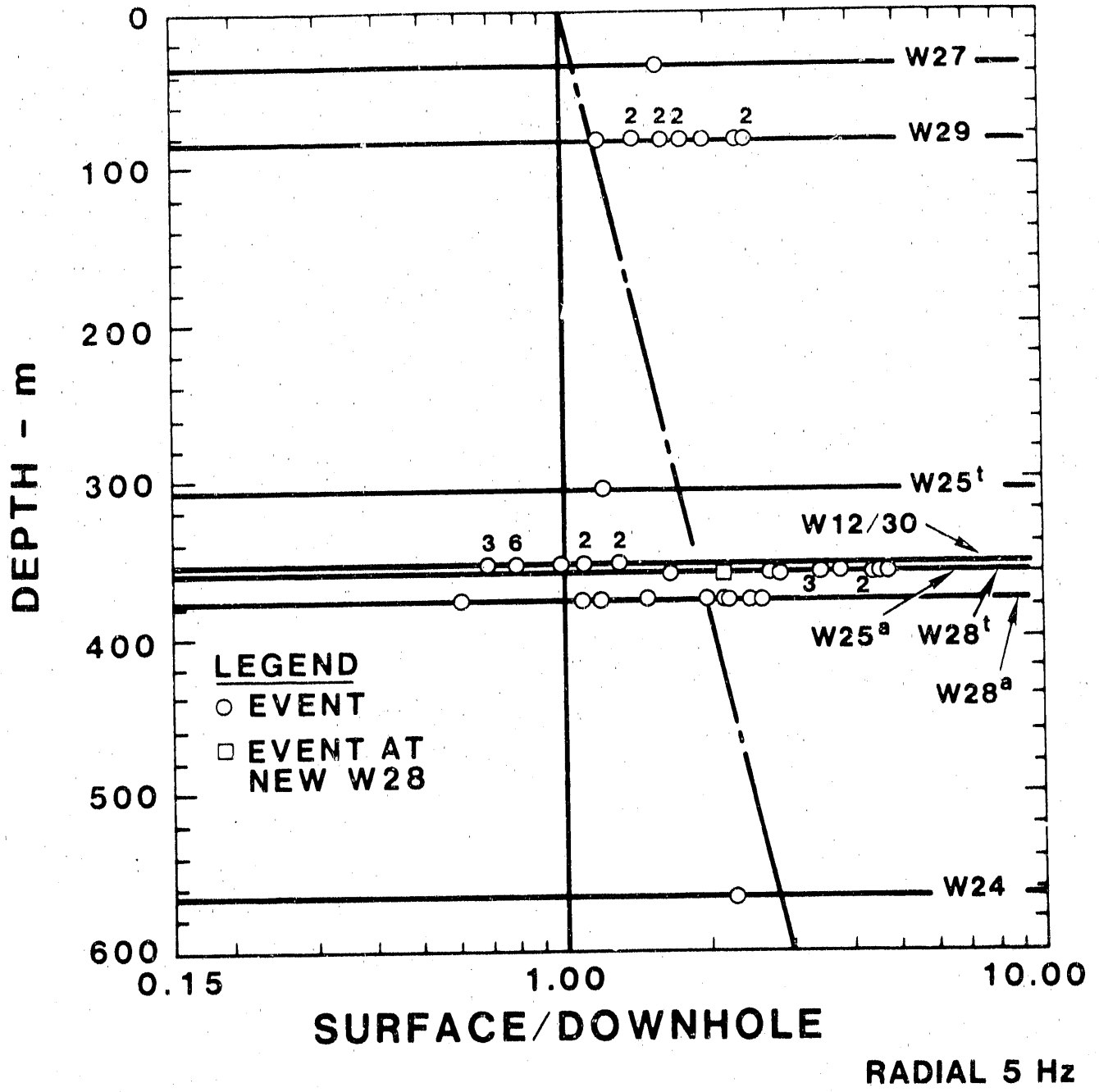

NOTES:
1. DOWNHOLE STATIONS AT W25 and W28 HAVE BEEN INSTALLED AT DIFFERENT DEPTHS. "a" DENOTES ORIGINAL DEPTH. "t" DENOTES NEW DEPTH. NEW DEPTH OF W28 SAME AS OLD W25.
2. NUMBERS ABOVE POINTS INDICATE SEVERAL EVENTS WITH SAME RATIO.
3. LINE SHOWN IS FIT DISCUSSED IN TEXT.

Figure A-4.17. Surface/Downhole Ratios vs Depth for PSRVs of Radial Motions at 5 Hz

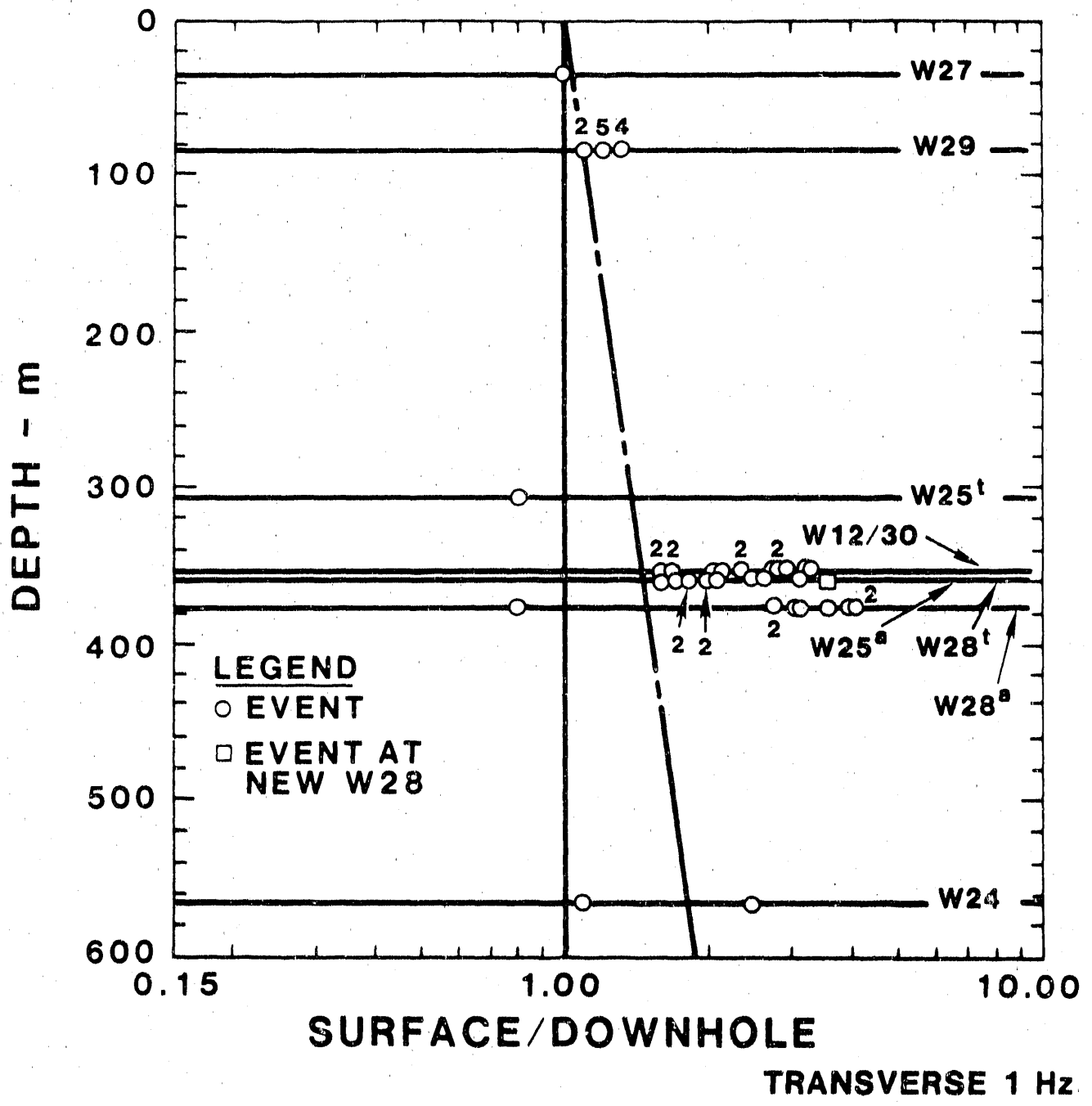

NOTES:
1. DOWNHOLE STATIONS AT W25 and W28 HAVE BEEN INSTALLED AT DIFFERENT DEPTHS. "a" DENOTES OLD DEPTH. "t" DENOTES NEW DEPTH. NEW DEPTH OF W28 SAME AS OLD W25.
2. NUMBERS ABOVE POINTS INDICATE SEVERAL EVENTS WITH SAME RATIO.
3. LINE SHOWN IS FIT DISCUSSED IN TEXT.

Figure A-4.18. Surface/Downhole Ratios vs Depth for PSRVs of Transverse Motions at 1 Hz

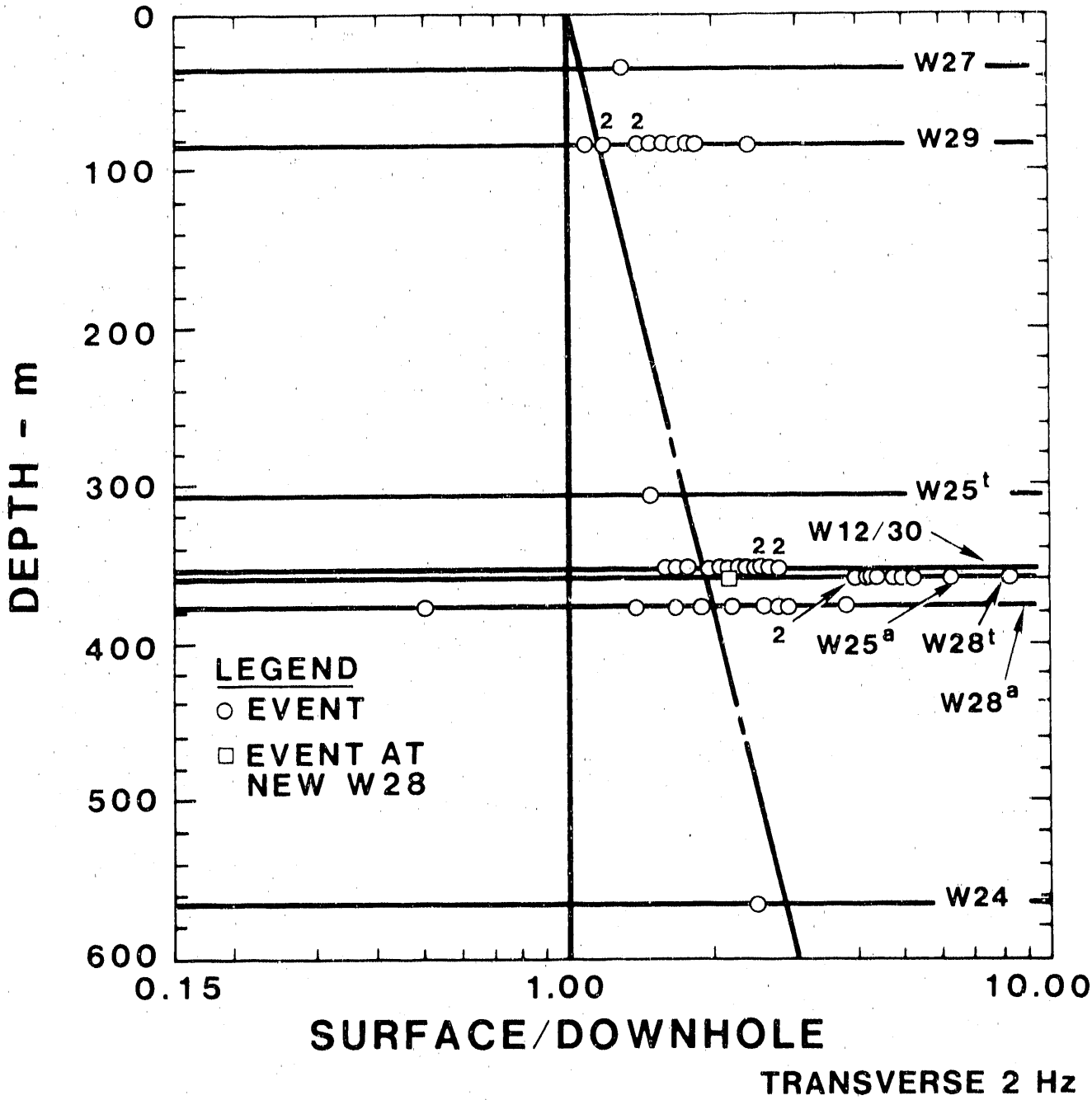

NOTES:
1. DOWNHOLE STATIONS AT W25 and W28 HAVE BEEN INSTALLED AT DIFFERENT DEPTHS."a" DENOTES OLD DEPTH. "t" DENOTES NEW DEPTH. NEW DEPTH OF W28 SAME AS OLD W25.
2. NUMBERS ABOVE POINTS INDICATE SEVERAL EVENTS WITH SAME RATIO.
3. LINE SHOWN IS FIT DISCUSSED IN TEXT.

Figure A-4.19. Surface/Downhole Ratios vs Depth for PSRVs of Transverse Motions at 2 Hz

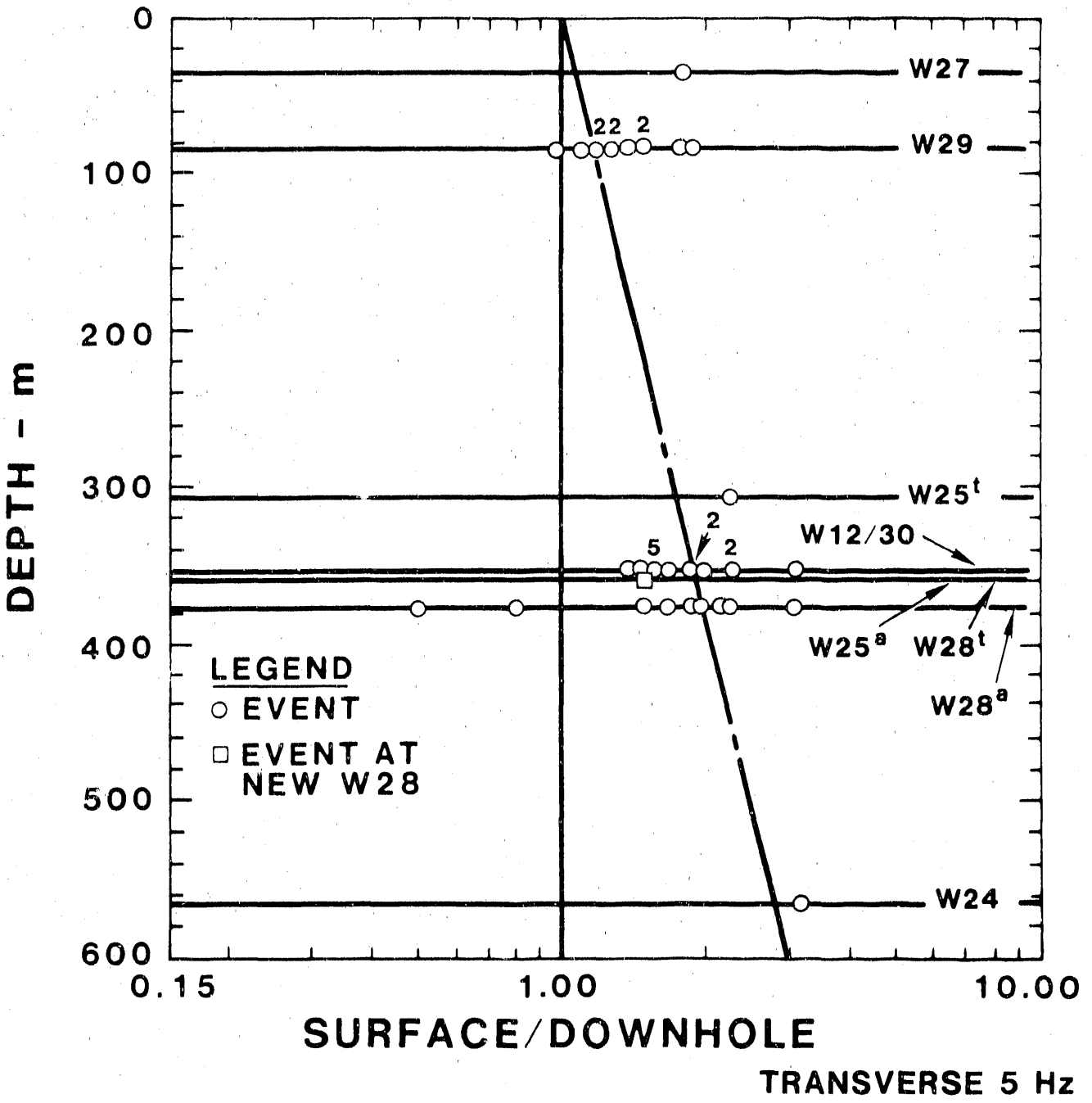

NOTES:
1. DOWNHOLE STATIONS AT W25 and W28 HAVE BEEN INSTALLED AT DIFFERENT DEPTHS. "a" DENOTES OLD DEPTH. "t" DENOTES NEW DEPTH. NEW DEPTH W28 SAME AS OLD W25.
2. NUMBERS ABOVE POINTS INDICATE SEVERAL EVENTS WITH SAME RATIO.
3. LINE SHOWN IS FIT DISCUSSED IN TEXT.

Figure A-4.20. Surface/Downhole Ratios vs Depth for PSRVs of Transverse Motions at 5 Hz

Table A-4.7

Summary of PSRV Depth Attenuation Curves for 1, 2, and 5 Hz

Component	Equation
Vertical @ 1 Hz	downhole = surface / ($e^{1.2E-3\ z}$)
Vertical @ 2 Hz	downhole = surface / ($e^{1.8E-3\ z}$)
Vertical @ 5 Hz	downhole = surface / ($e^{2.3E-3\ z}$)
Radial @ 1 Hz	downhole = surface / ($e^{1.2E-3\ z}$)
Radial @ 2 and 5 Hz	downhole = surface / ($e^{1.8E-3\ z}$)
Transverse @ 1 Hz	downhole = surface / ($e^{1.1E-3\ z}$)
Transverse @ 2 & 5 Hz	downhole = surface / ($e^{1.8E-3\ z}$)

Table A-4.8

Depth Attenuation of PSRVs at 1, 2, and 5 Hz

Depth	Vertical			Radial			Transverse		
(m)	1 Hz	2 Hz	5 Hz	1 Hz	2 Hz	5 Hz	1 Hz	2 Hz	5 Hz
0	1	1	1	1	1	1	1	1	1
100	0.9	0.8	0.8	0.9	0.8	0.8	0.9	0.8	0.8
200	0.8	0.7	0.6	0.8	0.7	0.7	0.8	0.7	0.7
300	0.7	0.6	0.5	0.7	0.6	0.6	0.7	0.6	0.6
400	0.6	0.5	0.4	0.6	0.5	0.5	0.6	0.5	0.5
500	0.6	0.4	0.3	0.6	0.4	0.4	0.6	0.4	0.4

APPENDIX B

Information Used in this Report from the Reference Information Base

Rock properties, including bulk density at in situ saturation and Poisson's ratio for rock mass, from draft Reference Information Base Version 03.001, were used in preparing Table 6-1.

Candidate Information for the Reference Information Base

The following information is recommended as candidate information for the NNWSI Reference Information Base.

1. Recommended surface control motions given in the Executive Summary.
2. Recommended design basis UNE control motions given in Table 3-1.
3. Recommended dynamic rock properties for seismic design given in Section 6. (Calculations of S-wave velocities, dynamic deformation modula, and tabulated rock properties should be made consistent with expected changes in reference rock properties.)

Candidate Information for the Site and Engineering Properties Data Base

This report contains no candidate information for the Site and Engineering Properties Data Base.

END

DATE FILMED

11 / 1 / 90